Seismic Ground Response Analysis of Soil Sites

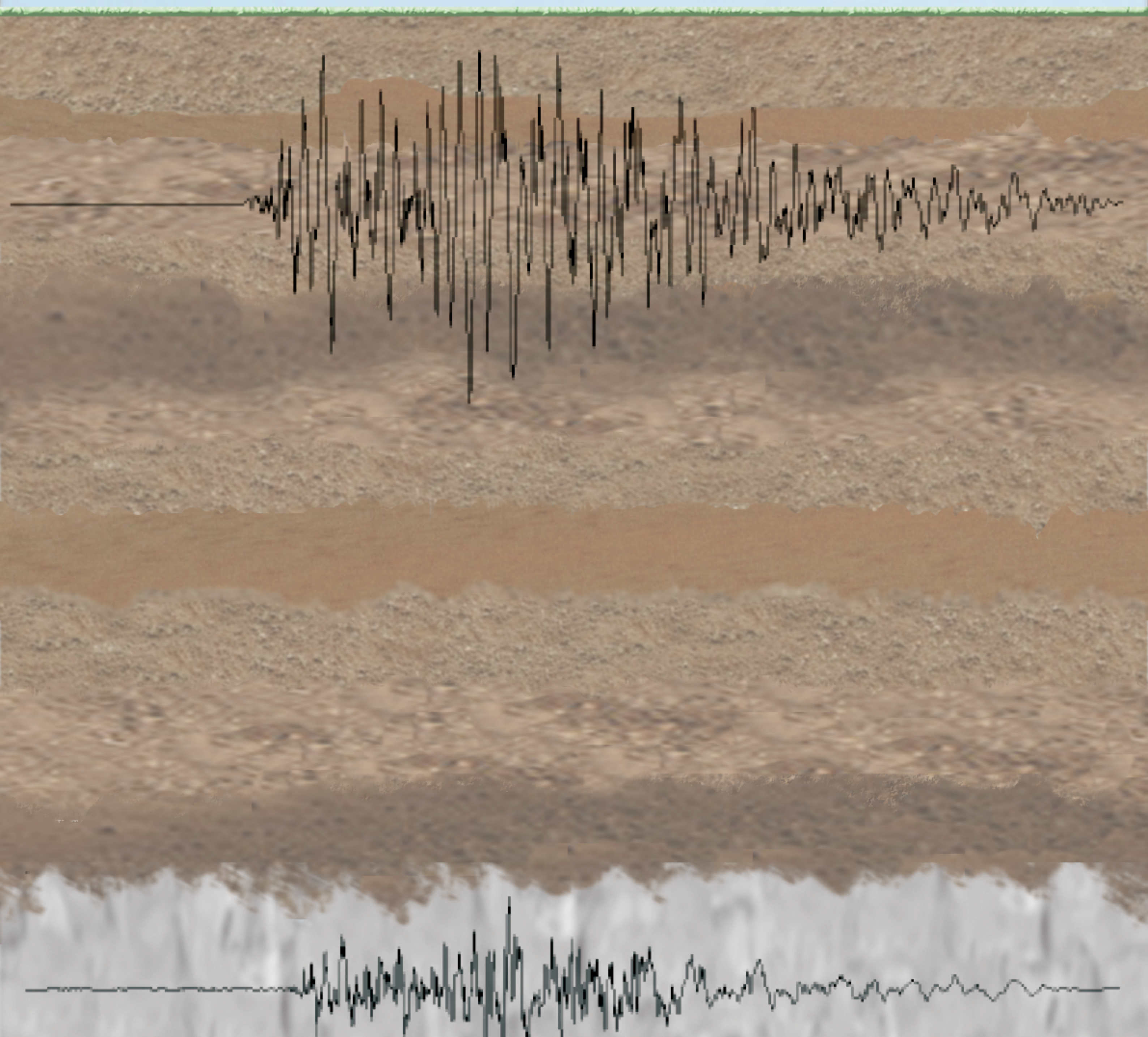

Master Thesis

by Casper Holmgaard Jensen
Department of Civil Engineering - Aalborg University - 2008

Seismic Ground Response Analysis of Soil Sites

Casper Holmgaard Jensen

Aalborg University

June 2008

Preface

This master thesis is prepared at the Department of Civil Engineering at the Faculty of Engineering, Science and Medicine at Aalborg University by the undersigned. The thesis is prepared in the period from the 4th of February 2008 through the 11th of June 2008.

The title of this thesis is *Seismic Ground Response Analysis of Soil Sites*. The thesis concerns a series of methods for ground response analyses for seismic excitation and seeks to discover the effects of each method on the resulting surface motion. The thesis is written based on knowledge acquired at courses taken at the University of California at Berkeley as part of a 9th semester study abroad period. Further needed knowledge is acquired through literature studies with the references located in the reference list at the end of the thesis.

The master thesis is prepared with the supervision from Associate Professor Lars Andersen and Professor MSO John Dalsgaard Sørensen. I thank them for their highly appreciated supervision.

Casper Holmgaard Jensen

Abstract

This thesis present analysis methods for describing the seismic ground response and the influence of soil overlaying a firm elastic bedrock. The site is not for a specific location but the analyses are performed for a soil profile with soil to a significant depth and for an area with large seismic hazard.

The thesis describes the altering of the earthquake ground motion as it propagates through the soil from bedrock to surface. The ground motion analyses are compared with the approach described by Eurocode 8,EN1998.

Detailed analyses are performed by an equivalent linear and by a nonlinear modelling of the soil. The equivalent linear model includes strain dependant dynamic soil properties and rate independent damping. The nonlinear model is performed by modelling the soil with the extended Masing model which furthermore includes the hysteretic behaviour and plastic deformation of the soil.

The comparison of the analyses methods indicates that the nonlinear model gives the best results. The equivalent linear model also gives reasonable results for well described input motions and for lower strain levels of the soil. For large strains the equivalent linear model fails to describe the nonlinear behaviour of the soil.

The procedure given by Eurocode EC8 gives satisfactory results for low period input motions but fails to describe the amplification of the motion at higher period. For bedrock input motions with significant energy at high periods this amplification results in an underestimation of the surface motion and in such cases the equivalent linear and the nonlinear models are recommended.

Table of contents

1. Introduction 1

2. Preliminaries 3

2.1. Earthquake generation and propagation 3
2.2. Location of site 6
2.3. Assumptions and simplifications 7
2.4. Soil profile 8

3. Soil response by Eurocode EC8 11

3.1. Definition of response spectrum 11
3.2. General design procedure by Eurocode EC8 12
3.3. Shape of design spectrum 14
3.4. Design spectrum at defined site 18

4. Analysis methods 21

4.1. Equivalent linear method using power spectrum input 21
4.2. Equivalent linear method using Fourier series input 22
4.3. Nonlinear method using time history input 22

5. Input bedrock motion 25

5.1. Target response spectrum 25
5.2. Bedrock motion by Kanai-Tajimi power spectrum 25
5.3. Bedrock motion by time history 28
5.4. Bedrock motion by Fourier series 32

6. Equivalent linear soil response 37

6.1. Dynamic soil properties 37
6.2. Application of the wave equation 39
6.3. Solution to the wave equation 43
6.4. Solution for power spectrum bedrock input 46
6.5. Solution for Fourier series input 55

7. Nonlinear dynamic soil analysis 61

7.1. Cyclic nonlinear model 61
7.2. General procedure 61
7.3. Implementation of model for specific site 67
7.4. Results for nonlinear analysis 69

8. Response spectrum for power spectrum 75

8.1. Combination by SRSS rule 75
8.2. Combination by time series simulations 79
8.3. Results for power spectrum motion 83
9. Response spectrum for Fourier series 85
9.1. Fourier series for SDOF system 85
9.2. Total acceleration time history 85
9.3. Response spectrum 86
10. Response spectrum for time history 87
10.1. Newmark algorithm 87
10.2. Response spectrum for nonlinear analysis 89
11. Comparisons 91
11.1. Surface response spectra comparisons 91
11.2. Soil response for 30 m soil profiles 96
11.3. Alternative bedrock input record 98
12. Conclusion 101
13. References 103

1. Introduction

When constructions are build in seismic active areas one of the design criteria is that the construction must perform satisfactory during an earthquake event. Therefore it is necessary to know which seismic ground motions the construction must be designed for. One of the challenges is to describe the magnitude of earthquakes that can be expected in the region and estimate how the earthquake waves travel from the centre of the rupture to the bedrock beneath the construction site. For sites where the bedrock is overlain by a layer of softer soil the bedrock ground motion can be greatly altered before it reaches the surface, and if not anticipated cause great damage. Different analysis methods for describing this effect called local site effect is described in this project.

An event where local site effects played a major role occurred during the Mexico City earthquake of 1985 where parts of the city was destroyed even thou the epicentre of the earthquake was 350 kilometres away and buildings in the vicinity of the epicentre was only moderately damaged. The damage in Mexico City was mainly caused by local site effects where soil overlaying firm bedrock altered and amplified the bedrock motion to such an extend where a large number of buildings in specific areas were unable to withstand the seismic load and collapsed.

To understand what happened during the Mexico City earthquake it is important to know the subsurface condition beneath Mexico City. The city is divided into three seismic zones with pronounced different subsurface conditions. In Figure 1.1 the foothill zone seen consist of shallow well compacted granular material. The lake zone consists of old and younger lake deposits with thick deposits of very soft soils, with the thickness decreasing towards the foothill zone as indicated in Figure 1.1 (right). Between the foothill zone and lake zone is the transition zone that consists of a thin layer of soft soils broken up by layers of denser soils.

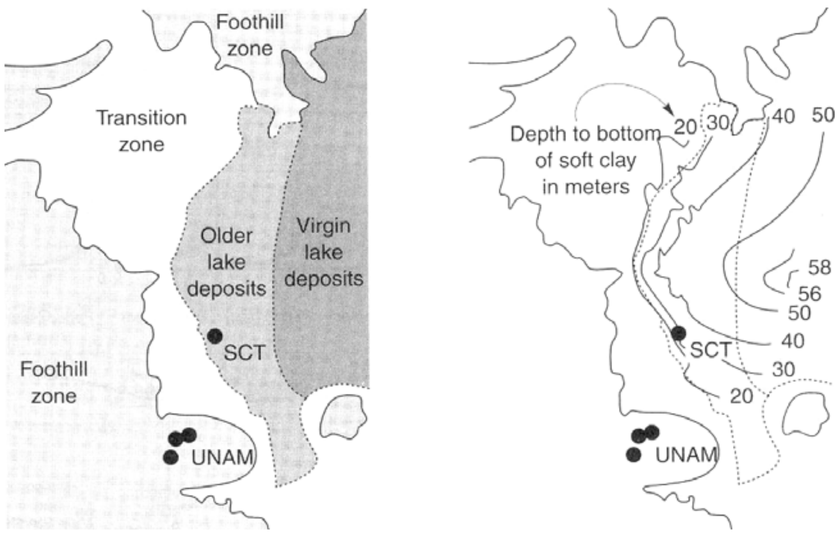

Figure 1.1. Subsurface of Mexico City divided into three zones (left). Depth of soft soil in lake zone (right). [Kramer 1996, p314]

From strong motion sensors placed at stations in the foothill and lake zone the ground surface acceleration showed significantly different motions as shown in Figure 1.2. In the foothill zone only minor ground motion was detected whereas in the lake zone large amplification of the motion was detected. It can also be seen the motion at the lake zone is oscillating at a lower frequency but for a longer duration.

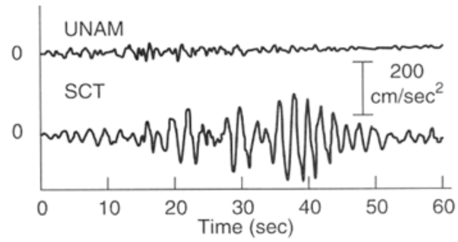

Figure 1.2. Acceleration ground motions recorded at Mexico City stations. UNAM: foothill zone. SCT: lake zone. [Kramer 1996, p314]

The reason for this difference is that the thick layer of softer soils in the lake zone acts as a filter that filters away high frequency motion and amplifies motion that corresponds to the natural period of the soil. The effect on the bedrock motion that happened at the lake zone caused many building to collapse in that region of the city. Especially building with a natural period in the same range as the natural period of the soil was heavily damaged since the motion in such cases was amplified twice, first by travelling through the soft soil to the surface and then again when travelling through the building. Buildings in the foothill zone suffered negligible damage.

The Mexico City earthquake is a good example of the importance of a good analysis of the seismic ground response at sites with soft soils or the consequences of neglecting them.

2. Preliminaries

In this chapter the preliminaries for the different analyses are described. This includes the possible location of the construction site and the defined soil profile for the site.

2.1. Earthquake generation and propagation

In this section the general terms and behaviour of earthquakes are described. Both the generation of earthquakes and the propagation of the following waves are described.

2.1.1. Generation of earthquakes

The majority of significant earthquakes are generated in the boundaries between tectonic plates as a consequence of their movement relative to each other. In Figure 2.1 a map of the major tectonic plates are shown where also the movement of the plates are given. The interrelationship between the plate boundaries are indicated with the fault environments given as subduction zone, ridge axis (spreading ridge) and strike slip fault.

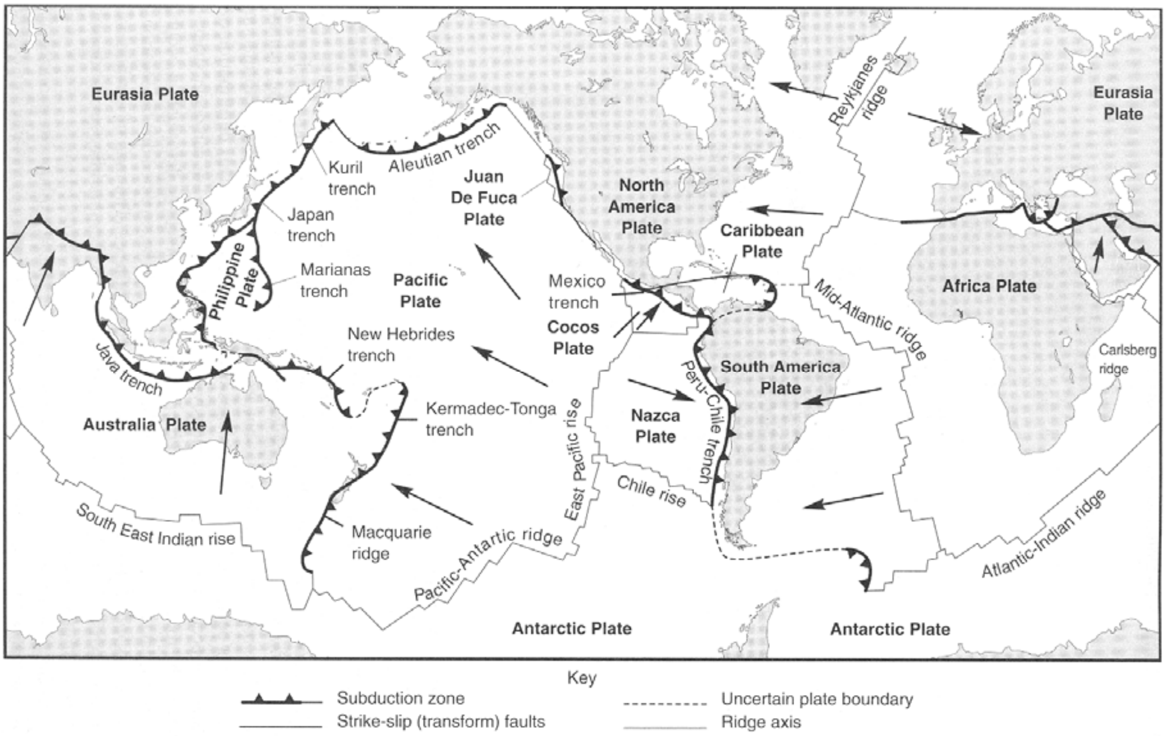

Figure 2.1. Worldwide map of major tectonic plates. Arrows indicate individual plate movement. [Kramer 1996, p26]

The three fault types are shown in Figure 2.2. The most severe earthquakes are mostly generated in areas with subduction zones and strike slip faults.

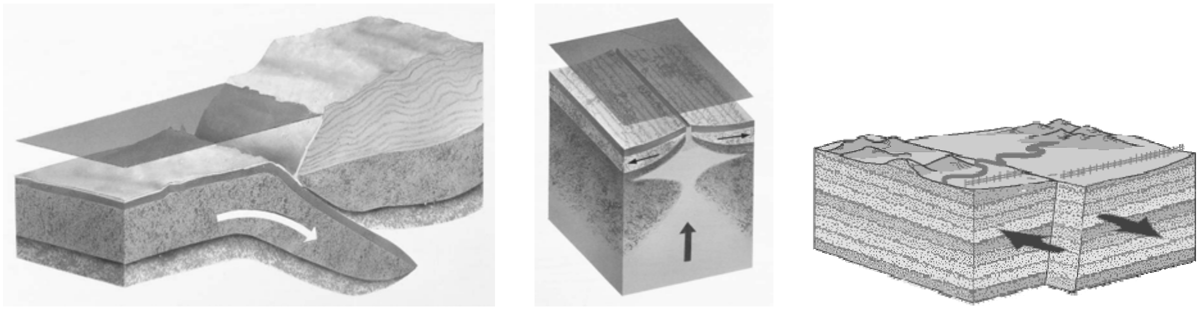

Figure 2.2. Subduction zone (left) [dkimages.com 2008], spreading ridge (middle)[dkimages.com 2008b] and strike slip fault (right) [usgs.com 2008].

The fundamental theory of energy build up in seismic active regions is called the elastic rebound theory. This theory states that when two tectonic plates moves relative to each other elastic strain energy is stored in the material near the boundaries between the two plates. When the shear stress in the fault plane separating the plates reach a certain level the stored energy is released which causes an earthquake.

A key feature of a fault is a parameter describing the annual strain energy build up. The slip rate of a fault is therefore defined as the annual relative movement of two adjoining plates and this parameter is a key parameter in the determination of the probability distribution of earthquake with a certain magnitude generated at the fault.

The hypocenter is the point where the strain energy of the earthquake is released and the depth of this point can be from a few kilometres to several hundred of kilometres.

2.1.2. Propagation of earthquakes

During a fault rupture the strain energy is released and body waves are generated and propagates away from the source. Body waves consist of two types of waves, namely p- and s-waves as shown in Figure 2.3.

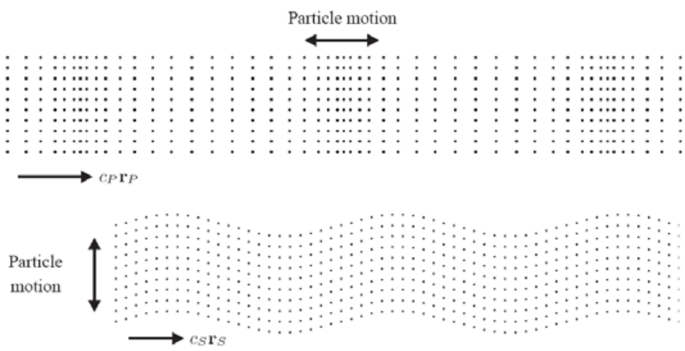

Figure 2.3. P-waves (upper) and s-waves (lower). The wave propagation is from left to right. [Andersen 2006, 11]

p-waves involves compression and rarefaction of the medium and are therefore often called compression waves. The particle motion is parallel to the direction of the wave propagation as indicated in Figure 2.3 (upper). s-waves involves shearing deformation of the medium and are therefore often called shear waves. The particle motion is perpendicular to the direction of the wave propagation as indicated in Figure 2.3 (lower). s-waves cannot travel through fluids since no shearing can occur in such medium.

The body waves are initially propagating away from the source as a sphere. Because the wave velocity decreases with decreasing stiffness of the soil a refraction phenomena occur. In general the stiffness of the rock is increasing with increasing depth and this tendency is even more pronounced in the shallower soil layers. Because of this decrease in stiffness and thereby decrease in wave velocity as the wave propagates towards the surface the incoming wave fronts will be refracted to a more vertical direction of propagation. An illustration of the refraction phenomena is given in Figure 2.4 where it is seen that the wave front changes direction due to the difference in velocity between the two sides of the wave orthogonals. The figure shows the path for s-waves but the same refraction phenomena applies to p-wave propagation.

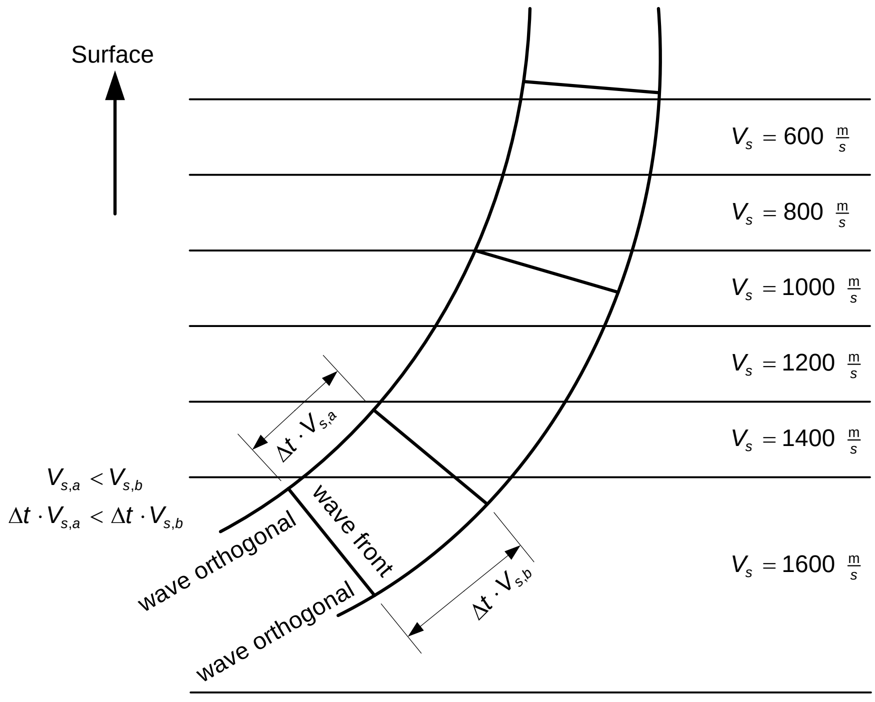

Figure 2.4. Refraction of inclined wave fronts. V_s is shear wave velocity.

The refraction phenomena for the body wave propagation is similar to the refraction phenomena in coastal hydraulics when ocean waves propagates toward the shore. The path of the body wave travelling from the source to the surface at the specified site is illustrated in Figure 2.5. As indicated in the figure the refraction is most predominant in the shallower layers where the decrease in stiffness between the layers are greater.

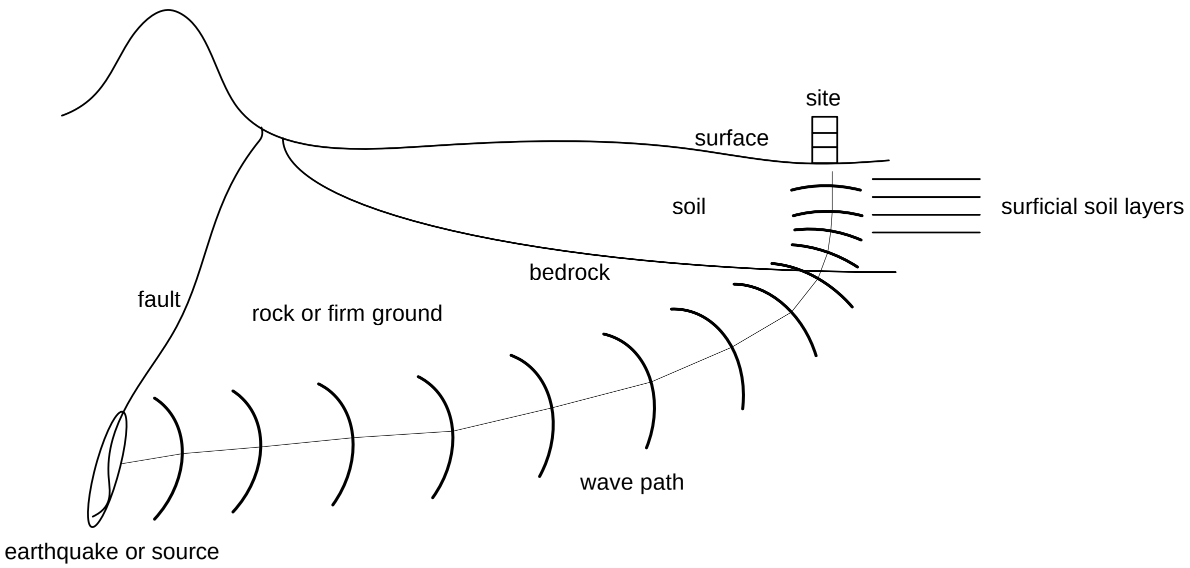

Figure 2.5. Earthquake wave propagation and refraction process.

2.2. Location of site

This project is not dealing with a specific site. Instead this project is a more general comparison of the different methods of analysing the soil and building response to earthquake loading. Since the Eurocode design method described in EN1998:2003 is one of the methods to be considered, it is assumed that the site is located in Europe. Also it is assumed that the site is on a location with noticeable earthquake hazards.

A site specific description of the seismic hazard level can be developed, but this requires extensive seismological knowledge of fault characteristics in the area and the use of attenuation relationships to attenuate the ground motion to the site. In the absence of such seismological information for this project the more general seismic hazard map is used to give the seismic hazard level.

The seismic hazard map as given in Figure 2.6 shows the level of peak ground acceleration corresponding to 10 % exceedence in 50 years. In this project the location is set to a site corresponding to a peak ground acceleration (PGA) of a_g = 0.5g for firm ground corresponding to bedrock with a 10 % exceedence in 50 years.

$z = 0$ m			surface
	$h = 12$ m	$V_{s,\max} = 200\ \frac{m}{s}$, $\rho = 1950\ \frac{kg}{m^3}$	soil type 1: silty sand
$z = 12$ m			
	$h = 18$ m	$V_{s,\max} = 300\ \frac{m}{s}$, $\rho = 2050\ \frac{kg}{m^3}$	soil type 2: silty sandy clay
$z = 30$ m			
	$h = 20$ m	$V_{s,\max} = 350\ \frac{m}{s}$, $\rho = 1850\ \frac{kg}{m^3}$	soil type 3: silty clay
$z = 50$ m			
	$h = 30$ m	$V_{s,\max} = 450\ \frac{m}{s}$, $\rho = 1850\ \frac{kg}{m^3}$	soil type 4: clay
$z = 80$ m			
	$h \approx \infty$	$V_{s,\max} = 1000\ \frac{m}{s}$, $\rho = 2600\ \frac{kg}{m^3}$	bedrock

Figure 2.7. Soil profile as used in the soil response analyses. h is thickness, z is depth, and ρ is unit density. $V_{s,max}$ is the measured shear wave velocity at an infinitesimal strain level.

3. Soil response by Eurocode EC8

In this chapter the soil response is analysed by use of the procedure described in Eurocode 8,EN1998. First a general description of the response spectrum concept and the design procedure for earthquake loads on buildings are given. Following is the design by Eurocode EC8 corresponding to the specific site of this project.

3.1. Definition of response spectrum

Seismic design by Eurocode EC8 involves the generation of a response spectrum. A response spectrum is defined as the maximum response of a single degree of freedom (SDOF) system with varying natural periods excited with a given ground motion. In earthquake design the response is taken as the maximum absolute acceleration of the mass. In Figure 3.1 the concept of a response spectrum is illustrated. As indicated in the figure the response spectrum is generated as the maximum mass response of a SDOF where the input motion is the earthquake ground motion.

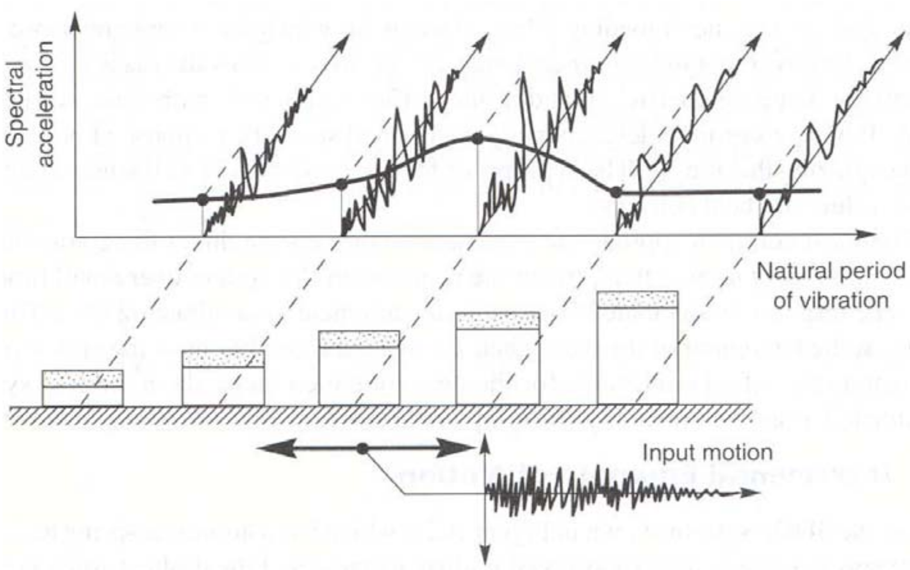

Figure 3.1. Illustration of the response spectrum concept.. [Kramer 1996, p571]

From the definition of the response spectrum a ground motion can be transformed into a response spectrum by letting a SDOF system with varying natural periods be excited with the ground motion. The response spectrum is then generated by plotting the maximum response of the system as a function of the natural period of the system.

In the following analyses two ground motions are transformed into response spectra. The first is the bedrock ground motion, since this motion is the basis of the following wave propagation through the soft soil layers. The bedrock motion is required to be as similar to the bedrock motion defined in Eurocode EC8 as possible, since this input motion is a prerequisite for the real analysis which is the analysis of the soft soil effect on the surface ground motion. The second ground motion is the surface ground motion after the wave propagation through the soft soil layers has been analysed. This ground motion is needed so the results from different analysis methods can be compared to the response spectrum defined in Eurocode EC8. An illustration of the two ground motions and their interpretation as a response spectrum are shown in Figure 3.2.

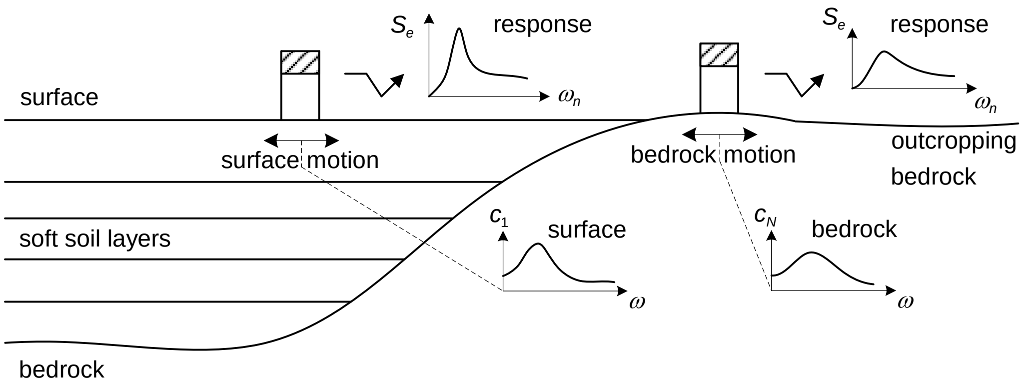

Figure 3.2. The two ground motions for which response spectra are generated. The outcropping bedrock has a ground motion assumed equal to the bedrock ground motion. c_N is the Fourier amplitude spectrum of the bedrock ground motion and c_1 is the Fourier amplitude spectrum of the surface motion. Note that the ground motions for the nonlinear analysis are given as time histories and not Fourier amplitude spectra.

3.2. General design procedure by Eurocode EC8

The design procedure by Eurocode EC8 can be divided into four sections.

1) Estimation of ground motion for firm ground
2) Correction of ground motion for sites with softer soil than firm ground
3) Generation of elastic response spectrum to describe the ground motion effect on structures
4) Calculate the response of the structure by use of the response spectrum

3.2.1. Estimation of ground motion for firm ground

The estimation of the ground motion for the site as if it were firm ground is most often found from seismic hazard maps. A seismic hazard map is a map of a region which indicates the expected peak ground motion of firm ground for a given return period. Such maps are generated on the basis of knowledge of distance to active faults and the characteristics of these. A seismic hazard map is seen in Figure 2.6.

3.2.2. Correction of ground motion for soft soil sites

For sites where softer soil is overlaying the bedrock a correction must be made since soft soils have a great effect on the ground motion as described in Section 1. The correction is done by classifying the soil profiles in different ground types corresponding to the grade of soil stiffness. The parameter dictating the ground type is the average shear wave velocity for the top 30 m of soil. In Figure 3.3 the design spectra for all the ground types defined in Eurocode EC8 are shown.

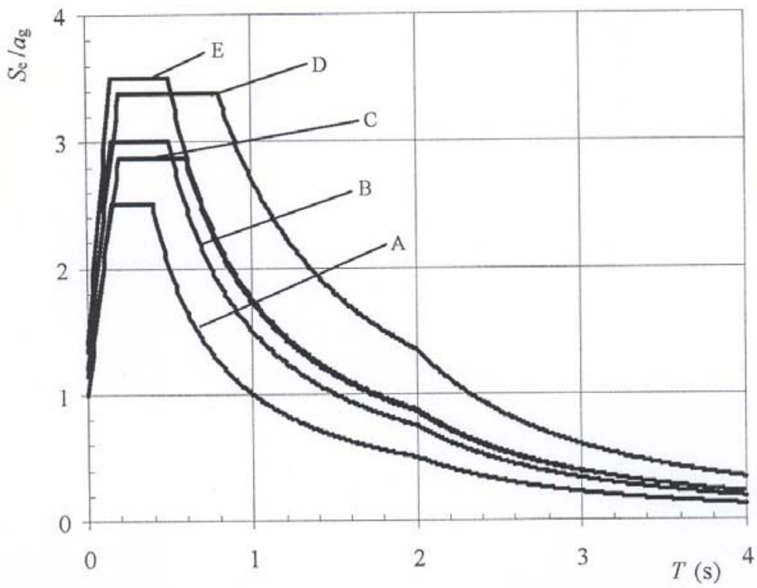

Figure 3.3. Normalized design response spectra as defined in EC8 for 5% damping. The ground stiffness decreases from ground type A to E. [EN1998:2003, p25]

3.2.3. Generation of elastic response spectrum

An elastic response spectrum is defined on the basis of the ground type and the firm ground motion found from the seismic map. The response spectrum is normally generated for an elastic and viscous damped one degree of freedom system with a damping ratio of 5 %. For systems with damping ratio different from 5 % a damping correction factor can be used to correct the response spectrum. The elastic response spectrum can also be modified to fit a structure where a some plastic deformation are allowed by use of a behaviour factor.

3.2.4. Response of structure by use of response spectrum

The total response of a multi degree of freedom system can be estimated by using the response spectrum. First the modes of the structure is found by modal analysis of the structure. A response for each mode is found as the value in the response spectrum corresponding to the frequency for the given mode. The response for each mode can then be combined to a total response of the structure by using the SRSS rule (Square Root of the Sum of Squares), where the response for each mode is squared, then summed and finally the square root of this sum is used as the total response of the structure. This method gives good estimates for well separated modes.

3.3. Shape of design spectrum

The response spectra defined in Eurocode EC8 are design spectra used to describe a whole group of individual site specific response spectra. The defined design spectra can be thought of as spectra which envelopes a broad variety of site specific spectra where the soil profiles are lumped together in classes as described in Section 3.2.2. For the period range of the response spectrum for a single site, different earthquake events can also be predominant at different periods which is further illustrated in Section 3.3.2. The design spectra defined in design codes are therefore often more conservative than site specific response spectra which on the other hand requires more information of the site and active faults in the area. In the following section the shape of the design spectra given by Eurocode EC8 are discussed.

3.3.1. Constant acceleration, velocity and displacement spectrum

In Figure 3.4 the general shape of a design spectrum defined in Eurocode EC8 is shown with indication of the different line segments.

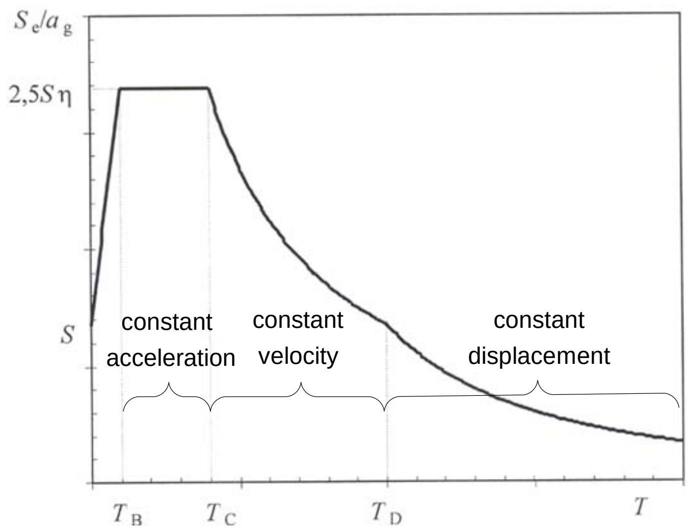

Figure 3.4. Shape of design spectra with indication of constant acceleration, velocity and displacement segments. [EN1998:2003, p24]

It is seen that the design spectrum are constructed of several line segments. By looking at the formulas defining these line segments, it can be shown that the lines relates to constant acceleration, constant pseudo velocity and constant pseudo displacement. The design spectra are defined by

$$\begin{aligned}
&0 \le T \le T_B : S_e(T) = a_g \cdot S\left(1 + \frac{T}{T_B}(\eta \cdot 2.5 - 1)\right) \\
&T_B \le T \le T_C : S_e(T) = a_g \cdot S \cdot \eta \cdot 2.5 \\
&T_C \le T \le T_D : S_e(T) = a_g \cdot S \cdot \eta \cdot 2.5\left(\frac{T_C}{T}\right) \\
&T_D \le T \le 4s : S_e(T) = a_g \cdot S \cdot \eta \cdot 2.5\left(\frac{T_C T_D}{T^2}\right)
\end{aligned} \tag{3-1}$$

where

$S_e(T)$	is the elastic response spectrum for acceleration
T	is the vibration period of a linear SDOF system
a_g	is the design ground acceleration on bedrock
T_B	is the lower limit of the period of the constant acceleration line segment
T_C	is the lower limit of the period of the constant velocity line segment
T_D	is the lower limit of the period of the constant displacement line segment
S	is the soil factor
η	is the damping correction factor with reference value of $\eta = 1$ for 5% viscous damping

[EN1998:2003, p23]

The values of T_B, T_C, T_D and S are given in [EN1998:2003, p24] for each ground type. a_g is most often found from seismic hazard maps of the area of the site. To show that the line segments in (3-1) correspond to constant acceleration, velocity and displacement the definition of pseudo velocity and pseudo displacement are discussed. These two quantities are given as

$$S_e = \omega_n S_V \text{ and } S_e = \omega_n^2 S_D \tag{3-2}$$

where

S_V	is the pseudo velocity spectrum
S_D	is the pseudo displacement spectrum
ω_n	is the circular natural frequency of the linear SDOF system

[Chopra 2007, p209-210]

The real velocity and displacement spectra can be found by integration of the Duhamel integral and it can be shown that these spectra are proportional to the acceleration spectra by a factor of ω_n^{-1} and ω_n^{-2} respectively except for a phase shift and that the phase shift does not have significant influence on the maximum response. Therefore the pseudo velocity and pseudo displacement defined in (3-2) gives a close approximation to the real velocity and displacement spectra. [Kramer 1996, p572]

Since the period T is inversely proportional to ω_n it can be seen that the line segment in (3-1) of the acceleration response spectrum from T_C to T_D corresponds to a constant velocity spectrum and the line segment of the acceleration response spectrum from T_D to 4 s corresponds to a constant displacement spectrum.

As an example, the constant velocity is calculated for a case with firm ground, damping ratio equal to 5% (η = 1) and firm ground motion equal to a_g = 0.5 g. For this case S = 1, T_C = 0.4 s, T_D = 2 s as found in [EN1998:2003, p24]. By insertion of these values in (3-1) for the line segment corresponding to constant velocity this gives a constant velocity of

$$\begin{aligned}
&T_C \leq T \leq T_D : S_e(T) = a_g \cdot S \cdot \eta \cdot 2.5\left(\frac{T_C}{T}\right) \\
&0.4s \leq T \leq 2s : S_e = \left(0.5 \cdot 9.81\tfrac{\mathrm{m}}{\mathrm{s}^2}\right) \cdot 1 \cdot 1 \cdot 2.5\left(\frac{0.4\mathrm{s} \cdot \omega_n}{2\pi}\right) \\
&0.4s \leq T \leq 2s : S_e = 0.78\tfrac{\mathrm{m}}{\mathrm{s}} \cdot \omega_n
\end{aligned} \tag{3-3}$$

By comparing (3-3) with (3-2) it is seen that $S_V = 0.78\,\frac{\mathrm{m}}{\mathrm{s}}$. Same procedure can be used to find constant displacement values.

3.3.2. Design spectra contra response spectra

A design spectra is used as a basis for design of earthquake resistant constructions. The shape with constant acceleration, velocity and displacement has been shown to give reasonable fits to response spectra based on recorded time histories of earthquake events. Response spectra from individual measurements will have a highly irregular shape with peaks at different periods and the design spectra seeks to include all these irregular shapes.

Another effect that requires the design spectrum to have a more smooth shape than for a single response spectrum is due to the difference in frequency contents for smaller magnitude and close earthquake events compared to larger magnitude and distant earthquakes. A design spectrum is often generated on the basis of a uniform seismic hazard, which therefore includes the contribution from all active faults which causes seismic hazard to the site.

The contribution to the seismic hazard from several faults are in the following illustrated by an example. The site is chosen as the Oakland side of the San Francisco–Oakland Bay Bridge, California, USA. Through the U.S. Geological Survey's homepage it is possible to generate the seismic hazard for the site by a probabilistic seismic hazard analysis, which gives the relative contribution for different distance and magnitude combinations for all nearby faults. For a more thorough description of probabilistic seismic hazard analysis the reader is recommended [Abrahamson 2000]. In Figure 3.5 the relative contribution to the hazard from different sources are shown for a 10 % exceedence in 50 years for the Bay Bridge site. A map is shown for both the relative contribution for the peak ground acceleration (PGA) and for the $S_e(2s)$ value corresponding to the maximum response for a SDOF system with natural period 2 s.

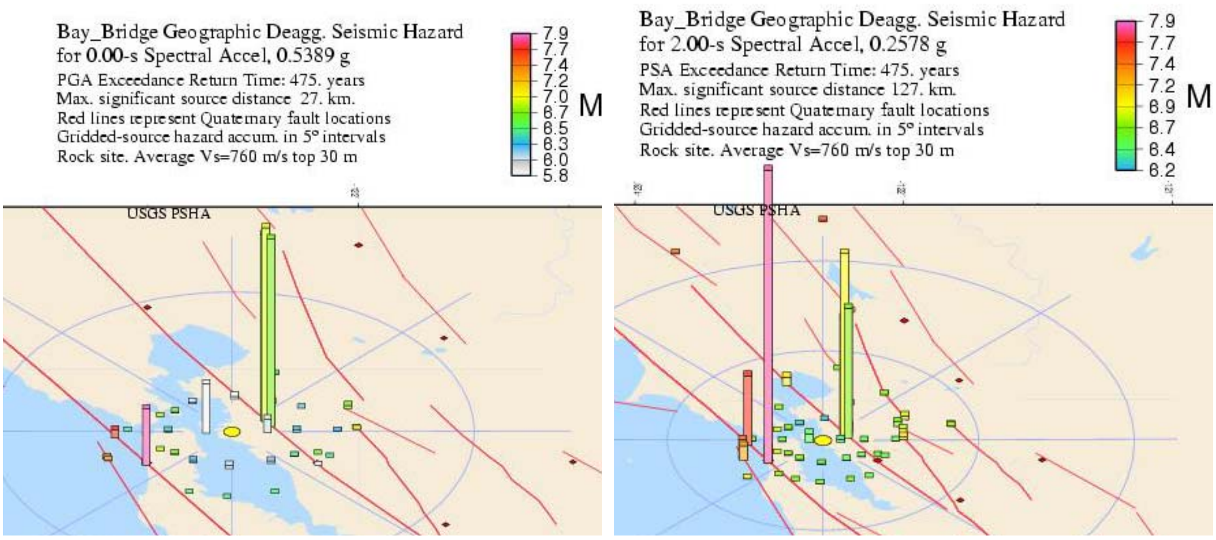

Figure 3.5. Relative contribution to seismic hazard from significant sources. Contribution to PGA (left) and to $S_e(2s)$ response (right). Site is indicated with yellow circle. [usgs.com 2008b]

It is seen from the contributions in Figure 3.5 that the most significant source is dependent on the wanted period value for the response spectrum. The short period values are often determined by closer but smaller earthquakes which also is the tendency in Figure 3.5 (left) while the longer period values more often is determined by larger earthquakes more distant from the site, which is the tendency seen in Figure 3.5 (right).

The reason for this is that the high frequency contents of the waves gets filtered while travelling from the source to the site. When the distance to the site is large most of the high frequent motion is filtered away. Therefore the predominant period of the ground motion increases with increasing distance between source and site. The same tendency is seen with the magnitude of the earthquake event, where larger magnitude more often increases the predominant period of the ground motion. The increase in the predominant period of the input ground motion then influences the response of the SDOF system so the value of the response spectrum for the chosen period follows the tendency of the frequency content of the ground motion. [Rathje et al. 2004]

The above mentioned tendencies are shown in Figure 3.6 where two response spectra and a design spectrum are shown. The response spectra are generated using attenuation relationships described by [Abrahamson & Silva 1997] for two earthquake events. One moderate sized at small distance and one large sized at large distance for a deep soil site and strike slip fault mechanism. As discussed above, the response at short periods are governed by the moderate sized but closer earthquake, while for the longer periods the more distant but larger sized earthquake governs the response. This is also the tendency shown in Figure 3.5. An imagined design spectrum for this case is included in Figure 3.6 but has no basis in Eurocode EC8 or similar codes.

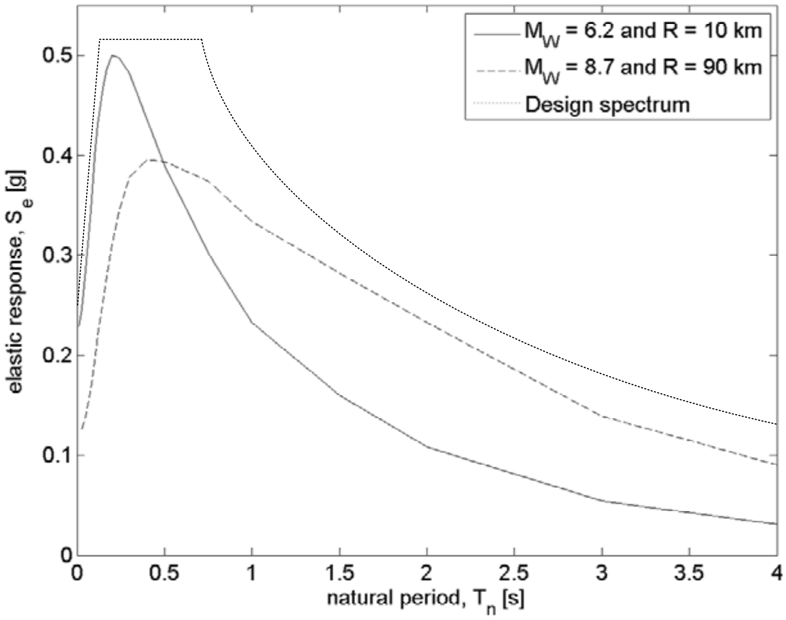

Figure 3.6. Response spectra from attenuation relationships described in [Abrahamson & Silva 1997]. M_W is the magnitude and R is the distance between site and source. An imagined design spectrum is included in the figure.

3.4. Design spectrum at defined site

In this section the generation of a response spectrum corresponding to the specified site is generated. The design ground acceleration for firm ground is given in Section 2.2 as a peak ground acceleration of a_g = 0.5 g. To find the ground type for the given soil profile the average shear wave velocity for the top 30 m of soil is calculated. This is done by

$$V_{s,30} = \frac{30\text{ m}}{\sum_{i=1}^{N} \frac{h_i}{V_{s,i}}} \tag{3-4}$$

where

$V_{s,30}$ is the average shear wave velocity for the top 30 m soil

h_i is the thickness of layer i in [m]

$V_{s,i}$ is the shear wave velocity of layer i

[EN1998:2003, p20]

For the soil profile defined in Section 2.4 the calculated average shear wave velocity as defined in (3-4) is $V_{s,30}$ = 250 m/s which corresponds to ground type C: *Deep deposits of dense or medium dense sand, gravel or stiff clay with thickness from tens to many hundreds of metres.* [EN1998:2003, p20]

For ground type C the horizontal elastic response spectrum for a 5% damped structure is shown in Figure 3.7. Here it is assumed that the earthquake event that contribute the most to the seismic hazard have a surface-wave magnitude grater than 5.5 so a type 1 spectrum is applied [EN1998:2003, p24].

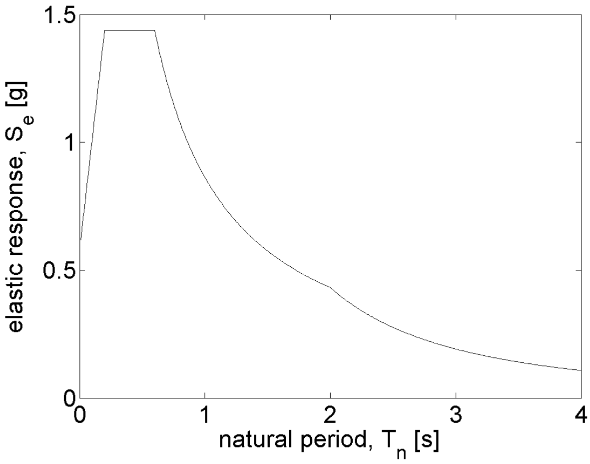

Figure 3.7. Elastic response spectrum for soil type C and 5 % damping. [EN1998:2003, p23]

4. Analysis methods

In this chapter an outline of the general procedures for the different ground response analyses used in this project are given.

4.1. Equivalent linear method using power spectrum input

This analysis uses an equivalent linear description of the soil response where the bedrock input motion is given as a power spectrum. The analysis is performed in the frequency domain by the procedure illustrated in Figure 4.1.

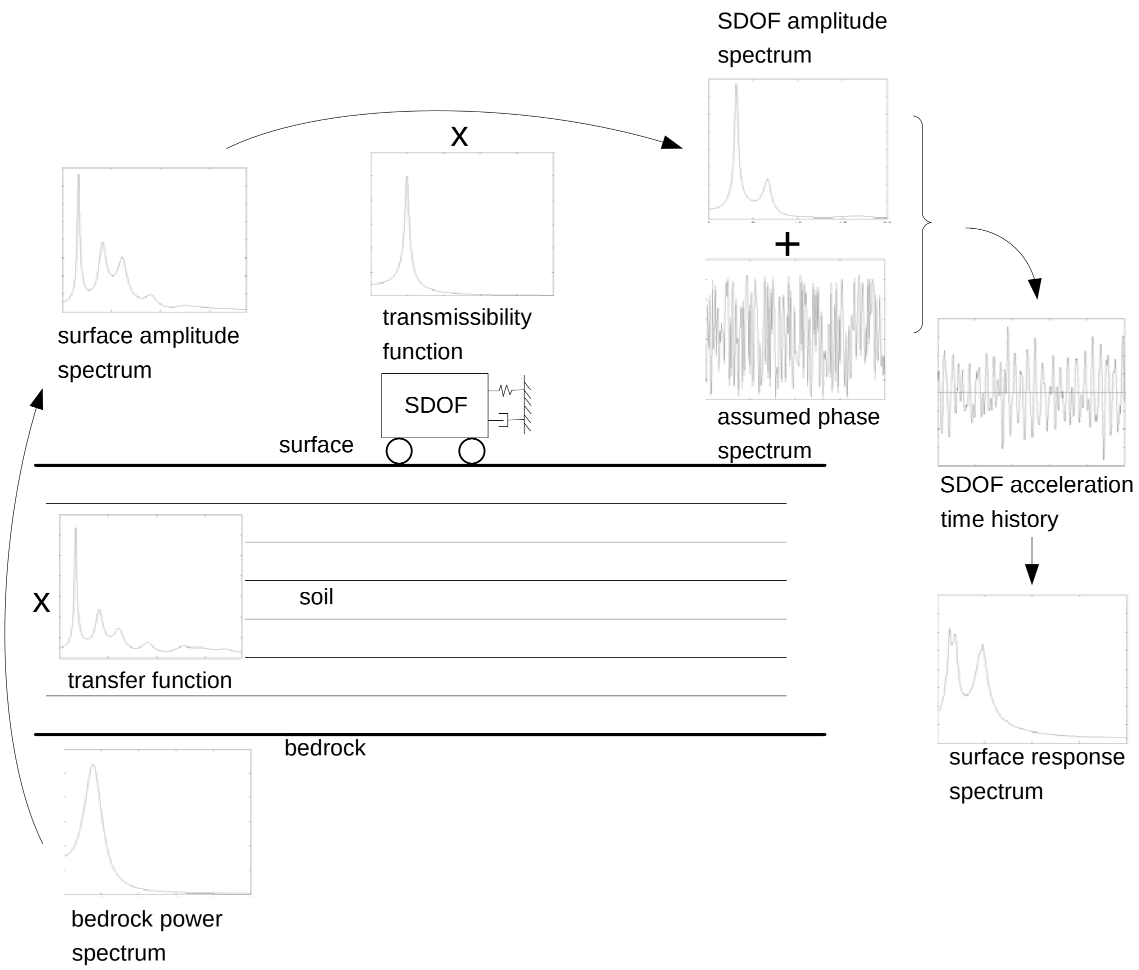

Figure 4.1. Equivalent linear method using a power spectrum bedrock input motion.

4.2. Equivalent linear method using Fourier series input

This analysis uses an equivalent linear description of the soil response where the bedrock input motion is given as a Fourier series including both amplitude and phase spectra. The analysis is performed in the frequency domain by the procedure illustrated in Figure 4.2.

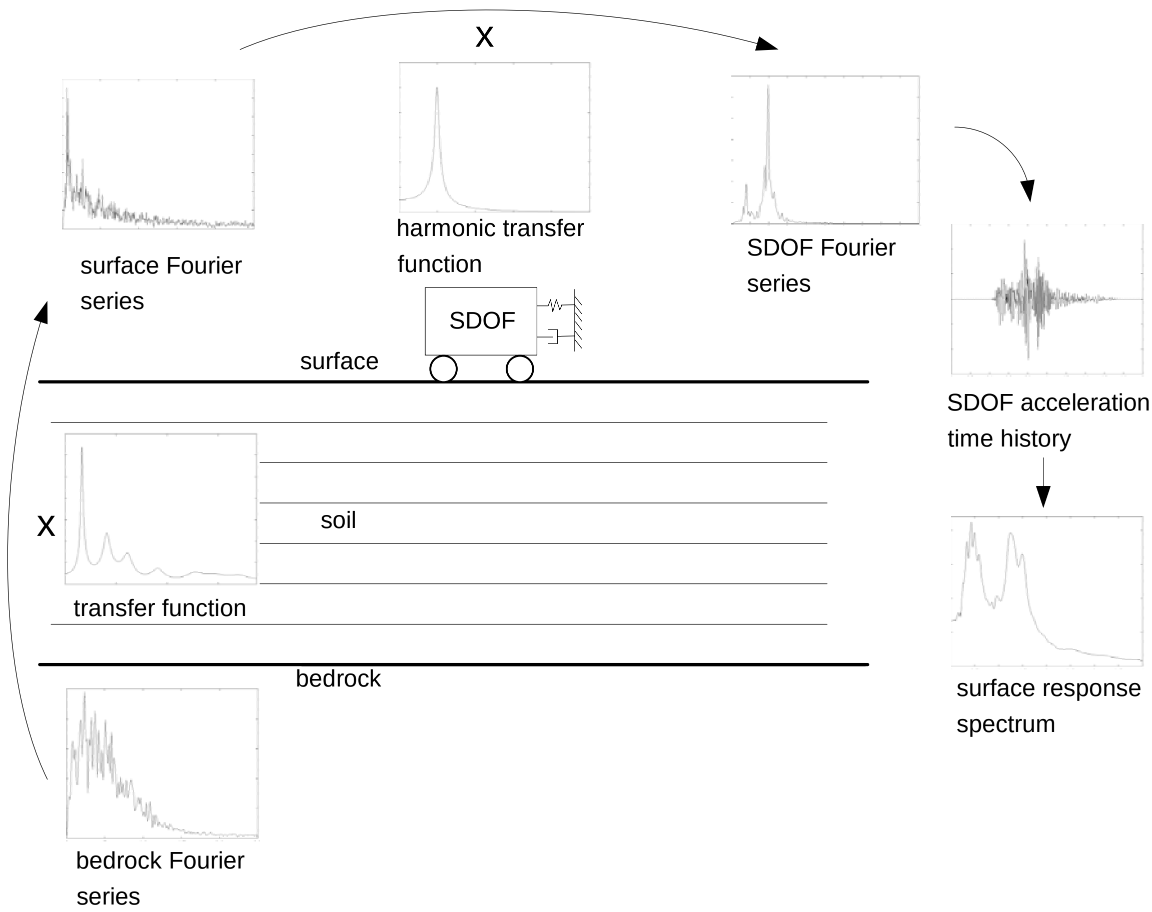

Figure 4.2. Equivalent linear method using a Fourier series bedrock input motion.

4.3. Nonlinear method using time history input

This analysis uses a nonlinear description of the soil response where the bedrock input motion is given as a time history. The analysis is performed in the time domain by the procedure illustrated in Figure 4.3.

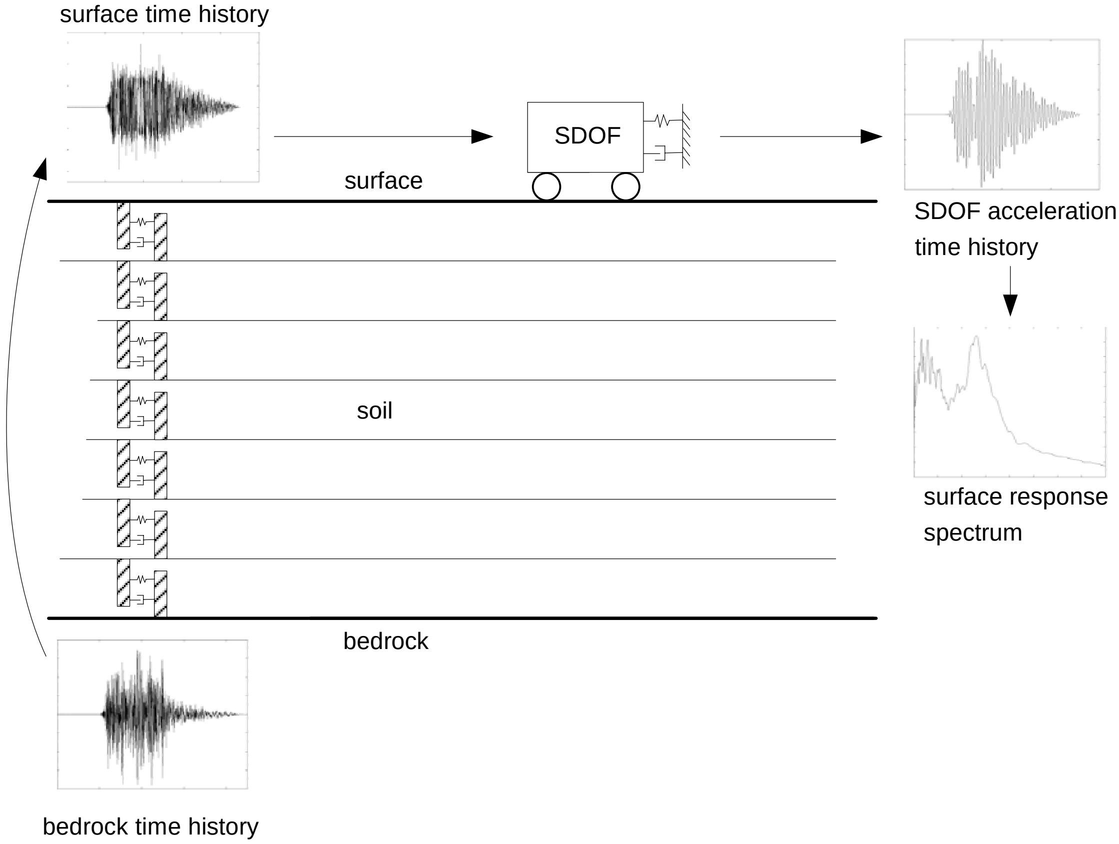

Figure 4.3. Nonlinear method using time history input.

5. Input bedrock motion

In this chapter the ground motion at bedrock is determined for the equivalent linear and the nonlinear analyses used in this project. The bedrock motion is used as input to the analyses and to be able to make a comparison of the analyses results the input motions for the equivalent linear analysis and the nonlinear analysis must be as similar as possible to the corresponding bedrock motion defined by the procedure in Eurocode EC8.

5.1. Target response spectrum

The basis for the bedrock motion is taken as the design response spectrum defined by the Eurocode EC8 procedure described in Section 3.2.2 for a rock site. A rock site is the stiffest of the sites defined in Eurocode EC8 and therefore this soil type corresponds well to bedrock. The use of a more general design spectrum is done, since generation of a site specific response spectrum on the basis of attenuation relationship needs more seismic data for the site than is known, see Section 2.2. The bedrock motions used in the equivalent linear and the nonlinear analyses must be calibrated to give values that resemble the target design spectrum as close as possible. Therefore the response spectrum given by Eurocode EC8 for rock site and with the same seismic hazard level as given in Section 2.2 is called the target response spectrum, see Figure 5.1.

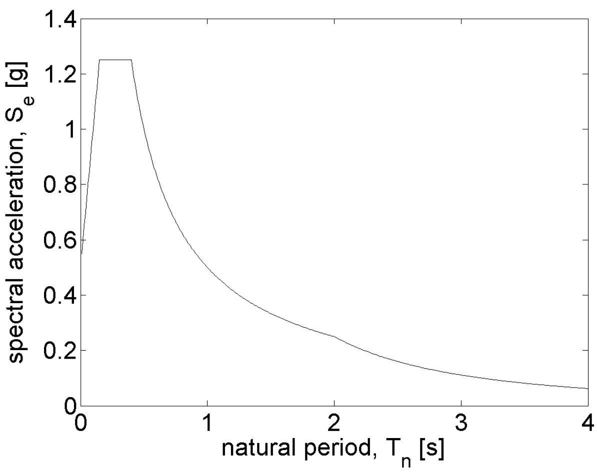

Figure 5.1. Target response spectrum. 5 % damping.

5.2. Bedrock motion by Kanai-Tajimi power spectrum

The input bedrock motion used for the equivalent linear analysis can be described by a power spectrum. An often used power spectrum for soil motion due to earthquake loading is the Kanai-Tajimi power spectrum.

The Kanai-Tajimi power spectrum is a filtered white noise defined by

$$G(\omega) = G_0 \frac{1+\left(2\zeta_g \dfrac{\omega}{\omega_g}\right)^2}{\left(1-\left(\dfrac{\omega}{\omega_g}\right)^2\right)^2+\left(2\zeta_g \dfrac{\omega}{\omega_g}\right)^2} \tag{5-1}$$

where

G_0 is the ground intensity

ω_g is the ground frequency. For rock site ω_g is set to 27.0 rad/s

ζ_g is the ground damping. For rock site ζ_g is set to 0.34

[Kramer 1996, p78]

The power spectrum is described for the bedrock motion where the ground frequency and ground damping values are given in (5-1). The ground intensity needs to be calibrated to the target spectrum as done later in this section.

A power spectrum describes the power of the signal. To rewrite it to the quantity of the signal as given by a Fourier amplitude spectrum of acceleration the following relation is used

$$\begin{aligned} G(\omega) &= \tfrac{1}{2}(c(\omega))^2 \\ c(\omega) &= \sqrt{2G(\omega)} \end{aligned} \tag{5-2}$$

where

$c(\omega)$ is the Fourier amplitude spectrum of acceleration

[Kramer 1996, p542]

It is noted that a power spectrum describes the power of the signal and by transferring a power spectrum to a Fourier amplitude spectrum a signal time history can not be fully described. To describe a time history also a Fourier phase spectrum is needed but information about the phase spectrum can not be extracted from the power spectrum. This problem is further discussed in Section 6.4.

To compare the result in the equivalent linear soil response analysis with the soil response analysis by Eurocode EC8 it is important that the seismic input load is of similar magnitude. Therefore the ground intensity factor G_0 must be determined in such a way that the bedrock power spectrum and the target response spectrum given in Figure 5.1 corresponds to similar seismic bedrock load.

This is done by generating an elastic response spectrum from the Kanai-Tajimi power spectrum and then compare this response spectrum with the target response spectrum. The transformation procedure from a power spectrum to a response spectrum is described in Chapter 8. A comparison of the response spectra for bedrock motion generated from a power spectrum are shown in Figure 5.2, where the motion are fitted using the time simulation curve as fitting curve to the target spectrum. The ground intensity in the power spectrum that gives the best fit to the target spectrum is $G_0 = 0.0016\,\mathrm{g}^2$ which is the value used for the input motion for the surface response analysis.

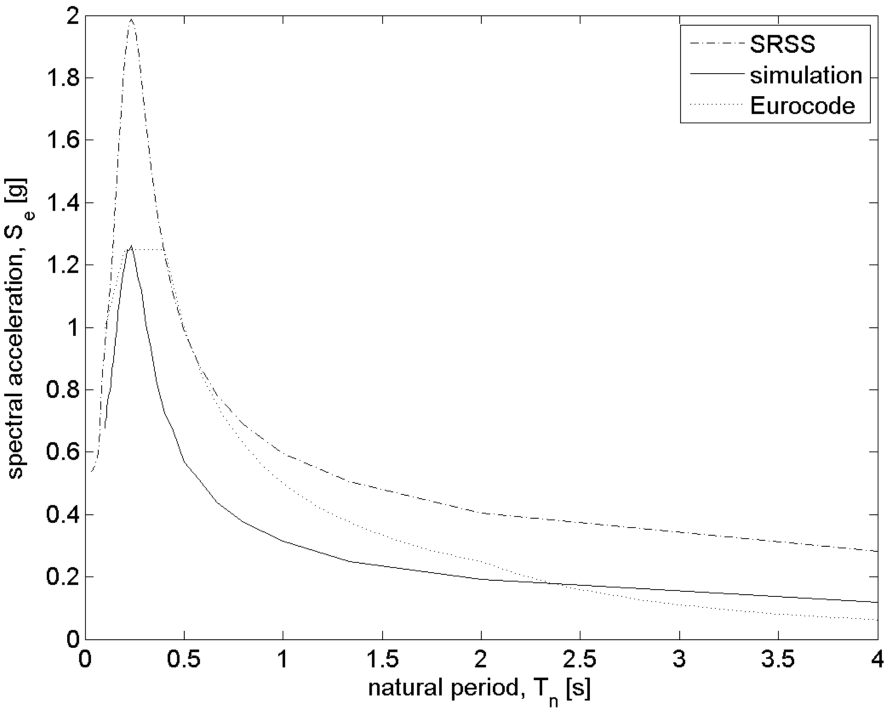

Figure 5.2. Response spectrum for bedrock motion. "SRSS" and "simulation" corresponds to generated response spectrum as described in Chapter 8. "Eurocode" is the target bedrock spectrum.

The power spectrum and the Fourier amplitude spectrum of the bedrock acceleration used in the equivalent linear analysis are given in Figure 5.3.

The bedrock motion described by a Fourier power spectrum needs assumptions of the phase spectrum in order to fully describe the time history of the motion. In the equivalent linear analyses using the bedrock motion described by the power spectrum assumptions of the phase spectrum are done after multiplication of the transfer function for the soil as described in Section 6.4.

An alternative approach is to assume a phase spectrum before the transmission through the soil layers and thereby give a fully described bedrock input motion. The phase spectrum could either be assumed uniform distributed and made to a transient time history by the procedure described in Section 5.3.1 or extracted from a time history for a recorded earthquake event.

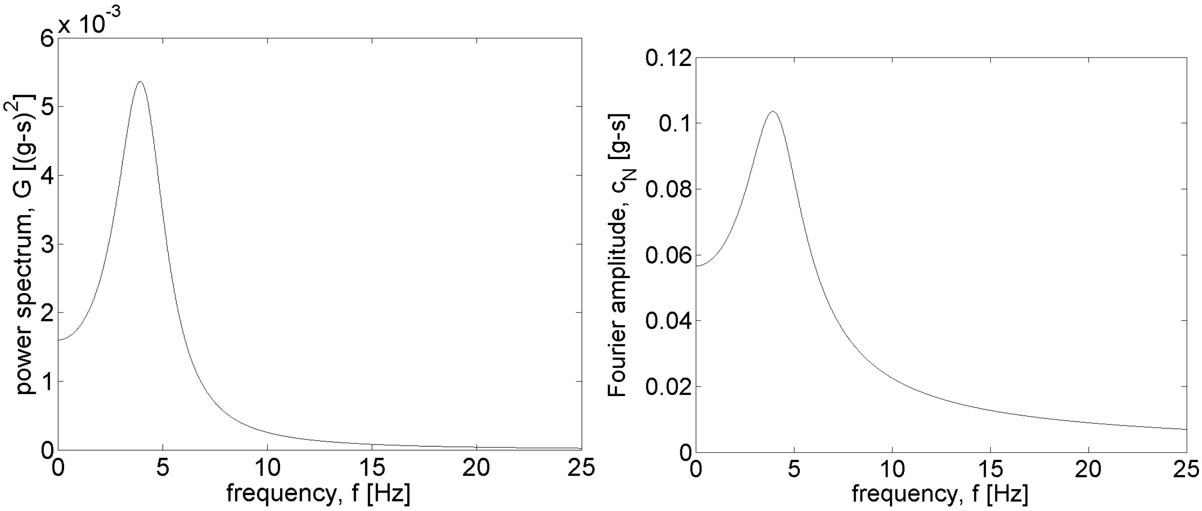

Figure 5.3. Input bedrock motion described by power and Fourier amplitude spectra.

5.3. Bedrock motion by time history

For the nonlinear analysis a velocity time series is needed. Two methods to find a time history is either by generating an artificially time history from an amplitude spectrum or by using a modified time history recorded from a past earthquake event. Both procedures are described here but for the nonlinear analysis the time history is found from a past earthquake event. In [EN1998:2003, p29] it is stated that at least 3 time histories must be used for the seismic analysis and if at least 7 time histories are used the response of the structure can be taken as the mean of the responses from the 7 time history analyses [EN1998:2003, p50]. In this project only one time history is used.

5.3.1. Artificially generated time history

An artificially generated time history can be generated on the basis of an amplitude spectrum by the following procedure. An illustration of the procedure is given in Figure 5.4.

First a phase spectrum of random uniform distributed phases are generated and combined with the known Fourier amplitude spectrum to give a stationary acceleration time history. The phase and amplitude spectra can either be combined by (8-14) in Section 8.2 or by taking the inverse FFT (Fast Fourier Transformation), see Section 5.4.

Next an envelope function is applied to the stationary time series to resemble the build-up and decay of a real earthquake motion. An envelope function only scales the amplitude of the time history so this procedure can not capture the nonstationary behaviour of the frequency contents which also is present in real earthquake motions.

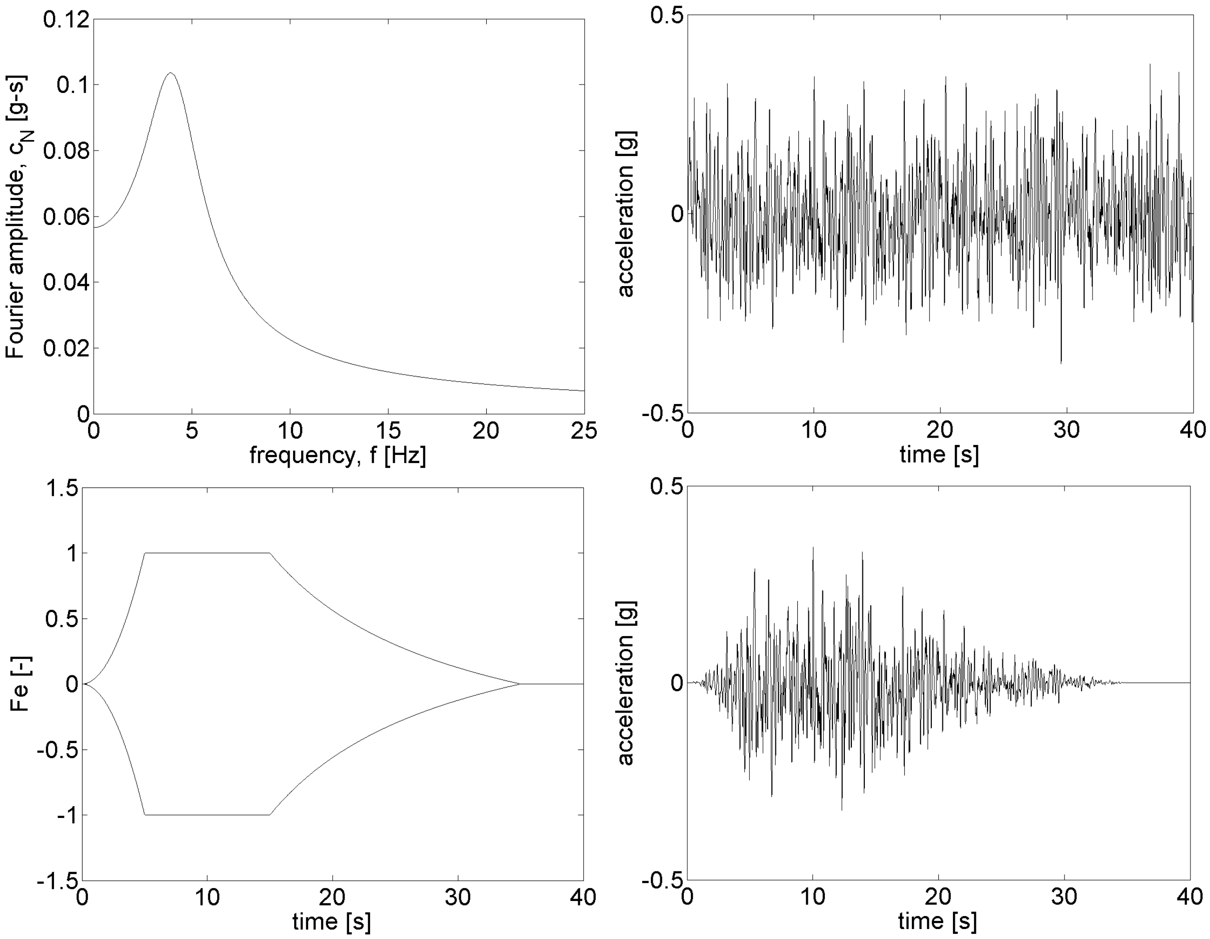

Figure 5.4. Illustration of artificially generated time history. Fourier amplitude spectrum (upper left), stationary time history (upper right), envelope function (lower left), nonstationary time history (lower right). The used parameter values are only chosen as example.

A problem with this method for time history generation is that the acceleration time history must be integrated to give a velocity time history which is needed in the nonlinear analysis. When this transformation from acceleration to velocity is performed a baseline error is introduced so the residual velocity is not equal to zero after the ground motion has subsided. An example of a velocity time history with baseline error is given in Figure 5.5.

A non-zero value of the velocity after the ground motion has ended is not physically meaningful so a baseline correction is needed in order to get a velocity time history with a residual velocity equal to zero. Such a correction is possible by modern data processing techniques but is not performed in this project [Kramer 1996, p62]. Another method to circumvent the baseline error is to generate the velocity time history directly from a velocity amplitude spectrum by the same procedure as the acceleration time history is generated by an acceleration amplitude spectrum. This method needs information of a velocity amplitude spectrum and since it most often is acceleration amplitude spectra that are specified this method is not used in this project.

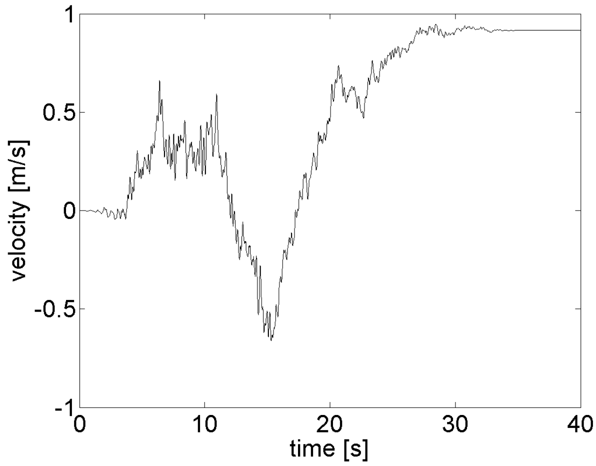

Figure 5.5. Velocity time history for the artificially generated time series.

By comparing the artificially generated velocity time history in Figure 5.5 with the recorded velocity time history in Figure 5.6, the problems with generating an artificial velocity time history is seen in that this gives a velocity time history without close resemblance to an actual velocity time history shown in Figure 5.6. Besides the baseline error, the artificially generated velocity time series also fails to describe the nonstationary behaviour of the frequency contents. In Figure 5.6 the velocity time series clearly shows a lower frequency for the decaying part of the time series (from 60 s to 90 s) which is not captures in the time series in Figure 5.5.

5.3.2. Modified time history records

Another method for getting time histories is by modification of recorded ground motions for past earthquake events. It is recommended that as many characteristics of the target ground motion is captured by the trial ground motion. The trial ground motion is the recorded time history used to simulate the wanted target earthquake. Of earthquake characteristics can be mentioned acceleration response spectrum, velocity response spectrum, duration but also fault and site characteristics such as fault type, distance to site, magnitude and soil type. It is generally accepted that a scaling of the magnitude can be done as long as the scaling factor is as close to 1 as possible and always between 0.25 and 4.0 [Kramer 1996, p340]. It is not recommended to scale the time scale since this also scales the frequency contents of the ground motion [Bray 2007b].

In this project only the target acceleration response spectrum is given, see Figure 5.1. Also a trial record corresponding to firm ground is recommended since the record must simulate bedrock motion. The chosen trial ground motion which has a matching response spectrum is a record from the Chi-Chi earthquake event in Taiwan. The record is from a site corresponding to firm ground and is the northern component of the record ID: P1450:TCU078-N [PEER 2008] and recorded with a sampling frequency of $f_s = 200$ Hz . The amplitude of the record is scaled by 1.3 to give the best fit.

The PEER database includes time histories of the velocity time histories where the records has been corrected for baseline error. In that way a velocity time history with residual velocity equal to zero is obtained from [PEER 2008] and thereafter scaled by the scaling factor 1.3 to give the time histories shown in Figure 5.6 where also the acceleration and displacement time histories are shown. The velocity time history in Figure 5.6 is used as bedrock input in the nonlinear analysis.

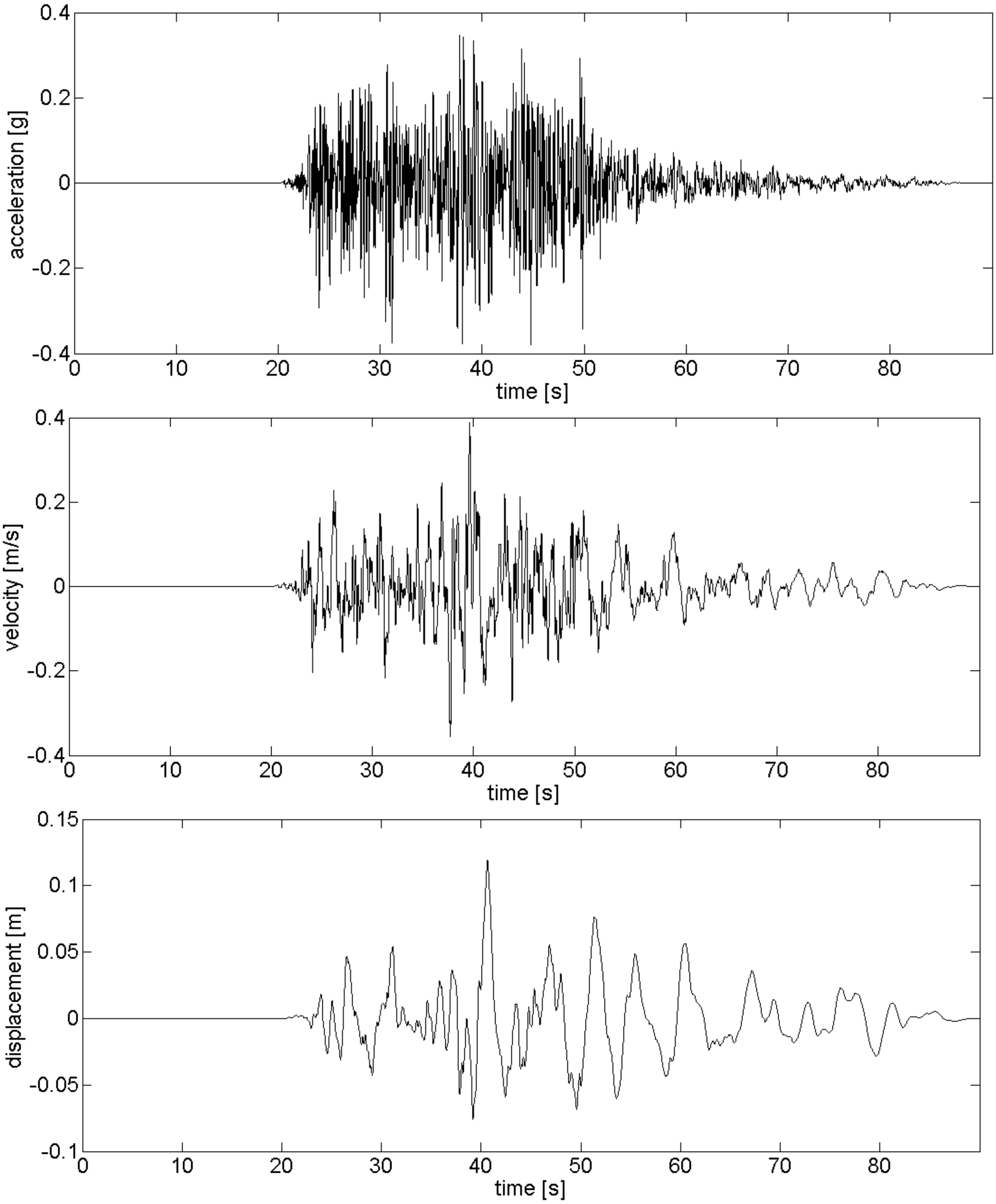

Figure 5.6. Scaled acceleration, velocity and displacement time histories for the used record from the Chi-Chi earthquake event.

In Figure 5.7 the target and trial response spectra are shown where the trial response spectrum is scaled by 1.3 to give a best fit to the target response spectrum. The response spectrum can be downloaded directly from the PEER database [PEER 2008] or can be calculated from the acceleration time history by the central difference method given in (7-12).

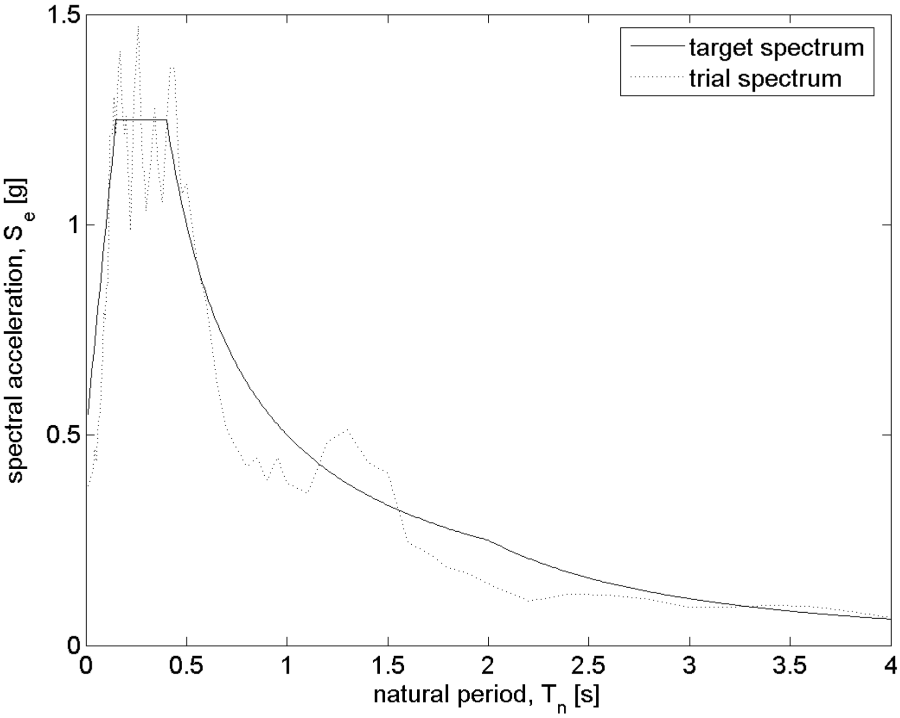

Figure 5.7. Target response spectrum and scaled trial response spectrum. Scaling factor is 1.3. 5 % damping.

5.4. Bedrock motion by Fourier series

The time histories found in Section 5.3 can be transformed to the frequency domain by using the theory of Fourier transformation. In this section it is done by the Fast Fourier Transformation (FFT), which has optimized the calculation speed of Fourier transformation. The transformation to Fourier series can be done for both acceleration, velocity and displacement time histories.

The sampling frequency for the time history is calculated as

$$f_s = \frac{1}{\Delta t} \tag{5-3}$$

where

f_s is the sampling frequency

Δt is the time step for the recorded time history

When taking the Fourier transform of a time history the maximum frequency which can be detected is the Nyquist frequency given as

$$f_{nyq} = \frac{f_s}{2} \tag{5-4}$$

where

f_{nyq} is the Nyquist frequency

The Fourier transformation is mirrored around the Nyquist frequency but at frequencies higher than f_{nyq} the values no longer gives a physical meaning.

The FFT algorithm is fastest when the number of data used is equal to a number where the *n*'th root is equal to 2, where *n* is a positive integer. Because of this, a number of trailing zeroes are added to the end of the recorded time series so the total number is equal to

$$N = 2^n > N_{recorded} \tag{5-5}$$

where

N is the total number of data points including trailing zeroes

n is a positive integer

$N_{recorded}$ is the number of recorded data points

The displacement time series from Figure 5.6 is shown in Figure 5.8 including trailing.

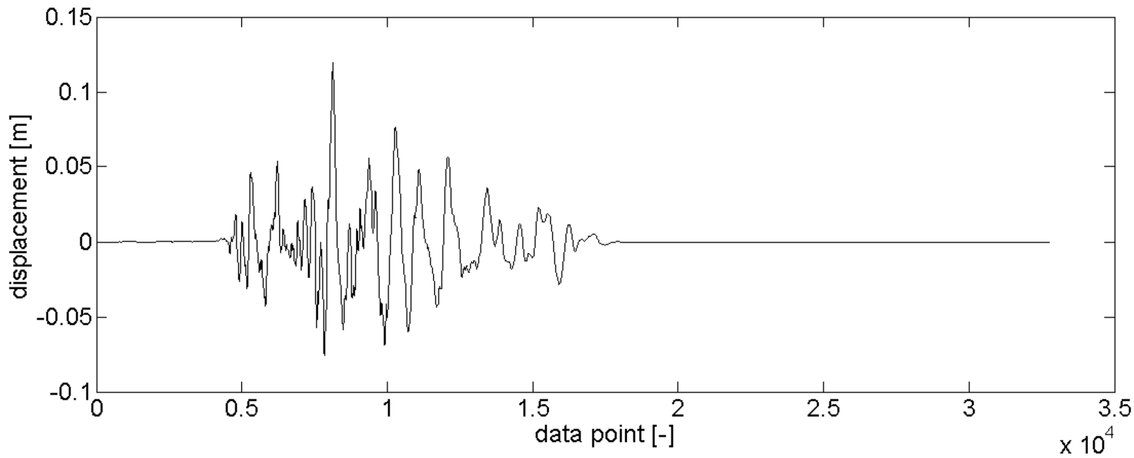

Figure 5.8. Displacement time history including trailing zeroes. Total number of points are 32768.

One of the concepts FFT is that it only can be done for periodic signals. This means that in the FFT algorithm the signal is treated as a periodic signal which repeats itself continuously as shown in Figure 5.9. By adding enough trailing zeroes it is assured that the response of the preceding sequence has no influence on the response of the succeeding sequence since the system again is at rest before the system is excited with the new input motion. Note that the periodic signal in Figure 5.9 is for the input motion and that the response motion first is at rest at a time after the input motion has stopped.

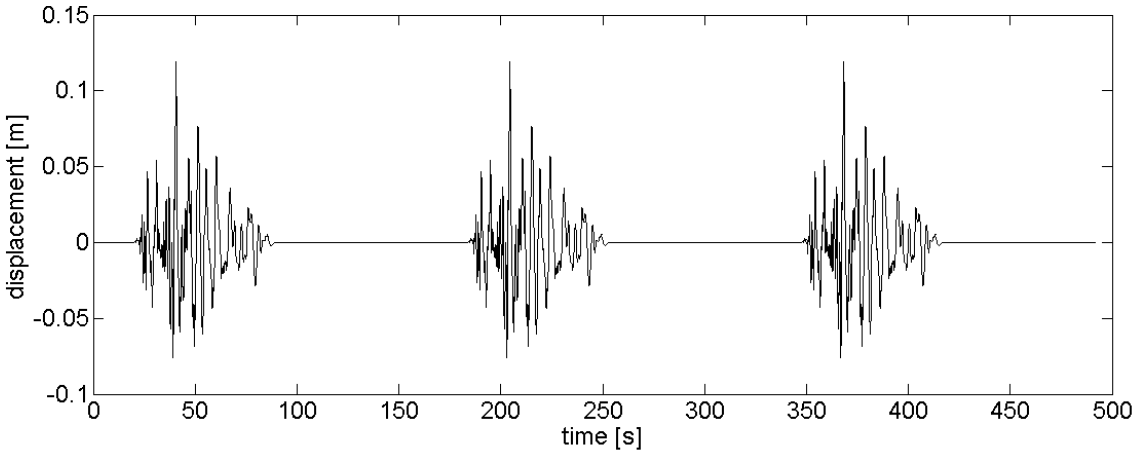

Figure 5.9. Periodic extension of the input signal.

The FFT algorithm is a built-in function in Matlab and in the discrete representation of the signal the Fourier series of the signal is given as

$$Y(f) = FFT\{y(t)\} \cdot \frac{1}{N} \text{ for } f = \left]0; f_s\right] \tag{5-6}$$

where

$Y(f)$	is the Fourier series of the signal as function of frequency
$y(t)$	is the time history of the signal as function of time
$FFT\{.\}$	is the FFT algorithm defined in Matlab
Δf	is the frequency step given as $\Delta f = \dfrac{f_s}{N}$

A single sided Fourier series is wanted so the frequencies above the Nyquist frequency are discarded. The single sided Fourier series is given as

$$Y_{ss}(f) = 2 \cdot FFT\{y(t)\} \cdot \frac{1}{N} \text{ for } f = \left]0; f_{nyq}\right] \tag{5-7}$$

where

$Y_{ss}(f)$ is the single sided Fourier series as function of frequency

The Fourier series is a set of complex numbers where both amplitude and phase spectra can be extracted. The Fourier amplitude spectrum is generated as

$$c(f) = abs\{Y_{ss}(f)\} \text{ for } f = \left]0; f_{nyq}\right] \tag{5-8}$$

where

$c(f)$ is the Fourier amplitude spectrum as function of frequency

In Figure 5.10 (left) the Fourier amplitude spectrum for the acceleration time series in Figure 5.8 is given. The spectrum is also given for a smoothed amplitude spectrum by averaging over intervals of 25 values Figure 5.10 (right). The amplitude is normalized so the generated amplitude spectra can be compared independent of the sample frequency.

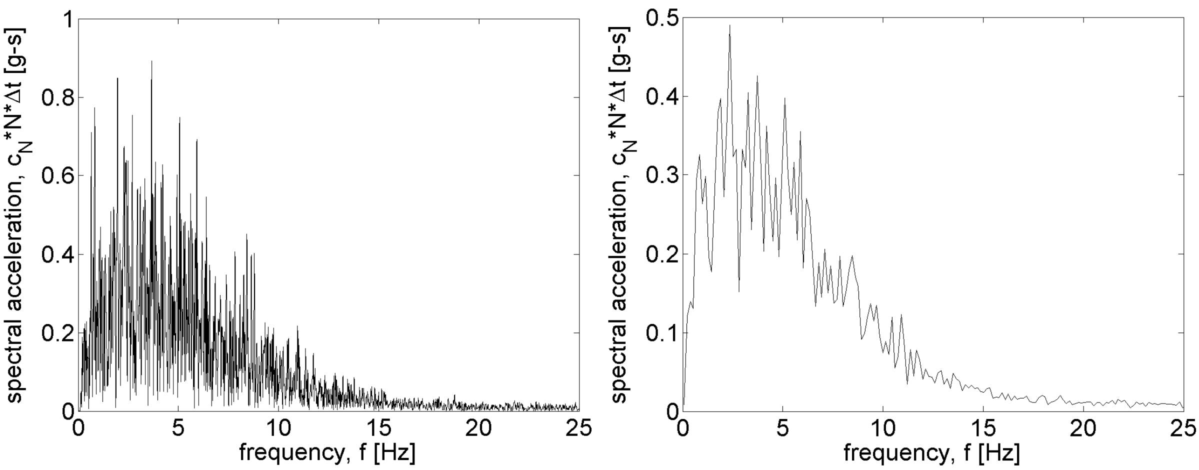

Figure 5.10. Fourier amplitude spectrum of acceleration for the time history given in Figure 5.6. Non-smoothed curve (left) and smoothed curve by averaging over intervals of 25 values (right). Sampling frequency is 200 Hz. Values between 25 Hz and the Nyquist frequency at 100 Hz are not shown due to negligible amplitudes in that interval.

6. Equivalent linear soil response

In this chapter the response of the soft soil is analysed in the frequency domain by use of the wave equation. The response is analysed for two types of input bedrock motions given as a power spectrum and a Fourier series as described in Section 5.2 and 5.4 respectively.

6.1. Dynamic soil properties

The soil properties have shown to vary with varying shear strain under dynamic loading. Under dynamic loading the stress strain behaviour is given as hysteresis loops where both energy dissipation and stiffness is varying with the magnitude of strain. The shear stiffness as a function of shear strain can be described in a simplified manner by use of a backbone curve, see Figure 6.1.

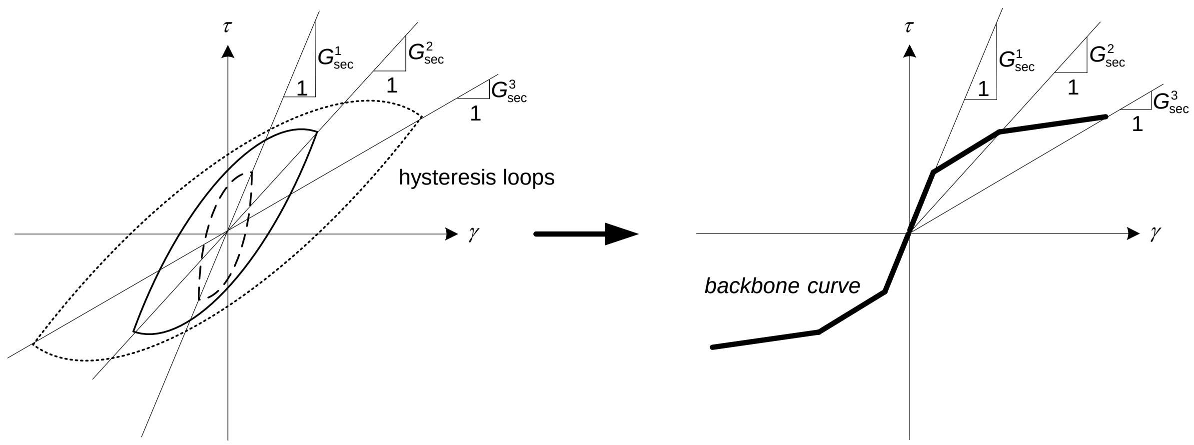

Figure 6.1. Hysteresis loops described by equivalent linear stiffness as the backbone curve.

Each soil type are assigned a curve with the shear modulus ratio as a function of shear strain. The shear modulus ratio is given as the ratio between the reduced shear modulus given from the backbone curve and the maximum shear modulus given as the shear stiffness corresponding to infinitesimal shear strain. The terms degraded and nondegraded stiffness are used for the reduced and the maximum stiffness respectively.

The maximum shear modulus is calculated by (6-1) with the measured shear wave velocities in the soil profile in Figure 2.7.

The relationship between shear wave velocity and shear modulus is given as

$$G = \rho V_s^2 \tag{6-1}$$

where

G is the shear stiffness

ρ is the density

V_s is the shear wave velocity

[Kramer 1996, p232]

Curves for the shear modulus ratio for each soil type are shown in Figure 6.2 (left).

The energy dissipation is given by introducing an equivalent viscous damping ratio which also varies with shear strain. The application of an equivalent viscous damping ratio is discussed further in Section 0. The equivalent viscous damping ratio curves are shown in Figure 6.2 (right).

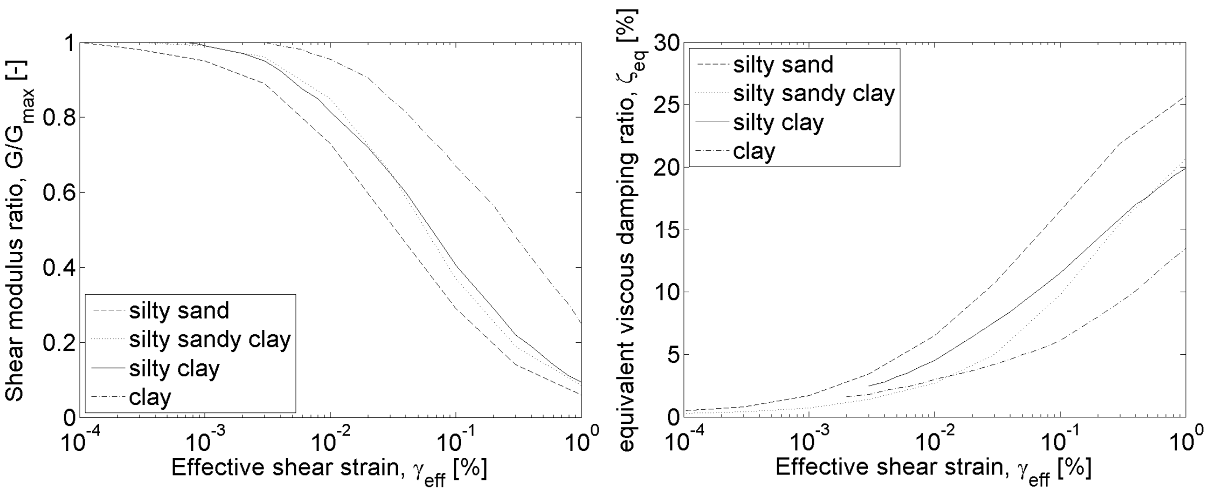

Figure 6.2. Shear modulus ratio curves (left) and equivalent damping ratio curves (right) for each soil type. For γ_{eff} see Section 6.4.2.

The used curves are found from published test results of various soils and the names of the used curves are listed in Table 6.1.

Table 6.1. Used reduction curves for shear modulus and damping ratio. [Bray 2007].

Soil type	Shear modulus curve	Damping ratio curve
1	Seed & Idriss, 1970, mean	Seed & Idriss, 1970, mean
2	Seed & Idriss, 1970, upper	Seed & Idriss, 1970, lower
3	Vucetic & Dobry, 1991, PI=15	Vucetic & Dobry, 1991, PI=15
4	Vucetic & Dobry, 1991, PI=50	Vucetic & Dobry, 1991, PI=50

6.2. Application of the wave equation

The equation of motion for vertically propagation s-waves are given as

$$\rho \frac{\partial^2 u}{\partial t^2} = \frac{\partial \tau}{\partial z} \tag{6-2}$$

where

ρ is the unit density

u is the displacement

t is the time

τ is the shear stress

z is the depth

[Kramer 1996, p177]

By using a Kelvin-Voigt solid the resistance to shearing consist of an elastic part and a viscous part. The stress – strain relationship for a Kelvin-Voigt solid is given as

$$\begin{aligned} \tau &= G\gamma + c\frac{\partial \gamma}{\partial t} \\ \tau &= G\frac{\partial u}{\partial z} + c\frac{\partial^2 u}{\partial z \partial t} \end{aligned} \tag{6-3}$$

where

G is the shear modulus

c is the viscous damping coefficient

γ is given as $\frac{\partial u}{\partial z}$ as derived in (6-28)

[Kramer 1996, p175]

By inserting (6-3) in (6-2) the wave equation for a Kelvin-Voigt solid can then be expressed as

$$\rho \frac{\partial^2 u}{\partial t^2} = G\frac{\partial^2 u}{\partial z^2} + c\frac{\partial^3 u}{\partial z^2 \partial t} \tag{6-4}$$

For soils it has been shown that viscous damping is a poor assumption and that damping is better estimated as rate-independent damping, sometimes also called hysteretic damping. Therefore a modification of damping term in the wave equation as given in (6-4) is discussed in the following section.

6.2.1. Viscous damping

First the damping term is discussed for the case with viscous damping and thereafter a modification is explained which gives an equivalent viscous damping.

The equation of motion for a damped single degree of freedom system excited with a harmonic vibration is given as

$$f_I + f_D + f_S = p_0 \sin(\omega t) \tag{6-5}$$

where

f_I is the inertia force

f_D is the damping force

f_S is the elastic resisting force

p_0 is the amplitude of the external force

ω is the forcing frequency

[Chopra 2007, p72]

For a viscous damped system the damping force is given as

$$f_D = c\dot{u} \tag{6-6}$$

where

$\dot{u}$ is the velocity

[Chopra 2007, p13]

The solution to (6-5) can be shown in a force-displacement diagram which gives a hysteresis loop as shown in Figure 6.3.

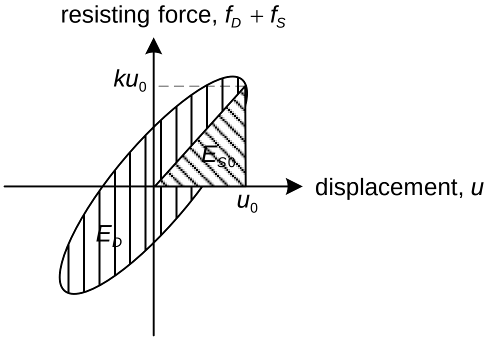

Figure 6.3. A hysteresis loop with definition of energy loss for a cycle.

The area encircled by the loop, as indicated in Figure 6.3, is the energy dissipation for one cycle and is for a viscous damped system given as

$$E_{D,\text{viscous}} = \pi c \omega {u_0}^2 \tag{6-7}$$

where

E_D is the dissipated energy in one cycle

u_0 is the maximum value of the displacement

[Chopra 2007, p99]

The energy in (6-7) for a viscous damped system can be rewritten by using the relation between the viscous damping coefficient and the viscous damping ratio and the value of the maximum strain energy both given in (6-8) as

$$\begin{aligned} c &= 2\zeta m\omega_n = 2\zeta \frac{k}{\omega_n} \\ E_{S0} &= \tfrac{1}{2} k {u_0}^2 \end{aligned} \tag{6-8}$$

where

ζ is the viscous damping ratio

E_{S0} is the maximum strain energy as shown in Figure 6.3

k is the system stiffness

m is the mass of the system

ω_n is the natural frequency of the system

[Chopra 2007, p48,102]

With the relations given in (6-8) the dissipated energy in (6-7) can be written as

$$E_{D,\text{viscous}} = 4\pi\zeta \frac{\omega}{\omega_n} E_{S0} \tag{6-9}$$

It is seen that the energy dissipation for a viscous damped system is proportional to the forcing frequency.

6.2.2. Rate independent damping

To modify the above procedure to account for rate independent damping the damping term in (6-6) is redefined as

$$f_D = \frac{\eta k}{\omega}\dot{u} \tag{6-10}$$

where

η is a damping coefficient for rate independent damping

[Chopra 2007, p106]

By replacing c with the term from (6-10) and inserting this in (6-7) the energy dissipation is expressed as

$$\begin{aligned} E_{D,\text{rate independent}} &= \pi\eta k u_0^2 \\ E_{D,\text{rate independent}} &= 2\pi\eta E_{S0} \end{aligned} \tag{6-11}$$

[Chopra 2007, p106]

It is seen that the energy dissipation for a rate independent damped system now is independent of the forcing frequency.

The energy dissipation for viscous and rate independent damping as a function of the forcing frequency are illustrated in Figure 6.4.

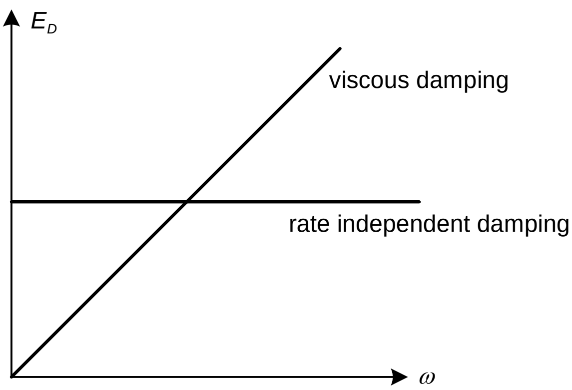

Figure 6.4. Energy dissipation for viscous and rate independent damping as a function of forcing frequency.

6.2.3. Equivalent viscous damping

For a structure which is not viscous damped the energy dissipated in one cycle is still given as the area, E_D, enclosed by the hysteresis loop. Therefore an equivalent viscous damping ratio can be found by equating E_D for the non-viscously damped system with the energy term for the viscous damped system as given in (6-9). This is done for the case with $\omega = \omega_n$ since the damping effect is most sensitive at this value.

$$E_D = E_{D,\text{viscous}}$$
$$E_D = 4\pi\zeta_{eq}\frac{\omega}{\omega_n}E_{S0} \tag{6-12}$$
$$\zeta_{eq} = \frac{1}{4\pi}\frac{E_D}{E_{S0}}$$

where

ζ_{eq} is the equivalent viscous damping ratio

[Chopra 2007, p103-104]

By inserting the term for the energy dissipation for rate independent damping the relation between equivalent viscous damping ratio and the damping coefficient η is given as

$$\zeta_{eq} = \frac{1}{4\pi}\frac{E_D}{E_{S0}}$$
$$\zeta_{eq} = \frac{1}{4\pi}\frac{2\pi\eta E_{S0}}{E_{S0}} \tag{6-13}$$
$$\zeta_{eq} = \frac{\eta}{2}$$

[Chopra 2007, p107]

With the relation between the damping coefficient η and the equivalent damping ratio ζ_{eq} an equivalent viscous damped system can be defined by the wave equation in (6-4) with c replaced by

$$c = \frac{\eta k}{\omega} = \frac{2k}{\omega}\zeta_{eq} \tag{6-14}$$

The wave equation can then by applied as if it was a viscous damped system but with the damping coefficient c replaced by (6-14). The system stiffness used in the wave equation is given as the shear modulus which leads to the modified wave equation given as

$$\rho\frac{\partial^2 u}{\partial t^2} = G\frac{\partial^2 u}{\partial z^2} + G\frac{2\zeta_{eq}}{\omega}\frac{\partial^3 u}{\partial z^2 \partial t} \tag{6-15}$$

6.3. Solution to the wave equation

By assuming harmonic waves the displacement can be written as

$$u(z,t) = U(z)e^{i\omega t} \tag{6-16}$$

By insertion of (6-16) in (6-15) the wave equation can be rewritten as

$$\begin{aligned}
-\rho\omega^2 U &= G\frac{d^2U}{dz^2} + i2G\zeta_{eq}\frac{d^2U}{dz^2} \\
-\rho\omega^2 U &= G\left(1+2i\zeta_{eq}\right)\frac{d^2U}{dz^2} \\
-\rho\omega^2 U &= G^*\frac{d^2U}{dz^2}, \qquad G^* = G(1+2i\zeta_{eq})
\end{aligned} \tag{6-17}$$

where

G^* is the complex shear modulus

The solution to (6-17) is given as

$$u(z,t) = Ae^{i(\omega t + k^* z)} + Be^{i(\omega t - k^* z)} \tag{6-18}$$

where

k^* is the complex wave number defined as $k^* = \omega\sqrt{\frac{\rho}{G^*}}$

A,B are integration constants describing the amplitude of the upward- and downward travelling wave respectively

[Kramer 1996, p177]

6.3.1. Application to multilayered soil

In the following determination of *A* and *B* it is assumed that the bedrock is modelled as elastic rock with parameters as given in Section 2.4 and damping in the soil layers are included. To include the damping and stiffness dependence of strain the soil is divided into a series of sublayers where the strain is assumed constant over the thickness of each sublayer and only a function of time.

The analysis is done by using the wave equation which is an analytical solution so the only requirement of the discretization is from the assumption that the strain is constant over the thickness of a sublayer. The discretization of the soil must be fine enough to describe the altered stiffness and damping throughout the soil types due to difference in maximum strain. Therefore the finest discretization is needed for the depth where the strain difference between sublayers are largest.

The sublayer thickness for each soil type are given in Table 6.2. Note that a finer subdivision is made for the soil types with larger strain variation, which is the upper soil types.

Table 6.2. Sublayer thickness for each soil type. Soil type refers to Figure 2.7.

Soil type	Sublayer thickness [m]
1	0.5
2	1
3	2
4	3

Due to the multilayered soil the depth z in (6-18) must be taken as the local depth corresponding to the depth from the top of the examined layer. By using that both displacements and shear stresses must be compatible in adjacent layer boundaries the relations between coefficients A and B for different layers can be expressed as

$$\begin{aligned} A_{m+1}(\omega) &= \tfrac{1}{2} A_m \left(1+\alpha_m^*\right) e^{ik_m^* h_m} + \tfrac{1}{2} B_m \left(1-\alpha_m^*\right) e^{-ik_m^* h_m} \\ B_{m+1}(\omega) &= \tfrac{1}{2} A_m \left(1-\alpha_m^*\right) e^{ik_m^* h_m} + \tfrac{1}{2} B_m \left(1+\alpha_m^*\right) e^{-ik_m^* h_m} \end{aligned} \tag{6-19}$$

where

α^* is the complex impedance ratio between layer m and m+1 given as (6-22) with complex values G^* and k^*

m is the layer index with 1 being the top layer

[Kramer 1996, p269]

The complex impedance ratio is derived from the definition of mechanical impedance, which is given as the resulting particle velocity in a medium generated from a unit force applied at the surface of the medium. For an analysis with only s-waves the mechanical impedance is defined as

$$Z = \rho V_s \tag{6-20}$$

where

Z is the mechanical impedance

V_s is the shear wave velocity

[Andersen 2006, p14]

The mechanical impedance ratio can then be rewritten by using the definitions of the wave number k from (6-18) and shear wave velocity V_s from (6-1)

$$\begin{aligned} Z &= \rho\sqrt{\frac{G}{\rho}} = \sqrt{\rho G} \\ Z &= \sqrt{\left(\frac{k}{\omega}\right)^2 G^2} = \frac{kG}{\omega} \end{aligned} \tag{6-21}$$

The impedance ratio can then be written as (6-22) which is used in (6-19) where the parameters consist of complex values

$$\alpha_m(\omega) = \frac{Z_m}{Z_{m+1}}$$
$$\alpha_m(\omega) = \frac{\frac{k_m G_m}{\omega}}{\frac{k_{m+1} G_{m+1}}{\omega}} \tag{6-22}$$
$$\alpha_m(\omega) = \frac{k_m G_m}{k_{m+1} G_{m+1}}$$

Since it is known that the shear stress at the surface must equal zero it can be shown that $A_1 = B_1$. Then the relations in (6-19) can be expressed as (6-23) where it has been exploited that $A_1 = B_1$ and rearranged since it for this analysis is the input bedrock motion A_N which is known

$$\begin{aligned} A_m(\omega) &= a_m \mathrm{A}_1 \Rightarrow A_m = A_N \frac{a_m}{a_N} \\ B_m(\omega) &= b_m \mathrm{B}_1 \Rightarrow B_m = A_N \frac{b_m}{a_N} \end{aligned} \tag{6-23}$$

By use of (6-19) a_m and b_m can be expressed as

$$a_m(\omega) = c_{m-1} a_{m-1} + d_{m-1} b_{m-1}$$
$$b_m(\omega) = e_{m-1} a_{m-1} + f_{m-1} b_{m-1}$$

where

$$\begin{aligned} \mathrm{c}_m(\omega) &= \tfrac{1}{2}(1+\alpha_m^*)e^{ik_m^* h_m} \\ d_m(\omega) &= \tfrac{1}{2}(1-\alpha_m^*)e^{-ik_m^* h_m} \\ e_m(\omega) &= \tfrac{1}{2}(1-\alpha_m^*)e^{ik_m^* h_m} \\ f_m(\omega) &= \tfrac{1}{2}(1+\alpha_m^*)e^{-ik_m^* h_m} \end{aligned} \tag{6-24}$$

From (6-24) it is seen that all the coefficients a_m and b_m for $m = [2;N]$ can be found by forward iteration when it from (6-23) is seen that $a_1 = b_1 = 1$.

6.4. Solution for power spectrum bedrock input

The following analysis is for the case when the input bedrock motion used for the equivalent linear analysis is described as a power spectrum as discussed in Section 5.2, where the power spectrum given as a Kanai-Tajimi power spectrum is used to create a Fourier amplitude spectrum.

The problem with a power spectrum or Fourier amplitude spectrum is that they do not fully describe the time history of the input signal since a phase spectrum also is needed. Therefore this method includes assumptions about the length of the signal and the distribution of phases as described later in this section.

6.4.1. Ground displacement amplitude

To get the quantity of the displacement amplitude input A_N as needed in (6-23) the Fourier acceleration amplitudes can be rewritten to Fourier displacement amplitudes as follows.

The displacement field defined by a harmonic wave can be expressed as stated in(6-16). By differentiation with respect to time, the displacement can be expressed as a function of the acceleration

$$\begin{aligned} u(z,t) &= U(z)e^{i\omega t} \\ \ddot{u}(z,t) &= i^2\omega^2 u(z,t) \\ u(z,t) &= -\frac{\ddot{u}(z,t)}{\omega^2} \end{aligned} \tag{6-25}$$

When combining (5-2) and (6-25) the displacement amplitude described as a function of the power spectrum is given as

$$\begin{aligned} A_N(\omega) &= \frac{c(\omega)}{\omega^2} \\ A_N(\omega) &= \frac{\sqrt{2G(\omega)}}{\omega^2} \end{aligned} \tag{6-26}$$

where

$A_N(\omega)$ is the displacement amplitude for a given frequency

6.4.2. Shear strain

The shear strain needed for the reduction curves described in Section 6.1 is the effective shear strain, γ_{eff}. The effective shear strain is calculated as a percentage of the maximal experienced shear strain during the earthquake loading and is often set to $\gamma_{eff} = 0.65\gamma_{max}$ [Kramer 1996, p271]. A time series of the effective shear strain is shown in Figure 6.6.

The shear strain is for this wave equation problem defined as the displacement differentiated with respect to depth. This is seen from the definition of shear strain and its relation to the strain tensor as shown in the following. For a one dimensional response analysis an infinitesimal element deformed by shear strain is given as shown in Figure 6.5.

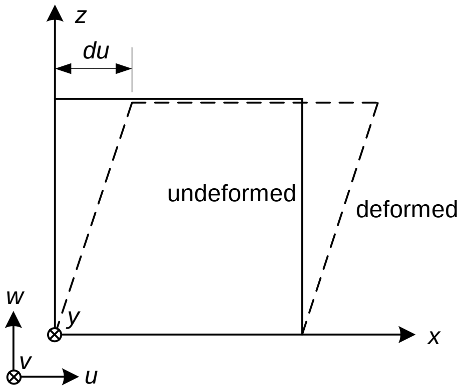

Figure 6.5. Shear deformation in one dimension.

By using the definition of infinitesimal strain tensors and that for the one dimensional problem as sketched in Figure 6.5 $v = w = 0$ the strain tensors defining the shear are given as

$$\begin{aligned} \varepsilon_{xz} &= \frac{1}{2}\left(\frac{\partial u}{\partial z} + \frac{\partial w}{\partial x}\right) = \frac{1}{2}\frac{\partial u}{\partial z} \\ \varepsilon_{xy} &= \varepsilon_{yz} = 0 \end{aligned} \tag{6-27}$$

The shear strain is defined as the following

$$\begin{aligned} \gamma = \gamma_{xz} &= 2\varepsilon_{xz} = \frac{\partial u}{\partial z} \\ \gamma_{xy} &= \gamma_{yz} = 0 \end{aligned} \tag{6-28}$$

The index on the shear strain is ignored in the following, since only one value is different from zero.

By differentiation of (6-18) the shear strain is given as

$$\gamma(\omega) = \frac{\partial u}{\partial z} = ik^*\left(Ae^{i(\omega t + k^* z)} - Be^{i(\omega t - k^* z)}\right) \tag{6-29}$$

The maximum shear strain in the top of each layer is found by setting $z = 0$ and taking the amplitude in (6-29) which gives

$$\gamma_{\max}(\omega) = |k^*(A - B)| \tag{6-30}$$

In the discretized calculation the strain contribution from each frequency step is added by the square root of the sum of squares (SRSS). This rule is used because the phases in the spectrum are unknown and assumed uncorrelated which gives a total strain for the top of each sublayer of

$$\gamma_{\max,total} = \sqrt{\sum_{i=1}^{I} \gamma_{\max}(\omega_i)^2 \Delta\omega} \tag{6-31}$$

where

i	is indicating shear strain contribution from frequency step i
I	is the total number of frequency intervals
$\Delta\omega$	is the frequency discretization

6.4.3. Effective shear strain

To illustrate the concept of an effective shear strain two strain time series are described in the following. Both a strain time series simulating the real time history and a time series consisting of a harmonic varying strain corresponding to the effective strain.

The real strain time history is simulated by generating a Fourier series with the discretized strain amplitudes and a set of random generated and uniformly distributed phase angles, δ_i. The strain time series for a given sublayer is then given as

$$\gamma(t) = \sum_{i=1}^{I} \gamma_{\max}(\omega_i)\cos(\omega_i t + \delta_i) \tag{6-32}$$

In Figure 6.6 a time series of the shear strain is shown for a sublayer at a depth of 10 m. In the same figure a harmonic wave corresponding to the effective shear strain $\gamma_{eff}(t) = \gamma_{eff}\sin(\omega t)$ is given. The amplitude γ_{eff} is set to $0.65 \cdot \max(\gamma(t))$ as described earlier in this section and the frequency ω is set to 5 rad/s.

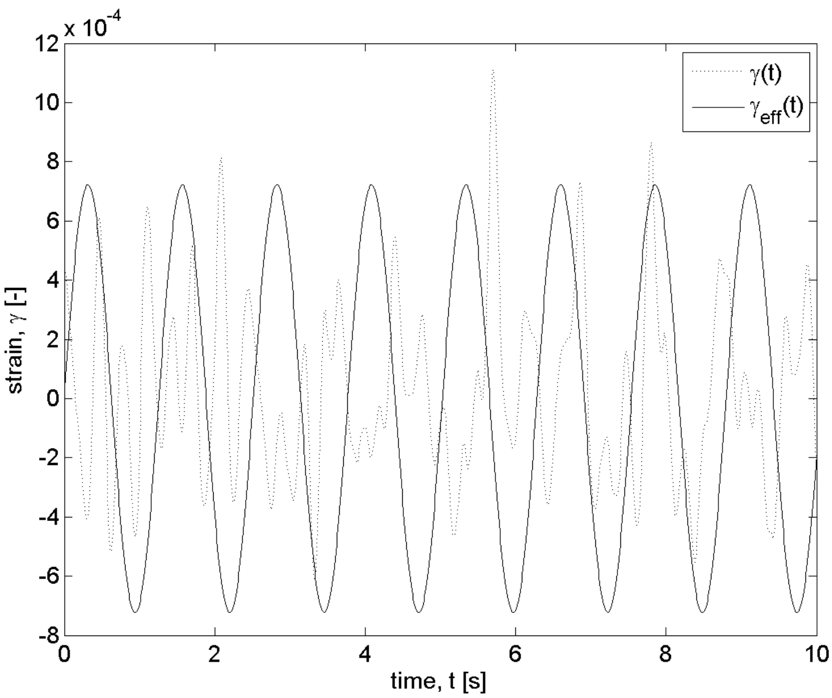

Figure 6.6. Strain time series for the sublayer at a depth of 10 m.

The harmonic wave for $\gamma_{eff}(t)$ can be seen as the time series used to get the dynamic soil parameters as described in Section 6.1.

6.4.4. Iteration procedure

The iteration procedure for the equivalent linear analysis using a power spectrum input is as follows

5) Use power spectrum as bedrock acceleration input
6) Guess initial effective shear strain values for each layer
7) Get degraded dynamic soil properties corresponding to the effective shear strain values
8) Calculate coefficients a_i and b_i
9) Calculate A_i and B_i values
10) Calculate effective shear strain
11) Unless convergence is achieved start next iteration from 3)

6.4.5. Results

From the described procedure above for the equivalent linear analysis using a power spectrum as bedrock input the following results are found.

Convergence of strain

As a control that the iteration procedure is converging the strain distribution for each iteration are recorded. The strain distribution for chosen iteration loops are shown in Figure 6.7 where it is seen that there is little change in the strain distribution from iteration #7 to iteration #10.

The shifts in shear strain at certain depths in Figure 6.7 corresponds to a shift in stiffness which happens at soil type boundaries. Since the stress must be continuous at these boundaries the shift in stiffness results in a shift in shear strain.

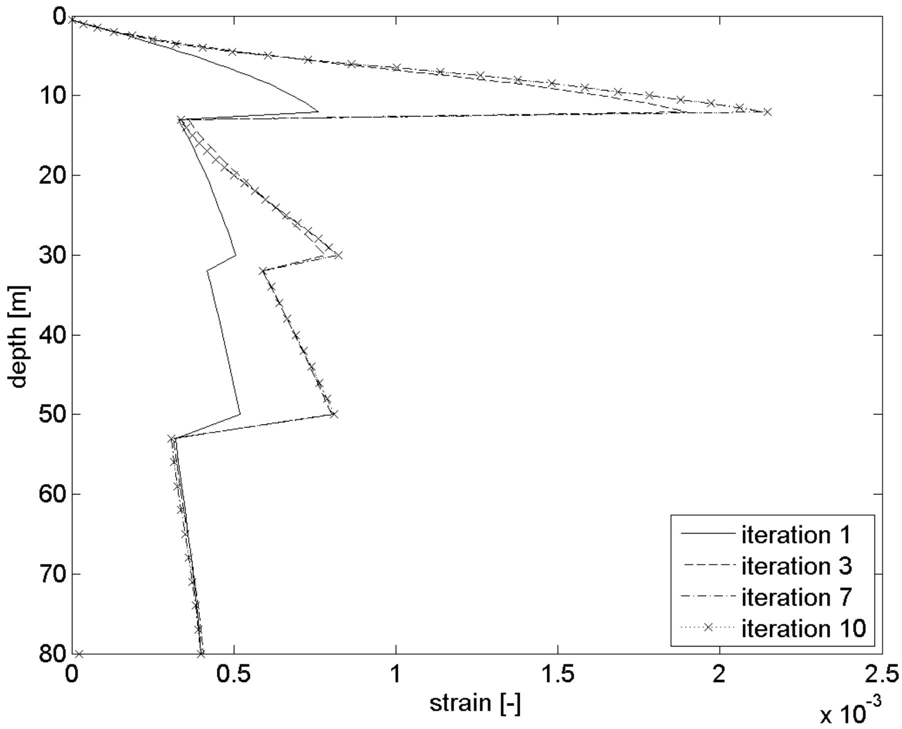

Figure 6.7. Maximum strain for chosen iteration loops.

To give a clearer picture of the change in the maximum strain from one iteration to the next the following quantity is defined

$$\gamma_{error,i} = \frac{1}{N}\sum_{j=1}^{N} abs\left(\frac{\gamma_{\max,i}^{j} - \gamma_{\max,i-1}^{j}}{\gamma_{\max,i}^{j}}\right) \tag{6-33}$$

where

$\gamma_{error,i}$ is the sum of the maximum strain difference between iteration i and i-1 for all sublayers

$\gamma_{\max,i}^{j}$ is the maximum strain of sublayer j for iteration i

N is the total number of sublayers

By plotting the sum of the strain difference for each iteration it is again seen from Figure 6.8 that with 10 iterations the strain distribution is converged.

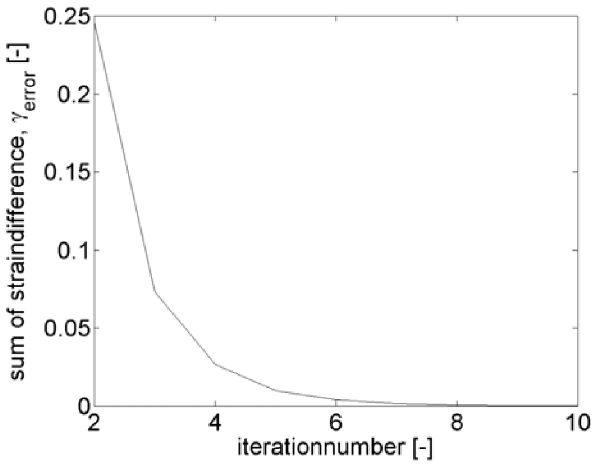

Figure 6.8. Sum of strain error as defined in (6-33).

Transfer function

The transfer function relates the motion at the surface with the bedrock motion and is given as the following

$$F_{iN}(\omega) = \frac{\langle \ddot{u}_i \rangle}{\langle \ddot{u}_N \rangle} \tag{6-34}$$

where

$F_{iN}(\omega)$	is the transfer function between bedrock and sublayer i as a function of frequency
$\langle \ddot{u}_i \rangle$	is the complex amplitude of the acceleration at the top of layer i

The amplitude of the acceleration of layer i is found from (6-18) with z = 0, since the acceleration is needed for the top of the layer. By using (6-23) and the fact that $A_1 = B_1$ the amplitude is given in (6-35)

$$\begin{aligned} u_i &= \Re e\{(A_i + B_i)e^{i\omega t}\} \\ \ddot{u}_i &= \Re e\{-\omega^2(A_i + B_i)e^{i\omega t}\} \\ \ddot{u}_i &= \Re e\{-\omega^2(a_i + b_i)A_1 e^{i\omega t}\} \\ \langle \ddot{u}_i \rangle &= \omega^2(a_i + b_i)A_1 \end{aligned} \tag{6-35}$$

Now the transfer function between sublayer i and bedrock is given as

$$\begin{aligned} F_{iN}(\omega) &= \frac{\langle \ddot{u}_i \rangle}{\langle \ddot{u}_N \rangle} = \frac{\omega^2(a_i + b_i)A_1}{\omega^2(a_N + b_N)A_1} \\ F_{iN}(\omega) &= \frac{a_i + b_i}{a_N + b_N} \end{aligned} \tag{6-36}$$

In Figure 6.9 the transfer function between bedrock and surface motion is shown as function of frequency for the degraded case where both stiffness and damping are functions of effective strain. As a comparison a result for a nondegraded case where it is assumed than the stiffness correspond to infinitesimal shear and that the damping ratio has a constant value of 5 % and that both stiffness and damping is unaffected of effective strain. The resulting dynamic soil parameters for both the degraded and nondegraded case are shown in Figure 6.11.

By comparing the degraded and nondegraded transfer functions it is seen that when degradation is included the peaks shifts towards lower frequencies corresponding to a softening of the soil. Also the peaks are lower corresponding to an increase in damping for the degraded analysis.

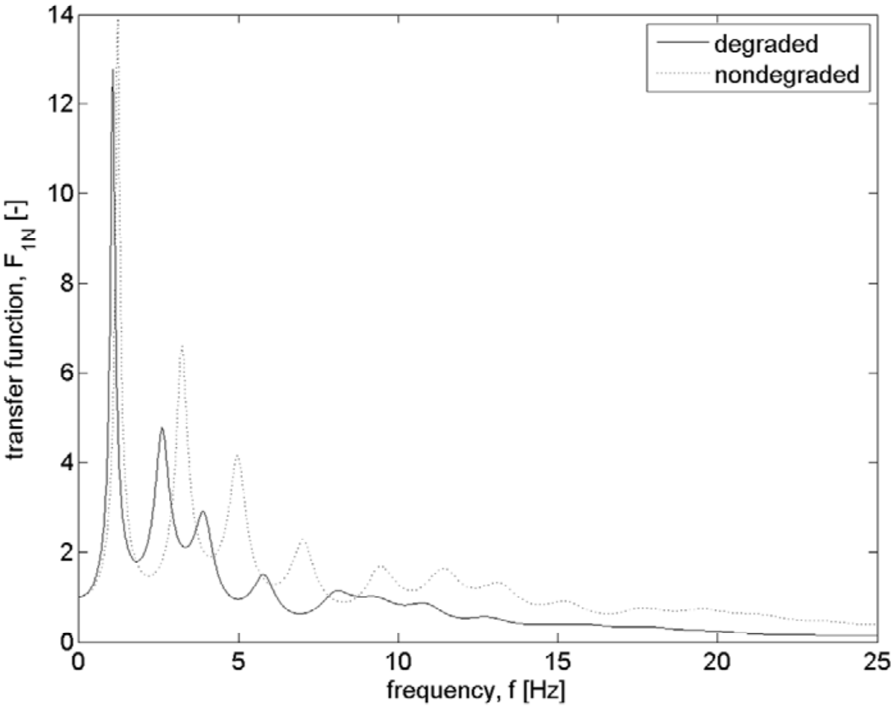

Figure 6.9. Transfer function between bedrock and surface motion.

Surface motion

The surface motion is calculated as the product of the transfer function and the bedrock Fourier amplitude spectrum as given in (6-37)

$$c_1 = F_{1N} c_N \tag{6-37}$$

where

c_1 is the surface Fourier amplitude spectrum

c_N is the bedrock Fourier amplitude spectrum as defined in Section 5.2

The Fourier amplitude spectrum for the surface is shown for both the degraded and nondegraded analyses. Again the degraded response gives lower amplitudes with peaks shifted towards lower frequencies.

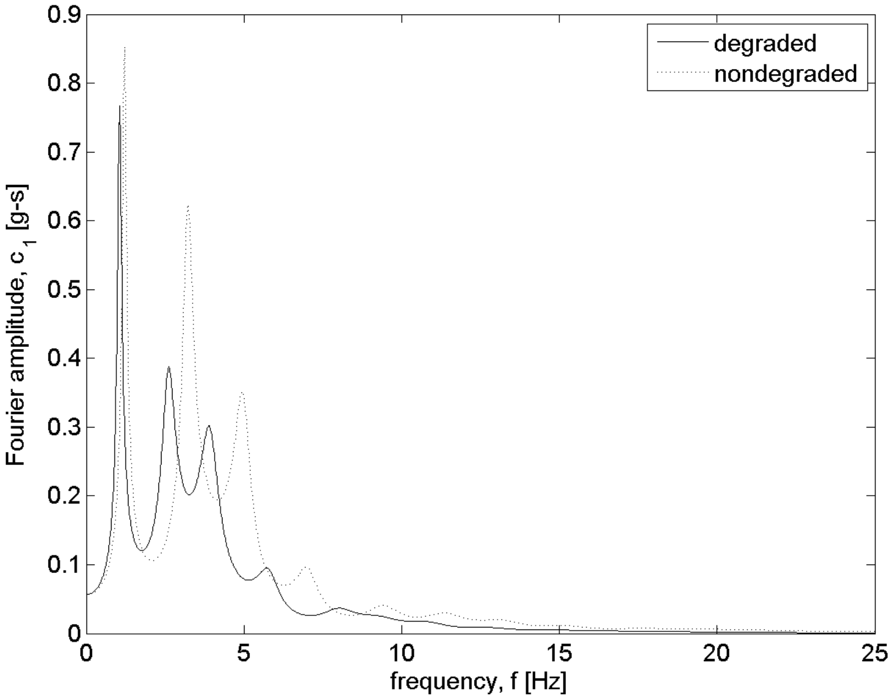

Figure 6.10. Surface Fourier amplitude spectrum.

Degraded soil parameters

A comparison between the degraded and nondegraded soil parameters are shown in Figure 6.11. It is seen that the shear wave velocity as expected is decreased in the degraded case and that the highest reduction is in the layers experiencing the highest maximum shear strain. The damping is for the most part increased for the degraded case and for large strains this increase is by a factor larger than three.

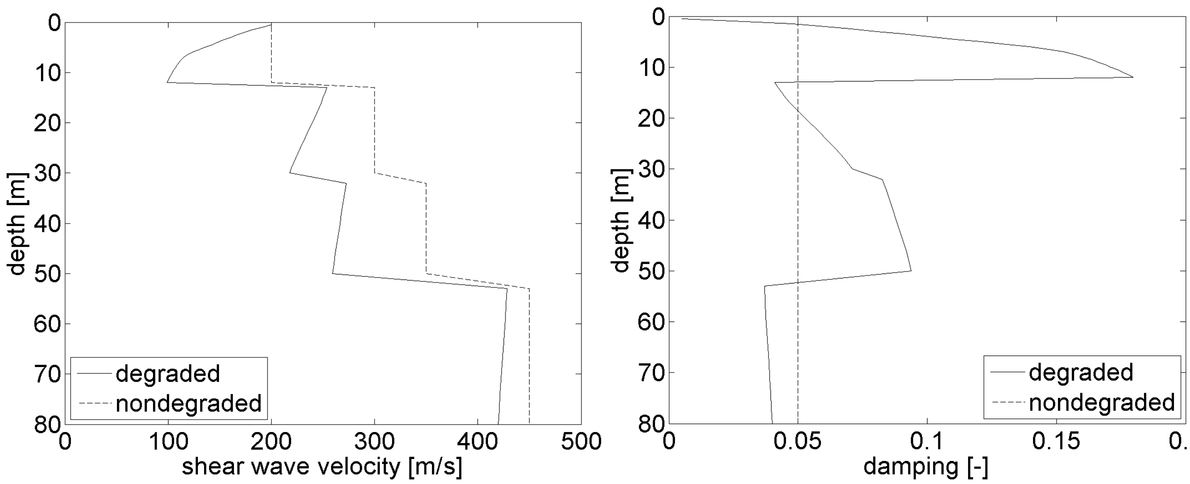

Figure 6.11. Degraded and nondegraded soil parameters.

It is assumed that an analysis using degraded soil parameters gives a better estimate of the soil response due to cyclic earthquake loading since this method better describes the behaviour of soil parameters when significant strain is present. The degraded analysis has shown to give good estimates for soils where the shear strain is below 1 % since dynamic soil properties at higher strains are poorly captured by reduction curves as described in Section 6.1 [Bray 2007b]. From Figure 6.7 it is seen that the maximum strain is below 1 % for all sublayers.

6.5. Solution for Fourier series input

When the bedrock input motion is described by a time series this can be transformed to the frequency domain using FFT as described in Section 5.4. By using FFT the bedrock input motion is given as a single sided complex Fourier series, $Y_{N,ss}$, which can be used for the equivalent linear analysis since this analysis is performed in the frequency domain.

For the iterative procedure the Fourier series of the displacement time history is used. This is done since the iterations seeks to find the maximum strain for each sublayer, where the strain is the derivative of displacement with respect to depth.

6.5.1. Fourier series for sublayers

The Fourier series for the sublayers are found by using the transfer function given in (6-36). The Fourier series for sublayer i is found by

$$Y_{i,ss}(f) = Y_{N,ss}(f) \cdot F_{iN}(f) \tag{6-38}$$

where

$Y_{i,ss}(f)$ is the single sided Fourier series for sublayer i

$Y_{N,ss}(f)$ is the single sided Fourier series for bedrock

$F_{iN}(f)$ is the transfer function between bedrock and sublayer i

6.5.2. Time history for sublayers

The time history of sublayer i is found by using the inverse FFT on the Fourier series of the sublayer. When the inverse FFT on a single sided Fourier series the series needs to be extended to the original length of the signal to get the right scale on the time history. Therefore trailing zeroes are added to the single sided Fourier series so the total number of frequencies are N, where N is the number of data points including trailing zeroes in the transformed input time series for the bedrock motion. The time history for sublayer i is found by

$$y_i(t) = N \cdot \Re e\{IFFT(Y_{i,ss}(f))\} \text{ for } f =]0; f_s] \tag{6-39}$$

where

$y_i(t)$	is the time history of sublayer i
N	is number of data points in the bedrock input time history including trailing zeroes
$IFFT(.)$	is the inverse FFT algorithm defined in Matlab
f_s	is the sampling frequency

6.5.3. Effective strain for sublayers

By using the displacement Fourier series as bedrock input motion the displacement time history for all sublayers can be found by use of (6-38) and (6-39). When all displacement time histories are known the strain can be calculated as the difference in displacement between two adjacent sublayers at time t

$$\gamma_i(t) \approx \frac{u_i(t) - u_{i-1}(t)}{\Delta z} \tag{6-40}$$

The effective strain for each sublayers are found as 65 % of the maximum strain as described in Section 6.4.3

$$\gamma_{i,eff} = 0.65 \cdot \max\{\gamma_i(t)\} \tag{6-41}$$

6.5.4. Iteration procedure

The following summary of the iteration procedure is given as

1) Use displacement Fourier series as input bedrock motion
2) Guess initial effective shear strain values for each layer
3) Get degraded dynamic soil properties corresponding to the effective shear strain values
4) Calculate coefficients a_i and b_i
5) Calculate transfer function F_{iN}
6) Calculate effective shear strain for each sublayer
7) Unless convergence is achieved start next iteration from 3)
8) When convergence is reached use acceleration Fourier series as bedrock motion and degraded soil properties to get surface acceleration Fourier series.

6.5.5. Results

From the described procedure above for the equivalent linear analysis using a time history bedrock as bedrock input the following results are found.

Convergence of strain

The convergence is for this analysis slower than for the analysis using a power spectrum as input. The slow convergence is seen in Figure 6.12 (left) where it is seen that convergence has stopped after iteration 6. To improve the convergence a new procedure for calculation of degraded soil parameters are used. Instead of calculation the degraded soil parameters from the maximum strain of the previous iteration, the mean of the maximum strain from the last two iterations are used instead. This method ensures that the strain value is not continuously shifting between two values without reaching converge. The convergence by this method is shown in Figure 6.12 (right), which is the method used for the results given later in this section.

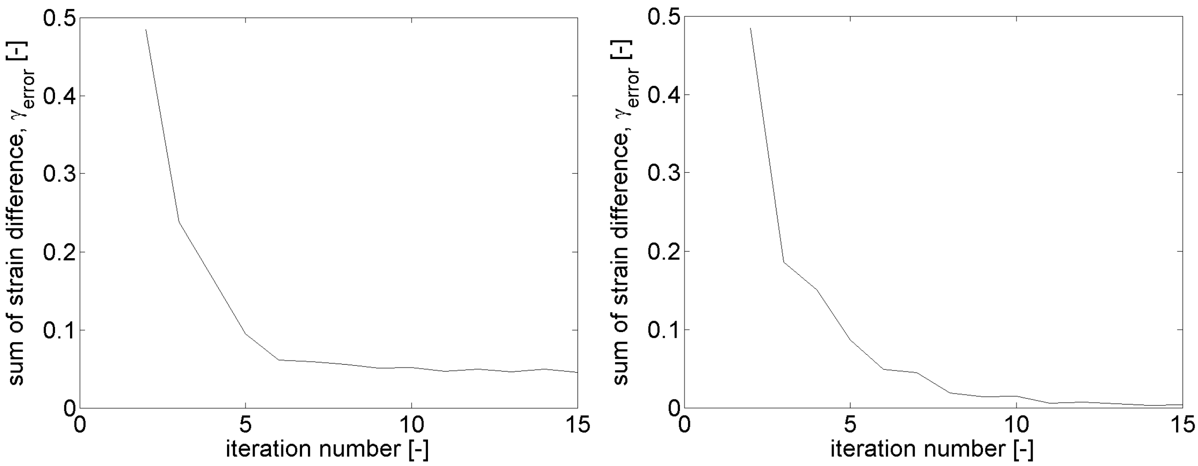

Figure 6.12. Sum of maximum strain difference between iterations. Convergence curve by using maximum strain from previous iteration (left). Convergence curve by using mean of last two maximum strain values (right).

The maximum strain distribution throughout the sublayers for chosen iteration loops are given in Figure 6.13.

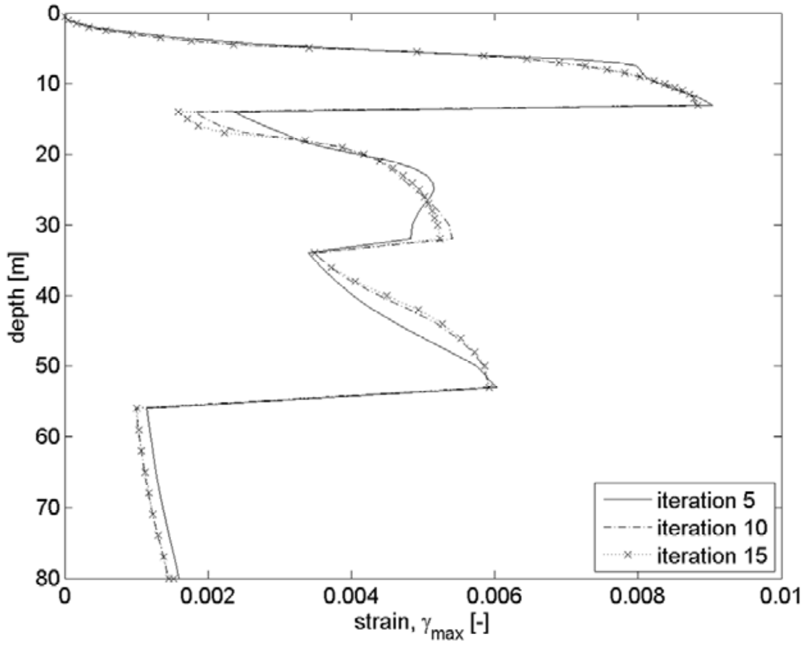

Figure 6.13. Maximum strain distribution for iteration 5, 10 and 15.

From Figure 6.13 it is seen that the maximum strain for all sublayers are below 1 % which is in the range where the dynamic soil properties are well captured by the reduction curves.

Transfer function

The absolute value of the degraded transfer function between bedrock and surface are shown in Figure 6.14.

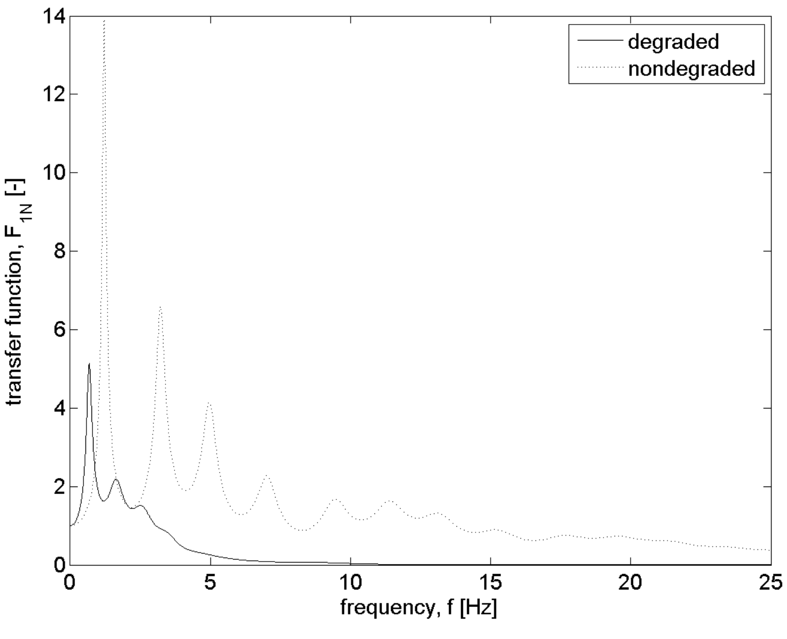

Figure 6.14. Transfer function between bedrock and surface.

The same tendency as the transfer function in Figure 6.9 are seen. The degraded transfer function is shifted towards lower periods and the magnitude is smaller than the non degraded transfer function.

Surface motion

Since this analysis has used a Fourier series and not only the Fourier amplitude spectrum it is possible to extract both the surface acceleration as a time history and as a Fourier amplitude spectrum. In Figure 6.15 the surface acceleration time history is shown for the degraded case.

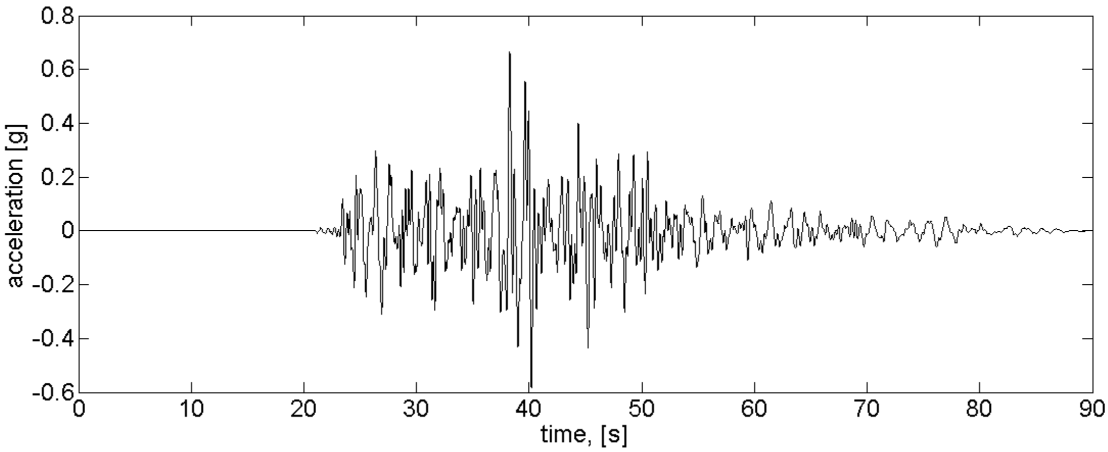

Figure 6.15. Surface acceleration time history.

The surface Fourier amplitude spectrum is shown in Figure 6.16. This figure also indicates the above observations of increase in amplitude and shift towards lower frequencies.

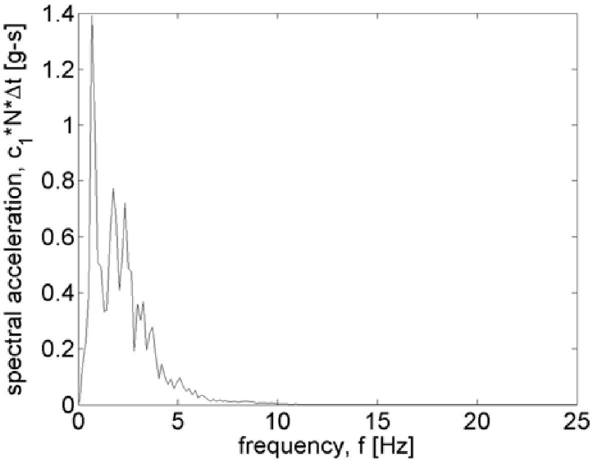

Figure 6.16. Fourier amplitude spectrum of acceleration for the surface. Smoothed curve by averaging over intervals of 25 values. Sampling frequency is 200.

7. Nonlinear dynamic soil analysis

In this chapter a nonlinear dynamic soil analysis is described. The nonlinear analysis is performed with the purpose of comparing the soil behaviour during an earthquake with the results from an equivalent linear analysis and the results from the procedure described in Eurocode EC8. This gives an insight into the effect of using more advanced analyses where it is assumed that the nonlinear analysis is the most advanced followed by the equivalent linear analysis.

7.1. Cyclic nonlinear model

It is chosen to use a relatively simple nonlinear model to describe the stress – strain behaviour during cyclic loading. The chosen model is the extended Masing model which will be discussed further in the following sections. The Masing model is able to describe a cyclic stress – strain behaviour which encapsulates the hysteretic behaviour of the stress – strain curves and thereby the inelastic behaviour of the soil. The model also includes the strain dependence of the shear stiffness and is likewise able to describe the development of permanent strain. The stress is described only in terms of effective stress and the model is not able to describe volumetric strain and pore pressure development.

7.2. General procedure

In this section the general procedure for the nonlinear analysis using the extended Masing model is described. In Section 7.3 the implementation of the general procedure for the specific case is further discussed. The nonlinear analysis is done in the time domain where the state of the soil is calculated at each time step.

7.2.1. Nonlinear algorithm

The nonlinear analysis is as the equivalent linear analysis based on the equation of motion given in Section 0 and here repeated as

$$\frac{\partial \tau}{\partial z} = \rho \frac{\partial \dot{u}}{\partial t} \tag{7-1}$$

where

ρ is the density of the soil

$\dot{u}$ is the particle velocity

t is the time

τ is the shear stress

z is the depth

[Kramer 1996, p275]

For the nonlinear analysis the soil is divided into a series of sublayers where the stress, strain, displacement and particle velocity is calculated by formulas given in the following. The numbering of the sublayers are shown in Figure 7.1.

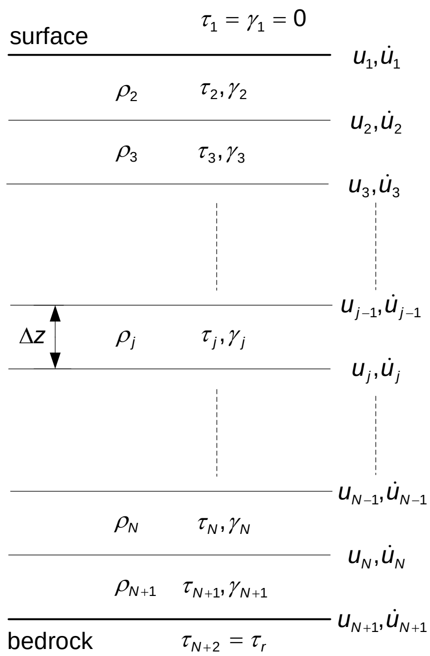

Figure 7.1. Definition of layer numbering. Displacement and velocity is taken as the value in the interface between two sublayers. Stress and strain is taken as the value in the middle of each sublayer. The soil is divided into N sublayers.

By using forward difference approximation the derivatives in (7-1) can be approximated as

$$\frac{\partial \tau}{\partial z} \approx \frac{\tau_{j+1,t} - \tau_{j,t}}{\Delta z} \tag{7-2}$$

and

$$\frac{\partial \dot{u}}{\partial t} \approx \frac{\dot{u}_{j,t+\Delta t} - \dot{u}_{j,t}}{\Delta t} \tag{7-3}$$

where

Δz is the sublayer thickness as indicated in Figure 7.1

Δt is the time step used in the analysis

u is the displacement at the sublayer interface

[Kramer 1996, p276]

by substituting (7-2) and (7-3) into (7-1) and solving for $\dot{u}_{j,t+\Delta t}$, the equation of motion can be approximated by the explicit finite difference equation given as

$$\frac{\tau_{j+1,t} - \tau_{j,t}}{\Delta z} = \rho_{j+1} \frac{\dot{u}_{j,t+\Delta t} - \dot{u}_{j,t}}{\Delta t}$$
$$\dot{u}_{j,t+\Delta t} = \dot{u}_{j,t} + \frac{\Delta t}{\rho_{j+1}\Delta z}\left(\tau_{j+1,t} - \tau_{j,t} \right) \tag{7-4}$$

The boundary conditions must be satisfied, which for the surface means that the stress and strain are both equal to zero as indicated in Figure 7.1. The boundary condition at bedrock depends on the behaviour of the bedrock. For the case with elastic bedrock, which is used for this analysis, the boundary condition that must be satisfied is that the stress at the interface between the bottom of the soil and the top of the bedrock must be equal. This boundary condition is shown to be satisfied when the shear stress at the top bedrock layer, τ_r, is given as

$$\tau_{r,t} \approx \rho_r v_{sr} \left(2\dot{u}_{r,t+\Delta t} - \dot{u}_{N+1,t+\Delta t} \right) \tag{7-5}$$

where

ρ_r is the density of bedrock

v_{sr} is the shear wave velocity of bedrock

$\dot{u}_r$ is the input bedrock velocity

τ_r is the shear stress at the top of bedrock as indicated in Figure 7.1

[Kramer 1996, p277]

Since $\tau_{N+2} = \tau_r$ the boundary condition at the bedrock can be expressed as a formula for the velocity at the interface between bedrock and sublayer N+1 by insertion of (7-5) into (7-4) and solving for $\dot{u}_{N+1,t+\Delta t}$. Thus the boundary condition is given as

$$\dot{u}_{j,t+\Delta t} = \dot{u}_{j,t} + \frac{\Delta t}{\rho_{j+1}\Delta z}(\tau_{j+1,t} - \tau_{j,t})$$
$$\dot{u}_{N+1,t+\Delta t} = \dot{u}_{N+1,t} + \frac{\Delta t}{\rho_{N+1}\Delta z}(\rho_r v_{sr}(2\dot{u}_{r,t+\Delta t} - \dot{u}_{N+1,t+\Delta t}) - \tau_{N+1,t})$$
$$\dot{u}_{N+1,t+\Delta t} = \frac{\dot{u}_{N+1,t} + \frac{\Delta t}{\rho_{N+1}\Delta z}(2\rho_r v_{sr}\dot{u}_{r,t+\Delta t} - \tau_{N+1,t})}{1 + \frac{\Delta t}{\rho_{N+1}\Delta z}\rho_r v_{sr}} \tag{7-6}$$

Note that the boundary condition in (7-6) are different than the condition in the procedure described in [Kramer 1996, p278] due to difference in definition of layer numbers.

Since the input bedrock motion is known for all time steps, the velocity profile for all sublayers can be calculated by knowledge of the velocity profile in the previous time step.

The incremental displacement from time step t to time step $t + \Delta t$ is given as

$$\Delta u_{j,t+\Delta t} = \dot{u}_{j,t+\Delta t}\Delta t \tag{7-7}$$

where

$\Delta u_{j,t+\Delta t}$ is the incremental displacement from time step t to time step $t + \Delta t$

[Kramer 1996, p278]

The displacement at time step $t + \Delta t$ is then found by summation of the incremental displacements from Δt to $t + \Delta t$ as shown in (7-8)

$$u_{j,t+\Delta t} = \sum_{t=\Delta t}^{t+\Delta t} \Delta u_{j,t} \tag{7-8}$$

The shear strain in each sublayer is given as

$$\gamma_{j,t+\Delta t} \approx \frac{u_{j,t+\Delta t} - u_{j-1,t+\Delta t}}{\Delta z} \tag{7-9}$$

[Kramer 1996, p278]

The strain is only found for $j = [2; N+1]$ since for $j = 1$ the strain is zero, see Figure 7.1 and for $j = N + 2$ the strain is not needed.

The shear stress is found from the shear strain by use of the defined stress-strain relationship. In this case the relationship is nonlinear and given as the extended Masing model.

7.2.2. Extended Masing model

One of the key elements in the extended Masing model is the backbone curve as discussed in Section 6.1. The backbone curve defines the strain dependency of the stiffness.

The extended Masing model consist of four criteria which describe the stress-strain relation. The criteria are as follows:

1) For initial loading, the stress – strain curve follows the backbone curve.
2) If a stress reversal point occurs at a point defined by (γ_p, τ_p), the stress – strain curve follows a path given by (7-10).
3) If the unloading or reloading curve exceeds the maximum magnitude of past strain and thereby intersects the backbone curve it follows the backbone curve until the next stress reversal.
4) If an unloading or reloading curve crosses an unloading or reloading curve from the previous cycle, the stress – strain curve follows that of the previous cycle.

$$\frac{\tau - \tau_p}{2} = F_{bb}\left(\frac{\gamma - \gamma_p}{2}\right) \tag{7-10}$$

where

τ_p	is the stress reversal point
γ_p	is the strain reversal point
F_{bb}	is the backbone function

[Kramer 1996, p241-242]

The criteria are easier understood by using an example which is done in the following. First it is noted that when a stress reversal point is reached a strain reversal point is reached at the same time. Since it is the strain that is known in this analysis the strain reversal point is instead used as an indicator. For this example the whole strain history is given beforehand as indicated in Figure 7.2.

For a given backbone curve and by applying the four rules for the extended Masing model, the stress – strain behaviour is as shown in Figure 7.3.

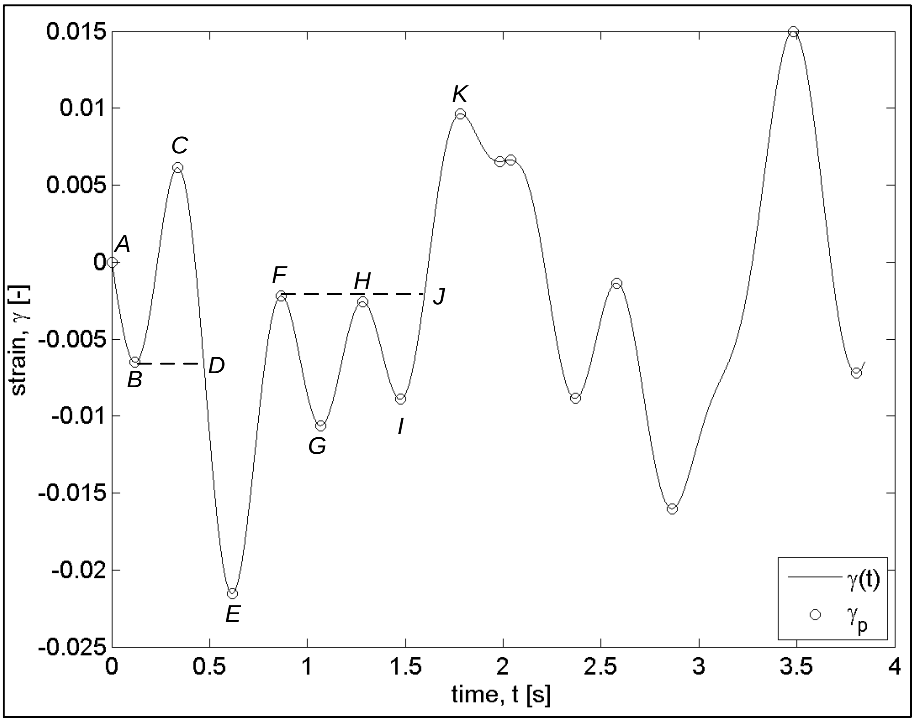

Figure 7.2. Strain time history for the extended Masing example.

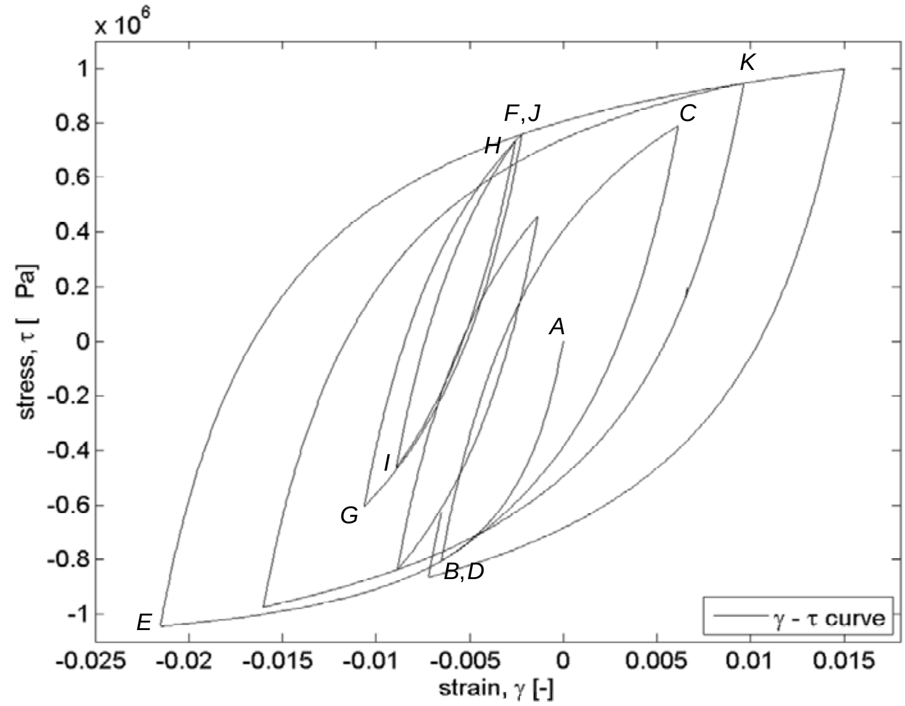

Figure 7.3. Stress – strain behaviour for the strain history example given in Figure 7.2 when the extended Masing model is applied. The letters correspond to the strain time history in Figure 7.2.

It is seen that for the initial unloading the curve follows the backbone curve from *A*-*B* according to rule 1). From *B*-*C* and *C*–*D* the curve follows the reloading and unloading curves defined by rule 2). At *D* the maximum strain is reached and the curve now follows the backbone curve as prescribed in rule 3). After a few unloading reloading curves the reloading curve *I*-*J* intersects the previous reloading curve at *J* and hereafter the curve follows the path of the previous reloading curve *E*-*F* until the strain reversal point at *K* as prescribed in rule 4).

7.3. Implementation of model for specific site

In this section a description of the implementation of the nonlinear model to the specific site is given. The site profile is given in Figure 2.7.

7.3.1. Backbone curves

The data sets describing the backbone curves for the four different soil types are simplified to hyperbolic functions where the quantities G_{max} and τ_{max} giving the shape of the hyperbola are fitted to the actual data sets. The hyperbolic functions are given as

$$\tau = F_{bb}(\gamma) = \frac{G_{\max}\gamma}{1 + \dfrac{G_{\max}}{\gamma_{\max}}|\gamma|} \tag{7-11}$$

where

G_{max} is a shape parameter corresponding to shear stiffness at infinitesimal strain

τ_{max} is a shape parameter corresponding to the shear strength of the soil

[Kramer 1996, p241]

The maximum shear modulus, G_{max}, can be calculated from the shear wave velocities given in the soil profile by (6-1). Instead of using the formula G_{max} is fitted since by fitting G_{max} the backbone curve described by the hyperbolic function gives a better fit to the data values in the whole range of γ. The backbone curve given by data values are derived from the data for the shear modulus reduction curves in Figure 6.2 (left). The maximum shear strength, τ_{max}, is also fitted and the backbone curves given by the data and the fitted curves for all four soil types are shown in Figure 7.4.

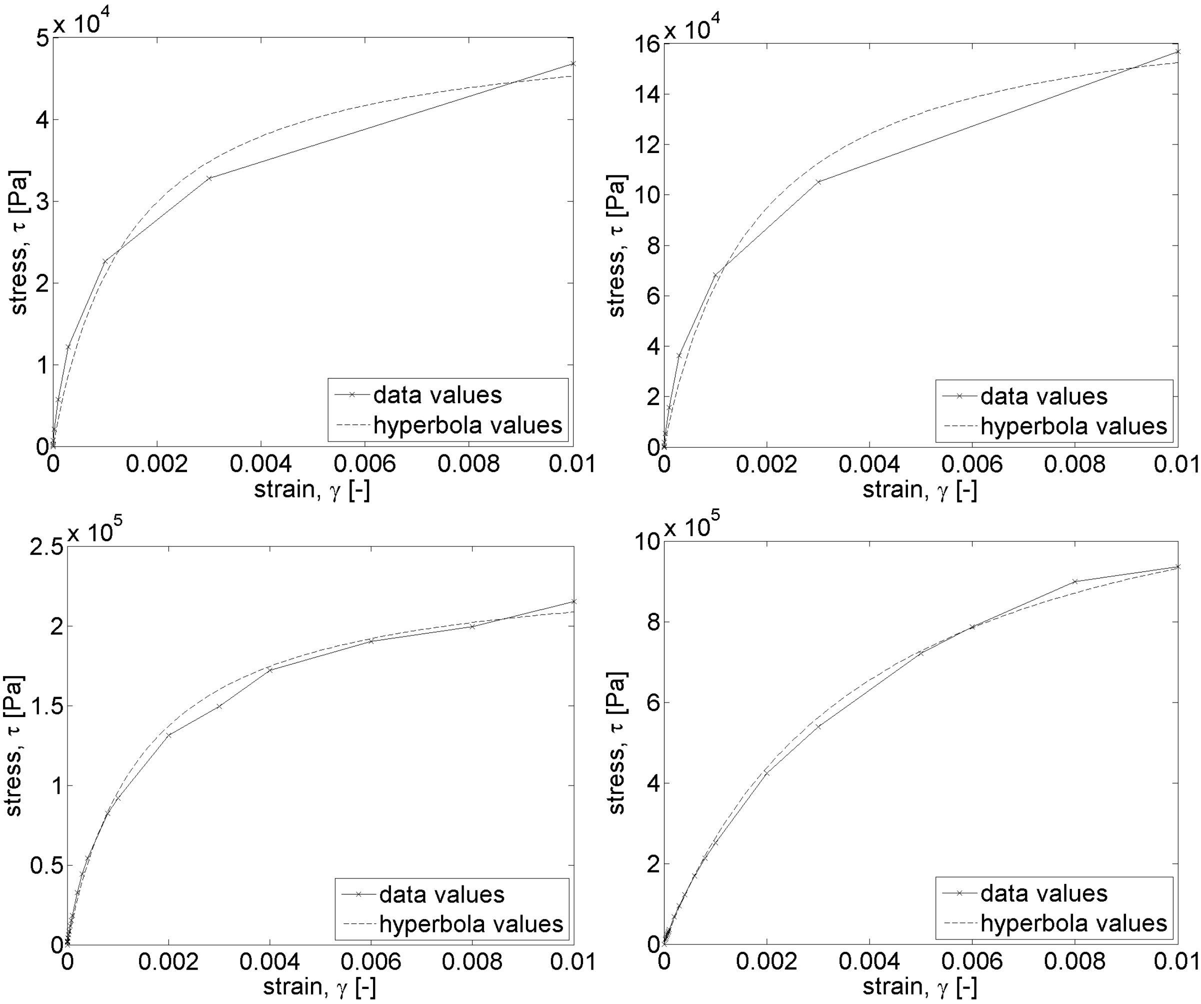

Figure 7.4. Data values for backbone curves for the four soil types fitted with hyperbola functions. Soil type 1 (upper left), soil type 2 (upper right), soil type 3 (lower left), soil type 4 (lower right). Soil types are indicated in Figure 2.7.

In Table 7.1 the fitted values of G_{max} and τ_{max} for the backbone curves described by the hyperbola functions in (7-11) are given.

Table 7.1. Used values for the hyperbolic backbone functions for all four soil types.

	Soil type 1	**Soil type 2**	**Soil type 3**	**Soil type 4**
G_{max} **[MPa]**	35	100	160	330
τ_{max} **[kPa]**	52	180	240	1300

7.3.2. Input velocity bedrock motion

The input velocity bedrock motion used for the nonlinear analysis must be described as a time history since the nonlinear method is in the time domain. The used bedrock motion is found as a scaled recorded time history from a past earthquake event as described in Section 5.3.2 and shown in Figure 5.6.

7.3.3. Algorithm for stress – strain relationship

In this section a note is made about how the algorithm for the stress – strain relationship is coded in Matlab. This is only a description of the overall procedure. For a complete description see the full Matlab code on the project CD-ROM.

The strain is known at time step *t* and all previous time steps by the nonlinear algorithm given in Section 7.2.1. With known strain history until time *t* the stress is found at time *t* for the extended Masing model by the following general procedure.

The procedure includes a set of key parameters described in the following

- **Base:** the stress – strain point used as parameters (τ_p, γ_p) for the unloading – reloading curve described in (7-10).
- **Target:** the stress – strain point where the current hysteresis loop crosses the previous hysteresis loop. This point indicates when the current curve needs to switch path to the previous curve, see rule 4. in Section 7.2.2.
- **Beta:** matrix storing the previous reversal points for all sublayers. This matrix is used when a redefinition of base and target are needed due to crossing of previous hysteresis loop.

The general procedure for determination of the stress when the strain is known is as follows

1) Test if new strain reversal point is reached
   a) If reversal point is reached new definition of base and target are made.
   b) If reversal point is **not** reached
      i) If target strain is reached redefine base and target to that of previous hysteresis loop.
      ii) If target strain is **not** reached base and target stays the same.
2) The stress value is calculated
   a) If the base is the backbone curve the stress is calculated by the backbone formula (7-11).
   b) If the base is **not** the backbone curve the stress is calculated by the strain reversal formula (7-10).

7.4. Results for nonlinear analysis

By the procedure and input as described in Section 7.3 the following results for the surface motion is found.

7.4.1. Surface velocity time history

The velocity time history for both the bedrock input motion and the calculated time history for the surface velocity are shown in Figure 7.5.

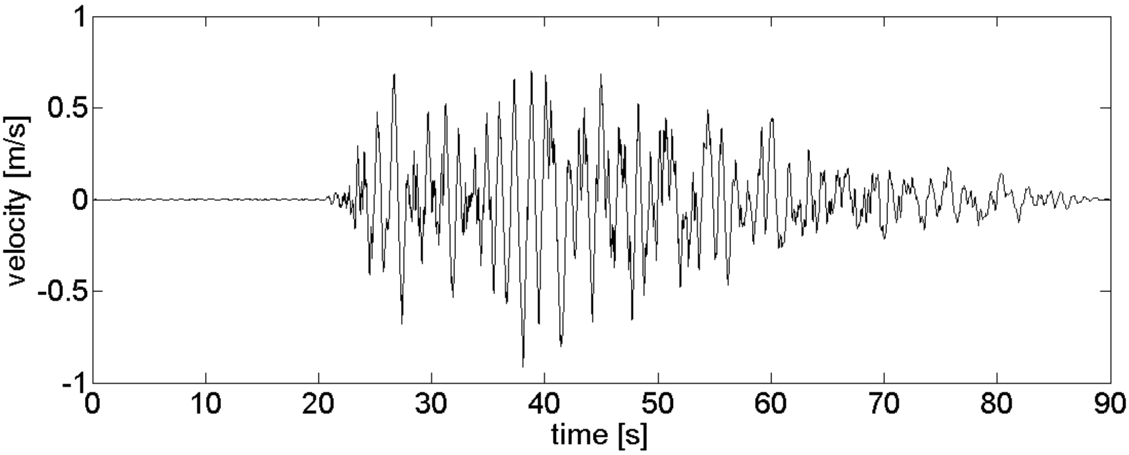

Figure 7.5. Surface velocity time history from the nonlinear analysis.

7.4.2. Surface acceleration time history

The output from the nonlinear model is the surface velocity time history. It is necessary to transform this to an acceleration time history which is used in the generation of an acceleration response spectrum as described in Chapter 10.

For constant time steps the time derivative of a discrete signal can be approximated by the central difference expression (7-12). Since the acceleration is the time derivative of the velocity an expression for the acceleration is the following

$$\ddot{u}_i = \frac{\dot{u}_{i+1} - \dot{u}_{i-1}}{2\Delta t} \tag{7-12}$$

where

$\ddot{u}_i$ is the acceleration of the mass relative to the ground at time step i

$\dot{u}_i$ is the velocity of the mass relative to the ground at time step i

Δt is the time step

[Chopra 2007, p171]

The above expression is used to get the acceleration time history for the surface response in the nonlinear analysis shown in Figure 7.6.

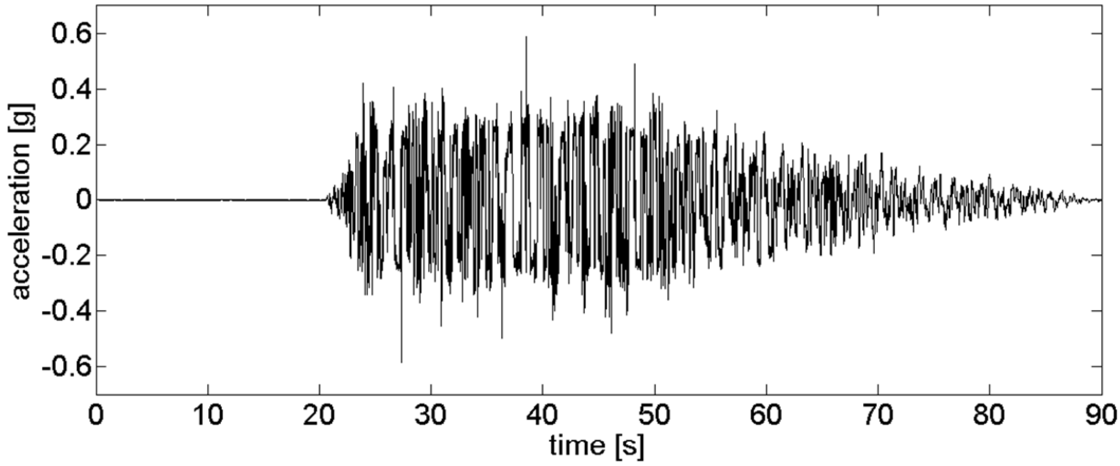

Figure 7.6. Surface acceleration time history from the nonlinear analysis.

7.4.3. Surface Fourier amplitude spectrum

The surface Fourier amplitude spectrum corresponding to the acceleration time history shown in Figure 7.6 can be generated by the procedure described in Section 5.4.

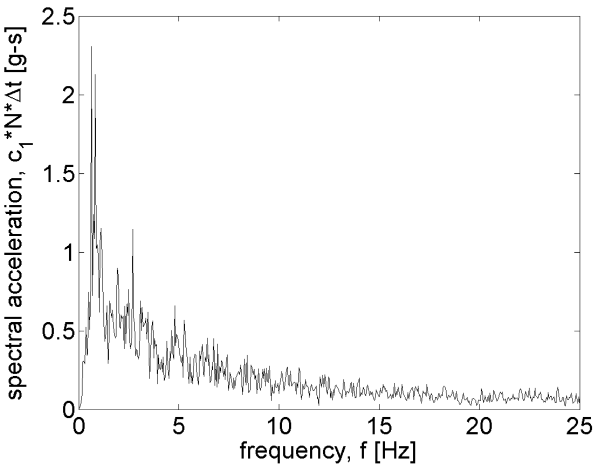

Figure 7.7. Surface Fourier amplitude spectrum.

7.4.4. Stress strain relationship

The stress-strain relationship for the sublayer at a depth of 10 metres is shown in Figure 7.8. Hysteresis loops of different sizes are seen along with the behaviour of shift in path when previous hysteresis loops are encountered. It can be noticed that for large magnitude strain cycles the area encircled by the hysteresis loops are much larger than for the small magnitude strain cycles. This indicates the effect that damping increases with increasing magnitude of strain cycles.

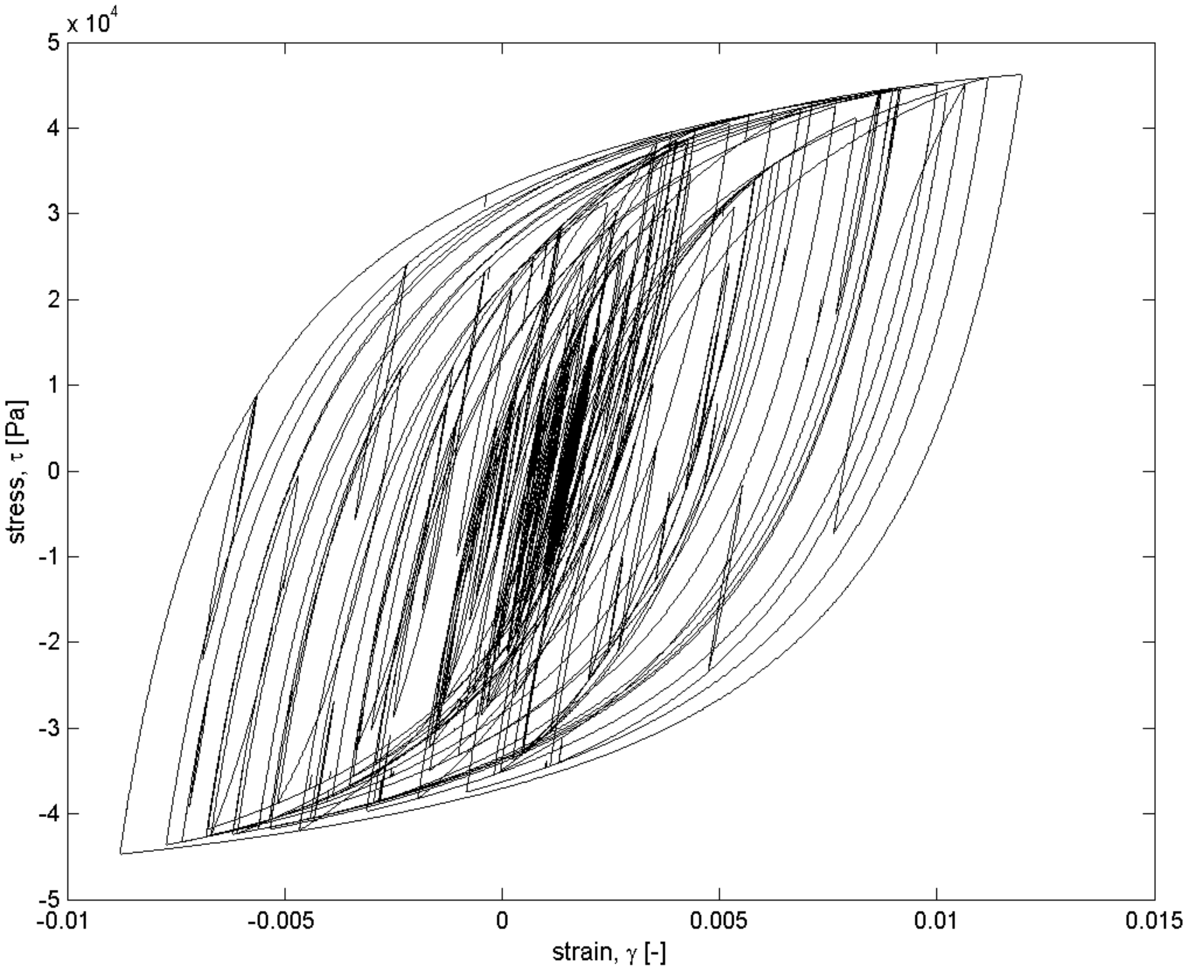

Figure 7.8. Stress-strain relationship for the sublayer at a depth of 10 metres.

7.4.5. Strain time history

A strain time history for the sublayer at a depth of 10 metres are shown in Figure 7.9.

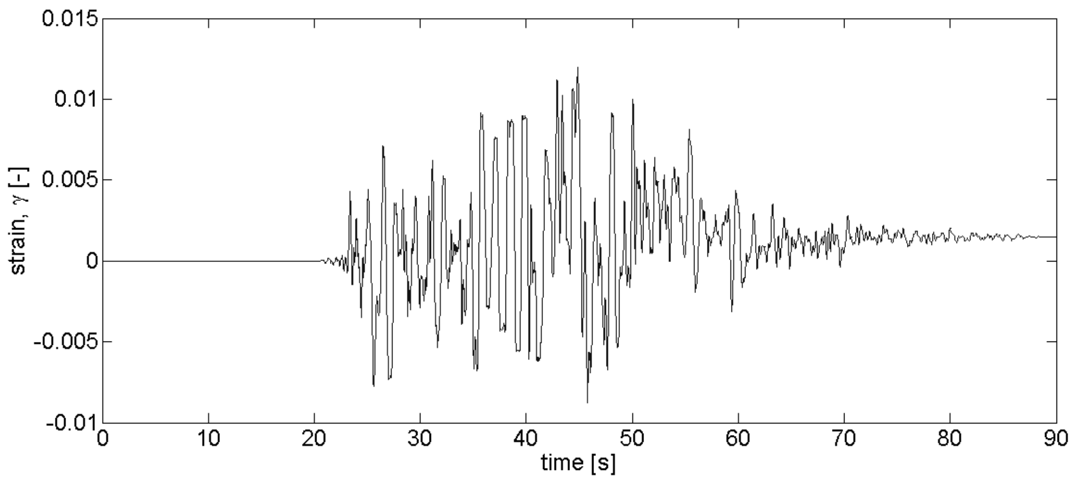

Figure 7.9. Strain time history for sublayer at a depth of 10 metres.

The given strain time history illustrates one of the features of the chosen nonlinear model in that a permanent strain is seen after the ground motion has subsided. This indicates that plastic deformation can be described by the nonlinear model, even thou only in a simplified manner.

8. Response spectrum for power spectrum

To compare the results from the equivalent linear and the nonlinear soil response analyses with the response spectrum defined in Eurocode EC8 it is necessary to transform the surface motions found in the equivalent linear and the nonlinear analyses to response spectra. A general description of the response spectrum concept are given in Section 3.1.

For the equivalent linear model using a Fourier amplitude spectrum the response spectrum is calculated on the basis of assumptions of the combination of the amplitudes for the different frequencies.

8.1. Combination by SRSS rule

This method combines the amplitudes in the amplitude spectrum by the SRSS rule where the amplitudes are combined by taking the square root of the sum of squares. The SRSS rule assumes that the contributions from amplitudes at different frequencies are uncorrelated. First the amplitudes of the total acceleration of the SDOF are found by the transmissibility formula.

8.1.1. Transmissibility formula

The maximum response for a SDOF system excited with harmonic ground motion can be determined by use of the transmissibility defined as (8-1) which gives the ratio between the amplitude of the vibration of the mass and the amplitude of the excitation.

$$TR(\omega) = \frac{\ddot{u}_0^t}{\ddot{u}_{g0}} = \left(\frac{1 + \left(2\zeta \frac{\omega}{\omega_n} \right)^2}{\left(1 - \left(\frac{\omega}{\omega_n} \right)^2 \right)^2 + \left(2\zeta \frac{\omega}{\omega_n} \right)^2} \right)^{\frac{1}{2}} \tag{8-1}$$

where

TR	is the transmissibility
$\ddot{u}_0^t$	is the amplitude of the total acceleration of the mass
$\ddot{u}_{g0}$	is the amplitude of a harmonic ground acceleration
ω	is the frequency of the harmonic ground motion
ω_n	is the natural frequency of the SDOF system

ζ is the damping ratio of the SDOF system

[Chopra 2007, p92]

The formula in (8-1) can be derived by using the expression for a harmonic transfer function as shown in the following. The following derivations are for a single degree of freedom system excited with harmonic ground motion and for stable response given as the stationary response after initial conditions are subsided. The total acceleration of the mass is given as

$$\ddot{u}^t(t) = \ddot{u}_g(t) + \ddot{u}(t) \tag{8-2}$$

where

$\ddot{u}^t(t)$ is the total acceleration of the mass

$\ddot{u}_g(t)$ is the ground acceleration

$\ddot{u}(t)$ is the acceleration of the mass relative to the ground

[Chopra 2007, p92]

The ground acceleration is given as

$$\ddot{u}_g(t) = \ddot{u}_{g0} \cdot e^{i\omega t} \tag{8-3}$$

[Chopra 2007, p91]

The response of the mass relative to the ground motion when a stationary response is achieved can be described by the harmonic transfer function. First the expression is given for the relative displacement excited with a harmonic motion

$$u(t) = H(\omega) \cdot \tilde{f}(\omega) \cdot e^{i\omega t} \tag{8-4}$$

where

$u(t)$ is the displacement of the mass relative to the ground motion

$H(\omega)$ is the harmonic transfer function

$\tilde{f}(\omega)$ is the Fourier amplitude of the harmonic excitation

[Lutes & Sarkani 2004, p235]

By taking the second derivative of (8-4) with respect to time the relative acceleration of the mass is given as

$$\ddot{u}(t) = -\omega^2 H(\omega) \tilde{f}(\omega) \cdot e^{i\omega t} \tag{8-5}$$

The Fourier amplitude of the excitation is for this case with ground motion given as

$$\tilde{f}(\omega) = -m\ddot{u}_{g0} \tag{8-6}$$

where

m is the mass of the system

[Chopra 2007, p91]

The harmonic transfer function can for the SDOF case be written as

$$H(\omega) = \frac{1}{m(\omega_n{}^2 + 2i\zeta\omega_n\omega - \omega^2)} \tag{8-7}$$

[Lutes & Sarkani 2004, p245]

By inserting (8-6) and (8-7) in (8-5) the relative acceleration is given as

$$\begin{aligned} \ddot{u}(t) &= \frac{\omega^2 \ddot{u}_{g0} e^{i\omega t}}{\omega_n{}^2 - \omega^2 + 2i\zeta\omega_n\omega} \\ \ddot{u}(t) &= \frac{\alpha^2 \ddot{u}_{g0} e^{i\omega t}}{1 - \alpha^2 + 2i\zeta\alpha}, \qquad \alpha = \frac{\omega}{\omega_n} \end{aligned} \tag{8-8}$$

By inserting (8-8) and (8-3) in (8-2) the total acceleration is given as

$$\ddot{u}^t(t) = \ddot{u}_{g0} \cdot e^{i\omega t} \left(1 + \frac{\alpha^2}{1 - \alpha^2 + 2i\zeta\alpha} \right) \tag{8-9}$$

The amplitude of the total acceleration is taken as the modulus of the complex value given in (8-9). This gives an amplitude of the total acceleration given as

$$\ddot{u}_0^t = \ddot{u}_{g0} \left(\frac{1 + (2\zeta\alpha)^2}{(1 - \alpha^2)^2 + (2\zeta\alpha)^2} \right)^{\frac{1}{2}} \tag{8-10}$$

The transmissibility as given in (8-1) is the ratio between the amplitude of the total mass acceleration and the amplitude of the ground acceleration. By dividing the expression in (8-10) with the amplitude of the harmonic ground acceleration $\ddot{u}_{g0}$ the transmissibility formula is derived as given in (8-11).

$$TR(\omega) = \frac{\ddot{u}_0^t}{\ddot{u}_{g0}} = \frac{\ddot{u}_{g0}\left(\frac{1+(2\zeta\alpha)^2}{(1-\alpha^2)^2+(2\zeta\alpha)^2}\right)^{\frac{1}{2}}}{\ddot{u}_{g0}}$$
$$TR(\omega) = \left(\frac{1+\left(2\zeta\frac{\omega}{\omega_n}\right)^2}{\left(1-\left(\frac{\omega}{\omega_n}\right)^2\right)^2+\left(2\zeta\frac{\omega}{\omega_n}\right)^2}\right)^{\frac{1}{2}} \tag{8-11}$$

8.1.2. Total response of mass

The transmissibility can be used for a single harmonic excitation. By discretization of the input Fourier amplitude spectrum of the surface acceleration, (8-1) can be used for each excitation frequency and corresponding amplitude. This gives a series of contributions to the total response of the mass. Each contribution is determined as

$$\ddot{u}_{0,\omega_i}^t = TR(\omega_i)\cdot\ddot{u}_{g0}(\omega_i) \tag{8-12}$$

where

$\ddot{u}_{0,\omega_i}^t$ is the distribution to the mass response from the excitation with ω_i

$\ddot{u}_{g0}(\omega_i)$ is the amplitude of the excitation with ω_i

To add all the contributions the square root of the sum of squares (SRSS) are used as adding rule. This gives an estimation of the maximum response of the mass given as

$$\ddot{u}_{0,\max}^t = \sqrt{\sum_{i=1}^{N}\left(\ddot{u}_{0,\omega_i}^t\right)^2\Delta\omega} \tag{8-13}$$

where

N is the number of components of the Fourier amplitude spectrum of the surface acceleration

$\ddot{u}_{0,\max}^t$ is the total maximum response of the mass when SRSS rule is assumed

$\Delta\omega$ is the frequency interval of the discretized input Fourier amplitude spectrum

8.1.3. Procedure for response spectrum generation

The following steps are used to generate the response spectrum for a given Fourier amplitude spectrum.

1) Set an array of the natural frequency values ω_n and for each value do the following
   a) Calculate TR by (8-1)
   b) Calculate the response distribution vector $\ddot{u}^t_{0,\omega_i}$ by (8-12)
   c) Calculate the total response $\ddot{u}^t_{0,\max}$ by (8-13)
2) Collect the total response values $\ddot{u}^t_{0,\max}$ and the corresponding ω_n values which gives the response spectrum $S_e(\omega_n)$

Response spectra for bedrock and surface motion generated by the procedure described in this section are given in Figure 8.2.

8.2. Combination by time series simulations

The SRSS rule used in Section 8.1 does not include the duration for which the earthquake loading is at its peak stationary period. The stationary duration has an influence on how the contributions from the discretized frequencies are added together in that a longer duration increases the probability of a crossing of a specified threshold. In this section an analysis is performed which includes the duration of the stationary part of the motion by generating an assumed Fourier phase spectrum and combine this with the Fourier amplitude spectrum for the mass of the SDOF.

8.2.1. Fourier series generation

Fourier series can be used to describe a signal which in this case is the acceleration time history of the mass in a SDOF system. The Fourier series for a given natural frequency is given as

$$\ddot{u}^t(t) = \sum_{i=1}^{N} \ddot{u}^t_{0,\omega_i} \cos(\omega_i t + \delta_i)\Delta\omega \tag{8-14}$$

where

$\ddot{u}^t(t)$ is the total response of the mass as function of time

δ_i is the phase angle corresponding to ω_i

t is time

The Fourier amplitudes $\ddot{u}^{t}_{0,\omega_i}$ is found in (8-12) whereas the phase spectrum is assumed to consist of random values uniformly distributed in the interval [0;2π[. In this way a time series of the mass acceleration can be generated and a maximum value in the given time interval corresponding to the stationary duration of the motion can be found for each simulation of a phase spectrum. The duration of the stationary part of the input bedrock motion is set to 10 s, which is the minimum duration recommended in Eurocode EC8 [EN8 2003, p29]. It is assumed that the stationary duration of the motion of the mass of the SDOF also is 10 s. It shall be noted that there is a possibility of the peak acceleration occurring after the stationary part of the earthquake motion is over, but this possibility is not included in this method.

Since the phase angles are random values each simulation will give a different time series and thereby a different maximum value. A number of simulations are therefore performed so a probability distribution of the maximum response is generated. In this analysis it is chosen to use the mean value of the generated distribution as the response value used for the response spectrum. By this procedure the response is given as the expected value of the maximum acceleration distribution. The mean value is chosen since the analysis is performed to give as realistic a result as possible and not to introduce extra safety in the earthquake response.

8.2.2. Procedure for time series simulation

By the above calculation a transformation of a Fourier amplitude spectrum can be transformed to a response spectrum by time series simulation. The following is the used procedure:

1) Define a fundamental frequency, ω_n, for the SDOF system
2) Generate N phase angles as random numbers uniformly distributed between 0 and 2π
3) Generate $\ddot{u}^{t}(t)$ and find the maximum acceleration in the specified time period
4) Repeat 2) and 3) 100 times to get a probability distribution and use the mean of the maximum values as a final response value
5) Repeat 1) – 4) for each ω_n to get the total response spectrum $S_e(\omega_n)$

8.2.3. Determination of discretization values

In Section 8.2 both time interval, Δt and number of simulations must be determined to give a accurate result. Also the frequency interval, $\Delta\omega$, is needed for both analyses in Section 8.1 and 8.2. In this section these three values will be determined on the basis of a series of convergence studies. The value of ΔT_n is set to 0.02 s.

Determination of Δt

By letting Δt vary and for a fixed set of δ_i, and for different values of T_n the response spectrum values for the surface motion are calculated. The values are shown in Table 8.1 and the index values of Table 8.1 are shown in Table 8.2.

Table 8.1. Response of mass in units of g for different time step and natural frequencies.

Δt \ T_n	0.2 s	0.5 s	1 s
0.3 s	1.793	1.192	2.597
0.1 s	1.793	1.192	2.597
0.03 s	1.793	1.192	2.611
0.01 s	1.830	1.193	2.619
0.003 s	1.830	1.195	2.619
0.001 s	1.831	1.195	2.619
0.0003 s	1.831	1.195	2.619

Table 8.2. Response values from Table 8.1 index after Δt = 0.0003 s values.

Δt \ T_n	0.2 s	0.5 s	1 s
0.3 s	0.980	0.998	0.992
0.1 s	0.980	0.998	0.992
0.03 s	0.980	0.998	0.997
0.01 s	1.000	0.998	1.000
0.003 s	1.000	1.000	1.000
0.001 s	1.000	1.000	1.000
0.0003 s	1.000	1.000	1.000

It is seen that the sensitivity of the time step value is not to sensitive so a time step of Δt = 0.01 s is used for the analysis.

Determination of number of simulations

A similar convergence analysis is performed for determination of number of needed simulations. Here an increasing number of simulations are performed and the result for different natural periods are given in Table 8.3 and index values in Table 8.4.

Table 8.3. Response of mass in units of g for different number of simulations (# sim) and natural periods.

# sim\ T_n	0.2 s	0.5 s	1 s
5	1.977	1.465	1.927
50	1.865	1.500	2.229
100	1.912	1.438	2.158
200	1.887	1.480	2.293
500	1.879	1.460	2.195
1000	1.882	1.470	2.226

Table 8.4. Response values from Table 8.3 index after # sim = 150 values.

# sim\ T_n	0.2 s	0.5 s	1 s
5	1.051	0.997	0.866
50	0.991	1.021	1.001
100	1.016	0.978	0.970
200	1.003	1.007	1.030
500	0.999	0.994	0.986
1000	1.000	1.000	1.000

The index values in Table 8.4 shows that there is no clear picture towards convergence. It is known that the quality of the estimate is better increasing number of simulations and therefore 100 simulations are chosen as a compromise between precision and calculation time.

Determination of $\Delta\omega$

A study of the influence of the frequency interval is carried out by generating a response spectrum for the bedrock motion using the SRSS method for different values of the frequency interval. The response spectrums are shown in Figure 8.1.

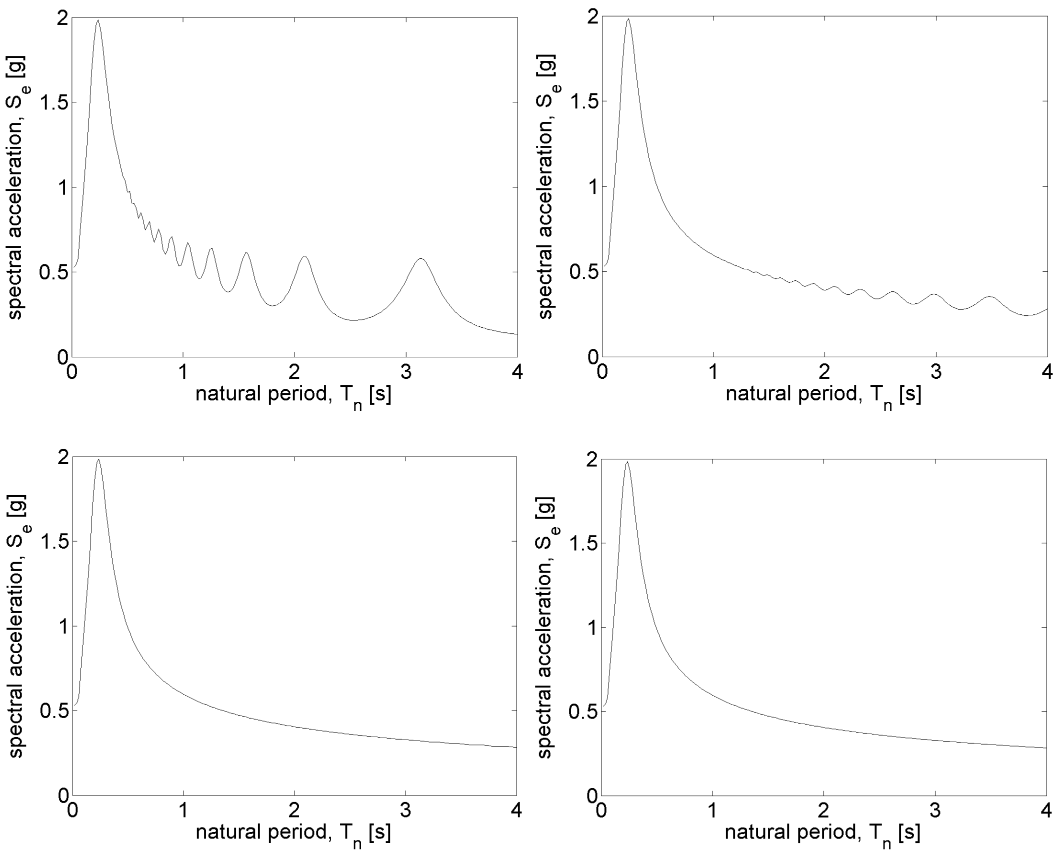

Figure 8.1. Response spectrum for bedrock for frequency interval values $\Delta\omega$ of 1 rad/s (upper left), 0.3 rad/s (upper right), 0.1 rad/s (lower left), 0.03 rad/s (lower right). ζ = 5 %.

From Figure 8.1 it is seen that the shapes of the four response spectra are similar except at higher natural periods, where irregularities are seen for the spectra corresponding to $\Delta\omega$ = 1 rad/s and $\Delta\omega$ = 0.3 rad/s. For $\Delta\omega$ = 0.1 rad/s and 0.3 rad/s no irregularities are seen and the shape of the response spectra looks as it should. A frequency interval of $\Delta\omega$ = 0.1 rad/s is chosen for the analysis.

8.3. Results for power spectrum motion

The transformation of a Fourier amplitude spectrum to response spectrum is performed by the equivalent linear method with combination of the amplitudes by both the methods described in Section 8.1 and 8.2. The values used for the time simulation method are, $\Delta\omega$ = 0.1 rad/s, Δt = 0.01 s and number of simulations = 100. The results are shown for degraded responses.

In Figure 8.2 the response spectrum for the surface motion is shown both for the response spectrum generated by the SRSS rule and for the time series simulation. It is seen that the time series simulation method gives a lower response than by using the SRSS rule. Since the time series simulation includes assumptions of the duration of the earthquake it is assumed that this analysis is more correct than the SRSS combination rule. Therefore the combination rule by time series simulation is used for fitting of the bedrock input motion as described in Section 5.2.

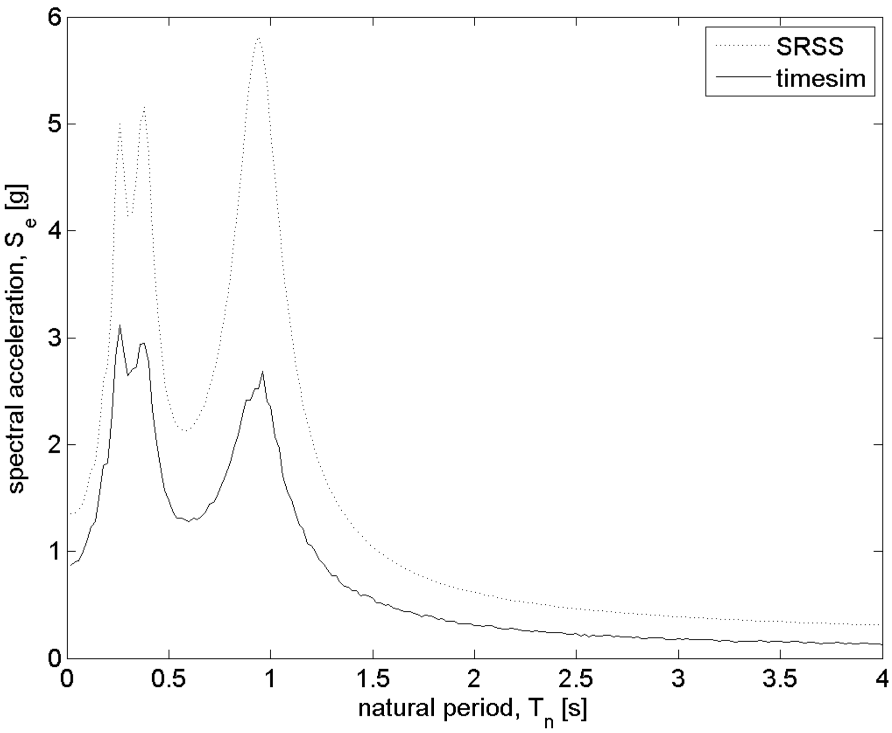

Figure 8.2. Response spectrum for surface motion. Damping is 5 %.

9. Response spectrum for Fourier series

In this chapter a description of how to generate a response spectrum from a ground motion given as a Fourier series. The method utilizes the harmonic transfer function for a SDOF system together with the inverse FFT.

9.1. Fourier series for SDOF system

The generated Fourier series for the surface motion calculated in (6-38) is transmitted through the SDOF in the frequency domain by multiplication with the harmonic transfer function for the SDOF system in the same way as the bedrock motion was multiplied with the transfer function of the soil as described in (6-38).

The harmonic transfer function for the SDOF system is given in (8-7) and the relative acceleration of the SDOF given as a Fourier series is calculated by

$$Y_{mass,ss}(f) = Y_{1,ss}(f) \cdot H(f) \tag{9-1}$$

where

$Y_{mass,ss}$ is the single sided Fourier series for the relative mass acceleration

$Y_{1,ss}$ is the single sided Fourier series for the surface acceleration

H is the harmonic transfer function for the SDOF system

9.2. Total acceleration time history

The Fourier series $Y_{mass,ss}$ is transformed to a time history using the inverse FFT algorithm as described in (6-39)

$$y_{mass}(t) = N \cdot \Re e\{IFFT(Y_{mass,ss}(f))\} \text{ for } f =]0; f_s] \tag{9-2}$$

The total acceleration of the SDOF used to get the response spectrum is found by adding the time history of the relative mass acceleration with the time history of the surface acceleration as described by

$$y^t_{mass}(t) = y_{mass}(t) + y_1(t) \tag{9-3}$$

where

$y^t_{mass}(t)$ is the total acceleration of the SDOF system

$y_1(t)$ is the surface acceleration

9.3. Response spectrum

The response spectrum value corresponding to the chosen natural circular frequency in the harmonic transfer function is found as the maximum value of the generated time history of total mass acceleration. For a series of generations with varying values of natural frequencies the response spectrum in Figure 9.1 is generated.

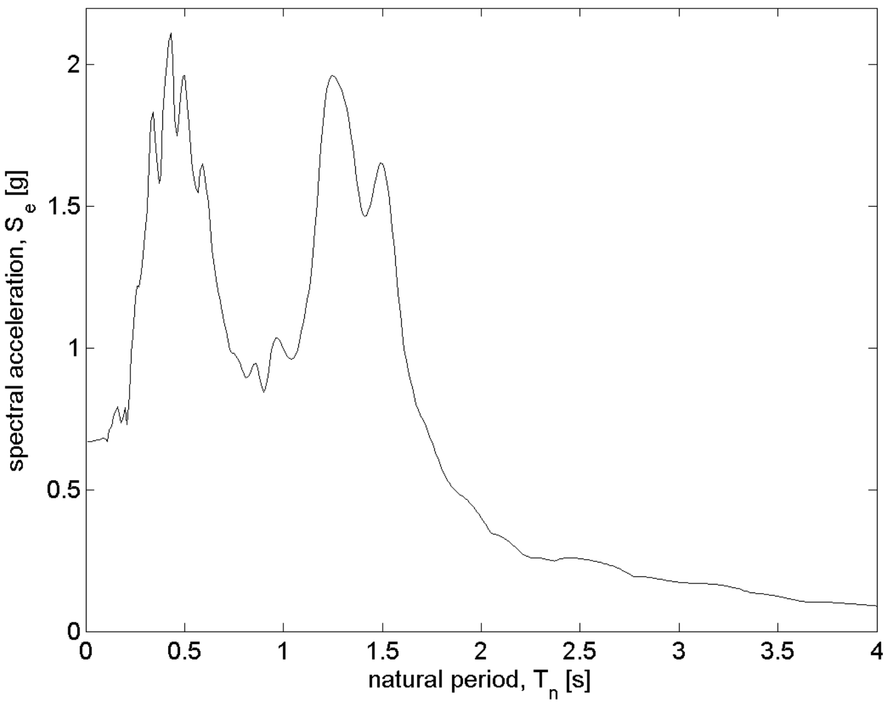

Figure 9.1. Surface acceleration response spectrum for the equivalent linear method using a Fourier series input.

10. Response spectrum for time history

In this chapter a description of how do generate a response spectrum from acceleration time histories is given. The Newmark time stepping algorithm is used to solve the equation of motion of a SDOF system excited with the ground acceleration.

10.1. Newmark algorithm

To generate a response spectrum corresponding to the surface acceleration time history a SDOF system is solved. In the time domain this can be done by the Newmark algorithm. In this section only the algorithm is given and criteria for stability and reasonable accuracy.

10.1.1. Initial conditions are calculated as

The initial conditions are calculated as

$$\ddot{u}_0 = \frac{p_0 - c\dot{u}_0 - ku_0}{m} \tag{10-1}$$

$$\hat{k} = k + \frac{\gamma}{\beta \Delta t}c + \frac{1}{\beta(\Delta t)^2}m \tag{10-2}$$

$$a = \frac{1}{\beta \Delta t}m + \frac{\gamma}{\beta}c \tag{10-3}$$

$$b = \frac{1}{2\beta}m + \Delta t\left(\frac{\gamma}{2\beta} - 1\right)c \tag{10-4}$$

where

$\ddot{u}_0$ is the initial acceleration of the mass

$\dot{u}_0$ is the initial velocity

u_0 is the initial displacement

p_0 is the initial excitation

c is the damping coefficient given as $c = 2m\zeta\omega_n$

k is the stiffness given as $k = m\omega_n{}^2$

m is the mass

ζ is the damping ratio

ω_n is the natural circular frequency

γ,β are a parameters set to $\gamma = \frac{1}{2}$ and $\beta = \frac{1}{4}$ corresponding to the average acceleration method

[Chopra 2007, p177]

In this analysis the initial conditions are all equal to zero. The damping ratio is set to $\zeta = 0.05$ which gives a response spectrum for 5% damping. The natural circular frequency is varied to give the response spectrum for a range of natural frequencies.

10.1.2. Time stepping calculation

For each time step in the analysis the following calculations are performed

$$\Delta\hat{p}_i = \Delta p_i + a\dot{u}_i + b\ddot{u}_i \tag{10-5}$$

$$\Delta u_i = \frac{\Delta\hat{p}_i}{\hat{k}} \tag{10-6}$$

$$\Delta\dot{u}_i = \frac{\gamma}{\beta\Delta t}\Delta u_i - \frac{\gamma}{\beta}\dot{u}_i + \Delta t\left(1 - \frac{\gamma}{2\beta}\right)\ddot{u}_i \tag{10-7}$$

$$\Delta\ddot{u}_i = \frac{1}{\beta(\Delta t)^2}\Delta u_i - \frac{1}{\beta\Delta t}\Delta\dot{u}_i - \frac{1}{2\beta}\ddot{u}_i \tag{10-8}$$

$$\begin{aligned} u_{i+1} &= u_i + \Delta u_i \\ \dot{u}_{i+1} &= \dot{u}_i + \Delta\dot{u}_i \\ \ddot{u}_{i+1} &= \ddot{u}_i + \Delta\ddot{u}_i \end{aligned} \tag{10-9}$$

where

Δp_i is the increment in excitation given as $\Delta p_i = p_{i+1} - p_i$

u_i is the displacement of the mass relative to the ground at time step i

p_i is the excitation at time step i

[Chopra 2007, p177]

Since the excitation in this case is ground acceleration the load p is given as $p_i = -m\ddot{u}_{g,i}$, where $\ddot{u}_g$ is the ground acceleration.

10.1.3. Time step criteria

The Newmark algorithm is stable for any chosen time step value when the average acceleration method is used.

To make sure the Newmark algorithm also gives accurate results the following criterion for the time step is typically used

$$\Delta t \leq 0.1 T_n \tag{10-10}$$

where

T_n is the natural period of the system given as $T_n = \dfrac{2\pi}{\omega_n}$

[Chopra 2007, p173]

In the response spectrum generation the smallest used value for T_n is set to $T_n = 0.02$ s so the time step criterion is $\Delta t \leq 0.002$ s . For the analysis a time step of $\Delta t = 0.0005$ s is used so the Newmark algorithm is assumed to give stable and accurate results.

10.2. Response spectrum for nonlinear analysis

A response spectrum is generated by using the Newmark algorithm described in Section 10.1 for a SDOF. For the response spectrum the total acceleration is needed and not the relative acceleration as calculated by (10-9). The total acceleration is given as

$$\ddot{u}_i^t = \ddot{u}_i + \ddot{u}_{g,i} \tag{10-11}$$

where

$\ddot{u}_i^t$ is the total acceleration of the mass at time i

[Chopra 2007, p177]

with the use of (10-11) the total acceleration time history for the SDOF system excited with the surface acceleration time history can be calculated. The values in the response spectrum is then found by varying T_n with values between $T_n = [0.02;4]$ s and for each chosen value of T_n take the maximum value of $\ddot{u}_i^t$ as stated in (10-12)

$$S_e(T_n) = \max\{\ddot{u}_i^t(T_n)\} \tag{10-12}$$

where

$S_e(T_n)$ is the response spectrum for a given T_n

The generated response spectrum for the surface acceleration time history from the nonlinear analysis is shown in Figure 10.1.

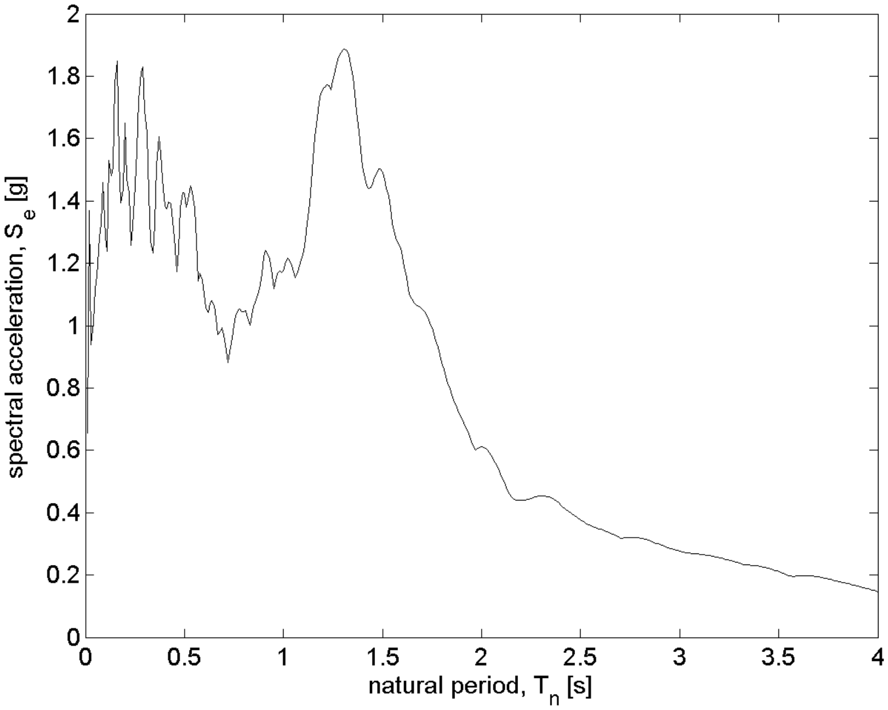

Figure 10.1. Response spectrum for the surface motion calculated from the nonlinear analysis. 5 % damping.

11. Comparisons

The seismic ground response has been analysed by different analysis methods and by different descriptions of the input bedrock motions by the procedures illustrated in Chapter 4. In this chapter a series of comparisons of the different methods are made in order to give an estimate of which analysis methods are the most accurate and for which cases simpler analyses gives satisfactory results.

The used analysis methods to get the surface ground motion is the following:

1) Procedure by Eurocode EC8
   a) Gives surface response spectrum
2) Equivalent linear model with power spectrum bedrock input motion
   a) Gives surface Fourier amplitude spectrum
   b) Gives surface response spectrum
3) Equivalent linear model with Fourier series bedrock input motion
   a) Gives surface Fourier amplitude spectrum
   b) Gives surface response spectrum
4) Nonlinear model with time history bedrock input motion
   a) Gives surface Fourier amplitude spectrum
   b) Estimates surface response spectrum

A comparison are made of the generated surface response spectra since this is the only representation of the surface motion defined in Eurocode EC8. Comparisons with alternative soil profile and bedrock input are also performed is Section 11.2 and 11.3 respectively.

11.1. Surface response spectra comparisons

The analysis results for the equivalent linear method and nonlinear method are compared with the procedure by Eurocode EC8 by comparing the generated surface acceleration response spectra. In Figure 11.1 the surface acceleration response spectrum for the equivalent linear method using both the power spectrum and Fourier series bedrock input are shown together with the nonlinear analysis and the surface acceleration response spectrum defined by Eurocode EC8.

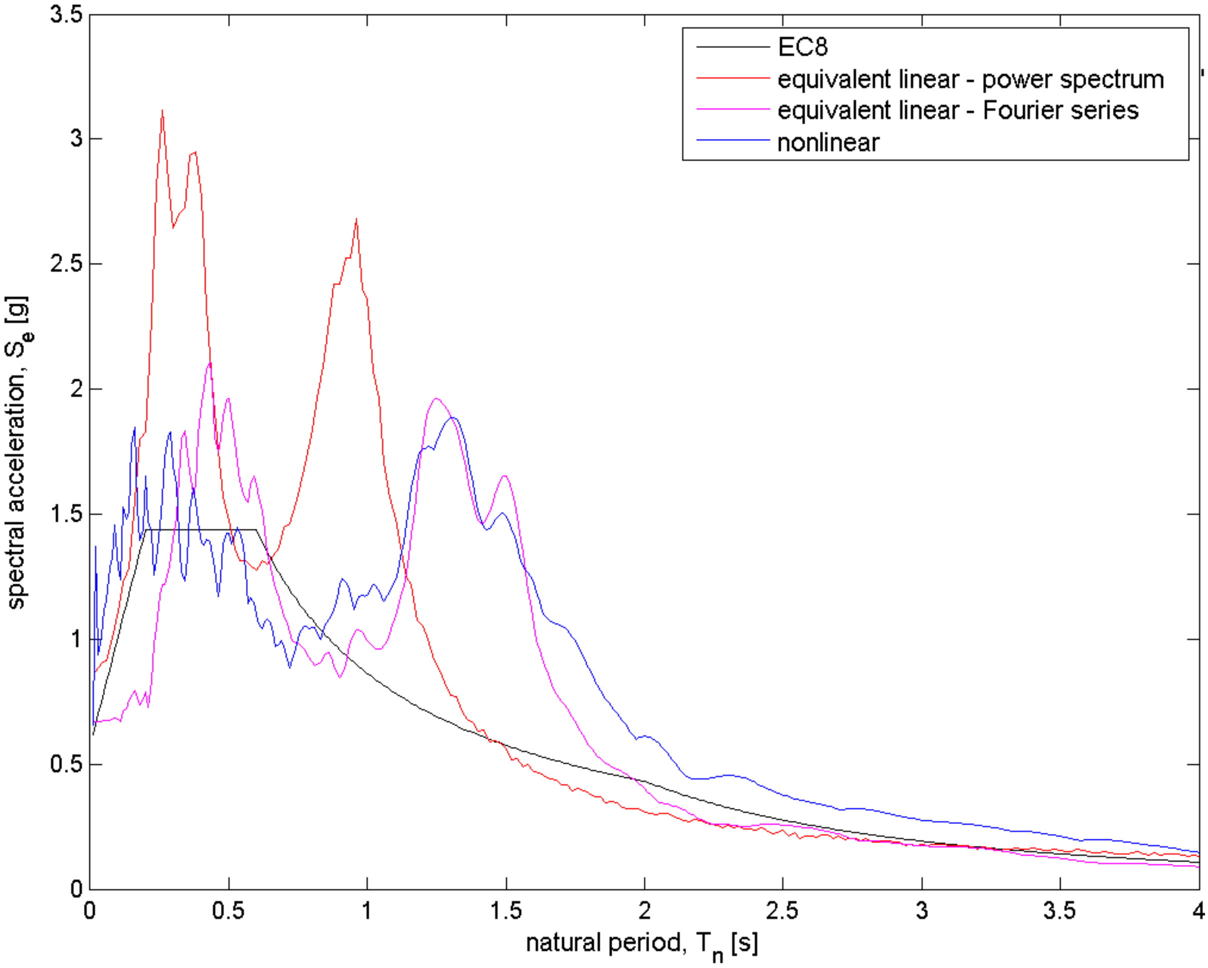

Figure 11.1. Surface acceleration response spectrum for all relevant analysis methods.

From the comparison of the response spectra it is seen that the equivalent linear method using a Fourier series input and the nonlinear analysis gives similar results, but the equivalent linear method has a tendency to overdamp the response at lower and higher periods than $T_n \approx 0.3$ s and $T_n \approx 1.6$ s respectively. The equivalent linear method using a power spectrum and assumed phase spectrum gives a much higher response. Compared with the response spectrum given by Eurocode EC8 the equivalent linear method using Fourier series and the nonlinear analysis fits the design spectrum quite well for periods in the range up to $T_n \approx 1$ s but with a tendency to give a higher response. The design spectrum given by Eurocode EC8 does not capture the large response in the region of $T_n \approx 1.5$ s as indicated by both the equivalent linear and the nonlinear analyses.

The high period peak at $T_n \approx 1$ s for the equivalent linear method using a power spectrum input is at a lower period than for the equivalent linear analysis using a Fourier series and for the nonlinear analysis. The reason for this peak at a lower period can be explained by comparing the range of effective shear strain and resulting transfer function for the soil of both the equivalent linear analysis using a power spectrum and the analysis using a Fourier series input.

The effective shear strain and transfer functions for the two analyses are seen in Figure 6.7, Figure 6.9, Figure 6.13 and Figure 6.14. The range of the effective shear strains for the analysis using a power spectrum are around $\gamma_{eff} \approx [0.06\,\%; 0.2\,\%]$ whereas the effective shear strain for the analysis using a Fourier series are around $\gamma_{eff} \approx [0.4\,\%; 0.9\,\%]$. The much lower shear strain for the analysis using a power spectrum results in a stiffer soil and by that a transfer function with modes at a higher frequency than for the analysis using a Fourier series. Large amplification is generated at frequencies in the regions of the modes, and the peak at the lower period for the analysis using a power spectrum therefore correspond well to this observation.

The second peak at a period around $T_n \approx 0.4$ s for the equivalent linear analysis using a power spectrum as input can also be explain on the basis of the transfer function in that the second peak in the transfer function, corresponding to the second mode, is significant compared to peak of the second mode for the analysis using a Fourier series.

To illustrate the change in ground motion from bedrock to surface the bedrock and surface acceleration response spectra for all four analysis methods are given in Figure 11.2.

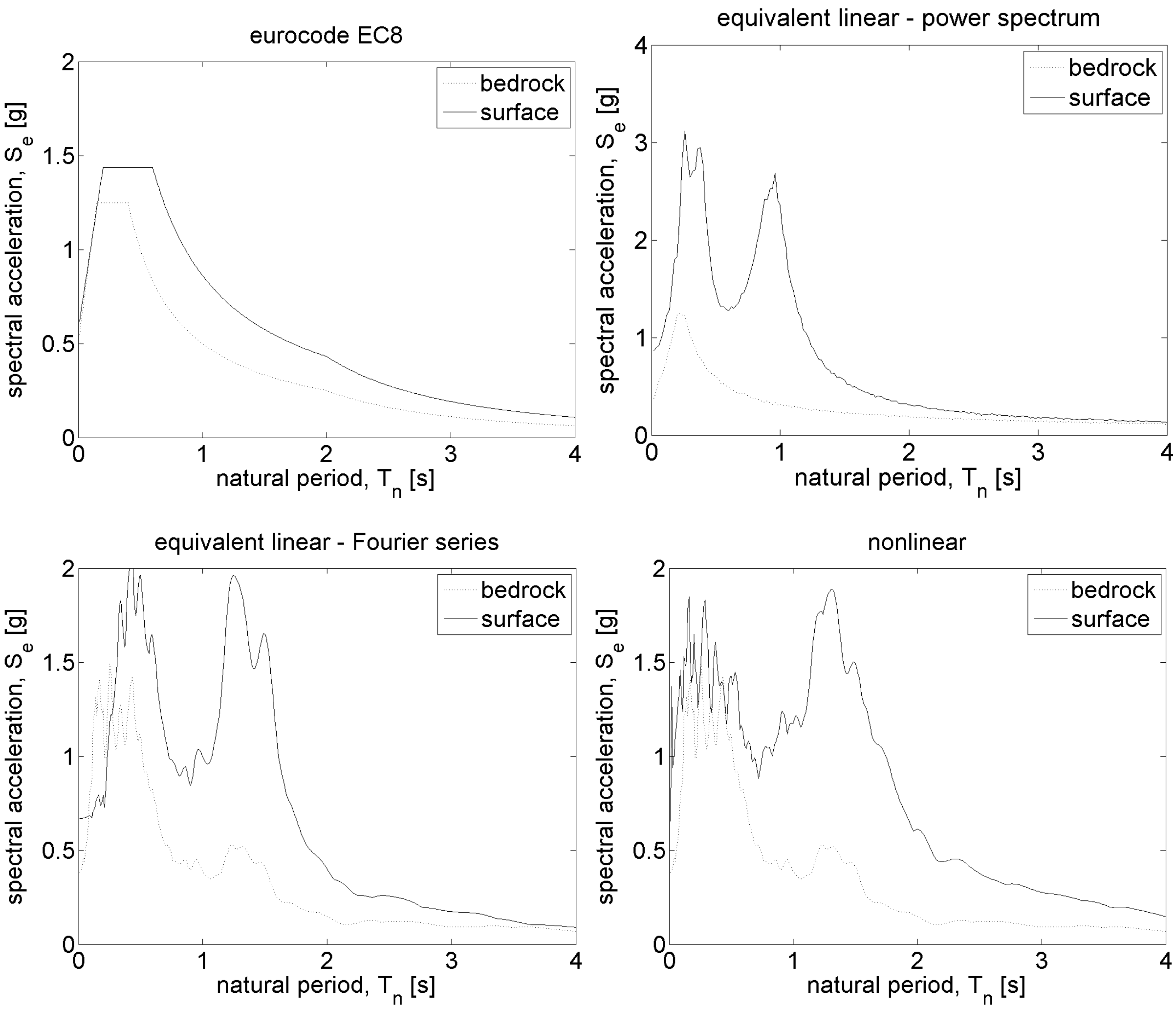

Figure 11.2. Bedrock and surface acceleration response spectra for the four compared analysis methods.

It is seen that the surface motion generally is higher than the bedrock motion for all analysis results. A shift in the frequency contents of the motion towards higher periods is seen for all analyses. From the figure for equivalent linear analysis using Fourier series and for the nonlinear analysis a small peak is seen at $T_n \approx 1.2$ s for the bedrock motion. The energy at this frequency range is partly what causes the large peak for the surface motion but by calculation of the amplification ratio as done in Section 11.1.1 it can be shown that the soil is still greatly amplified at this period range.

11.1.1. Amplification ratio

For a clearer picture of the amplification of the ground motion from bedrock to surface an amplification ratio can be calculated for the range of the natural period. The amplification ratio is defined as the ratio between the surface response value and the bedrock response value.

In Figure 11.3 the calculated amplification ratios on the basis of the response spectra in Figure 11.2 are shown.

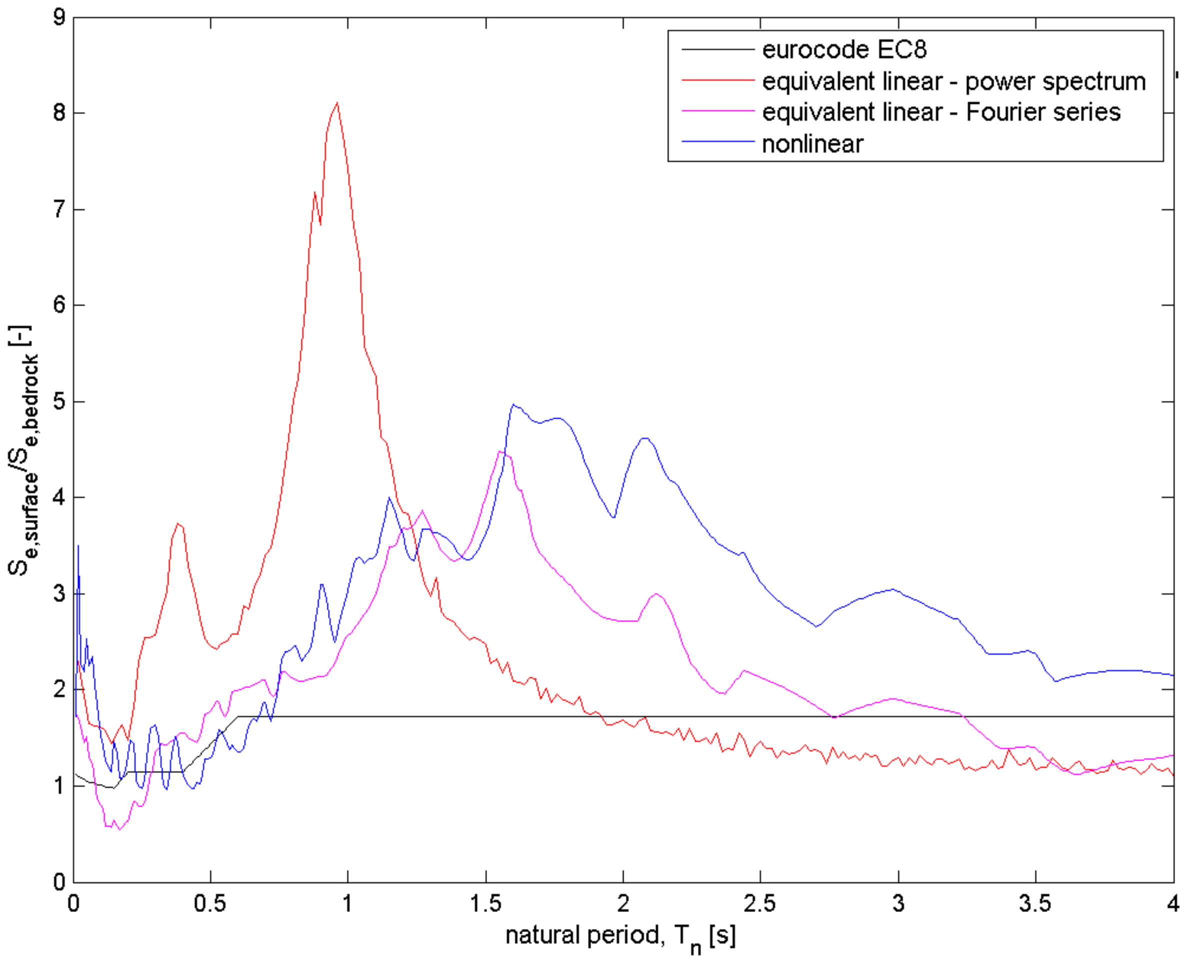

Figure 11.3. Amplification ratio curves for the four compared analysis methods.

By calculation of the amplification ratio it is easier seen, at which periods the motion is amplified the most. In Figure 11.3 it is seen that the periods around $T_n \approx 1.2\text{ s}$ to $T_n \approx 2.2\text{ s}$ gives the highest amplification of the motion for the equivalent linear and the nonlinear analyses.

An estimate of which period will give the highest amplification can be made on the basis of some basic estimation rules which gives an estimate of the degraded natural period. Excitation at the natural period of a soil site will be amplified the most, just as it is seen for all other dynamic systems.

Firstly the nondegraded natural period of a soil site can be estimated by (11-1), where nondegraded means a soil with stiffness not softened by shear strain

$$T_n \approx \frac{4H}{\overline{V}_s} \tag{11-1}$$

where

T_n is the nondegraded natural period of the site

H is the total thickness of the soil layers

$\overline{V}_s$ is the average nondegraded shear wave velocity for all soil layers

[Bray 2007b]

By the soil properties given in Figure 2.7 the nondegraded average shear wave velocity is calculated to $\overline{V}_s = 354\ \frac{\text{m}}{s}$. As an estimate the degraded natural period, T_n', is given as $T_n' \approx 1.5T_n$ [Bray 2007b]. With these basic estimation rules the degraded natural period of the site is given as

$$\begin{aligned} T_n' &\approx 1.5\frac{4H}{\overline{V}_s} \\ T_n' &\approx 1.4\text{ s} \end{aligned} \tag{11-2}$$

From (11-2) it is seen that this estimation correspond well with what is seen in Figure 11.3 but estimated slightly in the lower range of the period.

11.2. Soil response for 30 m soil profiles

In this section analyses of the soil response of an altered soil profile is performed. The motivation is that in Eurocode EC8 the soil type is defined on the basis of the average shear wave velocity for the top 30 m soil. The comparison in Section 11.1 are based on a soil profile with 80 m, where the soil from 30 m to 80 m of depth might have an influence on the surface response which the procedure by Eurocode EC8 does not take into account. The altered soil profile for this modified analysis is given in Figure 11.4 and is chosen as the top 30 m of the original soil profile from Figure 2.7 directly overlaying bedrock. With this altered soil profile the average shear wave velocity for the top 30 m is the same as for the original analysis and therefore the prescribed response by Eurocode EC8 is the same as for the original soil profile of 80 m soil.

$z = 0$ m			surface
	$h = 12$ m	$V_{s,max} = 200\ \frac{m}{s}$ $\rho = 1950\ \frac{kg}{m^3}$	soil type 1: silty sand
$z = 12$ m			
	$h = 18$ m	$V_{s,max} = 300\ \frac{m}{s}$ $\rho = 2050\ \frac{kg}{m^3}$	soil type 2: silty sandy clay
$z = 30$ m			
	$h \approx \infty$	$V_{s,max} = 1000\ \frac{m}{s}$ $\rho = 2600\ \frac{kg}{m^3}$	bedrock

Figure 11.4. Modified soil profile.

The surface motion for this soil profile is analysed using the equivalent linear analysis with the Fourier series input as described in 6.5 and by the nonlinear analysis described in Chapter 7. The surface motion is compared with the design response spectrum defined by Eurocode EC8 where all three response spectra are shown in Figure 11.5.

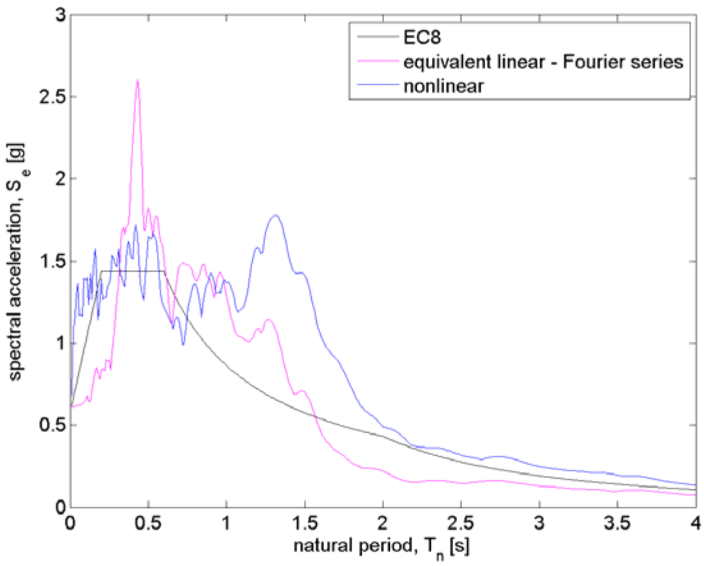

Figure 11.5. Surface acceleration response spectra using 30 m soil profile.

The response for this soil profile is generally smaller than for the analyses for the 80 m soil profile but with a significant large peak for the equivalent linear analysis. This peak corresponds to the first mode of the soil which is at a lower period than for the 80 m soil profile corresponding to the decreased value of *H* in (11-2). The large peak is partly caused by resonance but because the stiffness of the soil changes over the duration of the earthquake which is not captured by the equivalent linear model this high amplification due to resonance is likely to be an overestimation.

From the figure a peak for the nonlinear analysis is seen at a period around 1.5 s as with the original soil profile. As before this peak is not captured by the design spectrum defined by Eurocode EC8. The peak for the nonlinear analysis must correspond to the first mode in the analysis. The reason for the higher value of the period in the nonlinear analysis is because larger strains are calculated and thereby larger softening of the soil which shifts the first mode towards higher periods. The maximum strain distribution throughout the depth of the soil is shown in Figure 11.6.

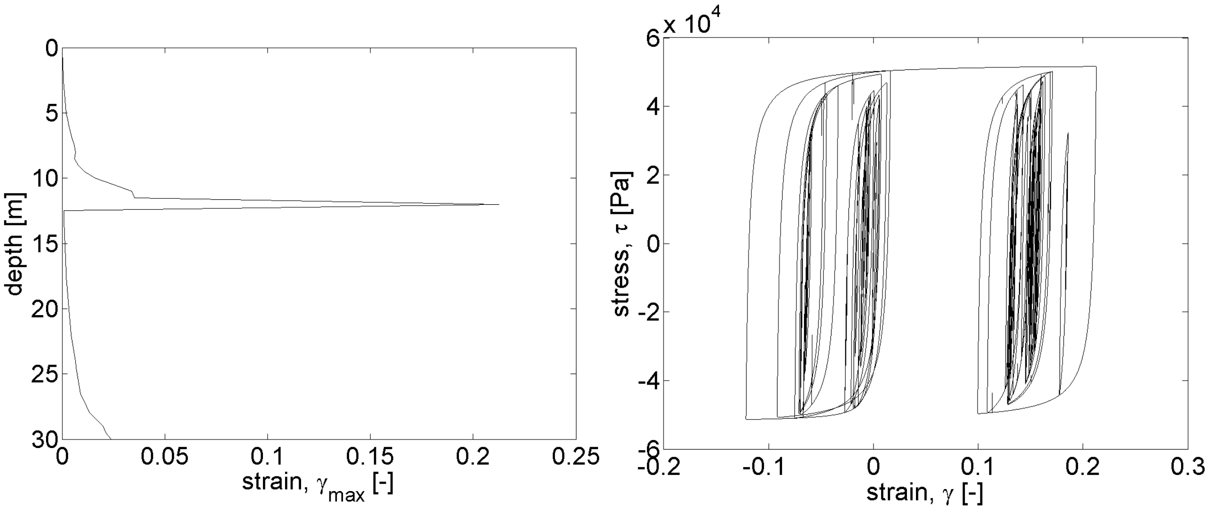

Figure 11.6. Maximum strain distribution (left). Stress-strain curve for sublayer at soil type interface at 12 m of depth (right).

As seen in Figure 11.6 large strains are experienced in the sublayers at 12 m of depth where a change in the soil type is present. The strain at that depth reaches values where the hyperbolic function describing the backbone curve gives deformations corresponding to failure of the soil. By looking at the actual measured backbone curve in Figure 7.4 it is seen that the measurements only are given for strain values below 1 %, but the tendency of the measured backbone curve is an continuously inclining curve. By comparing the fit of the hyperbolic function to the measured backbone curve in the region of strain values 1 %, it is seen that the inclination of the fitted curve is much less, indicating a shear strength lower than for the measured curve. The large softening of the soil in the nonlinear analysis might not be as large as calculated if a better fit of the backbone curve is used instead of the hyperbolic function.

11.3. Alternative bedrock input record

In this section an analysis of the effect of using another bedrock time history record as input is performed. The time history is chosen with the same target spectrum and by the same procedure as described in Section 5.3.2. The chosen trial ground motion is a record from the Northridge earthquake event in California, USA in 1994. The record is from a site corresponding to firm ground and with the record ID: P0926:MTW000 [PEER 2008] and recorded with a sampling frequency of $f_s = 50$ Hz. The scaled acceleration, velocity and displacement time history are shown in Figure 11.7.

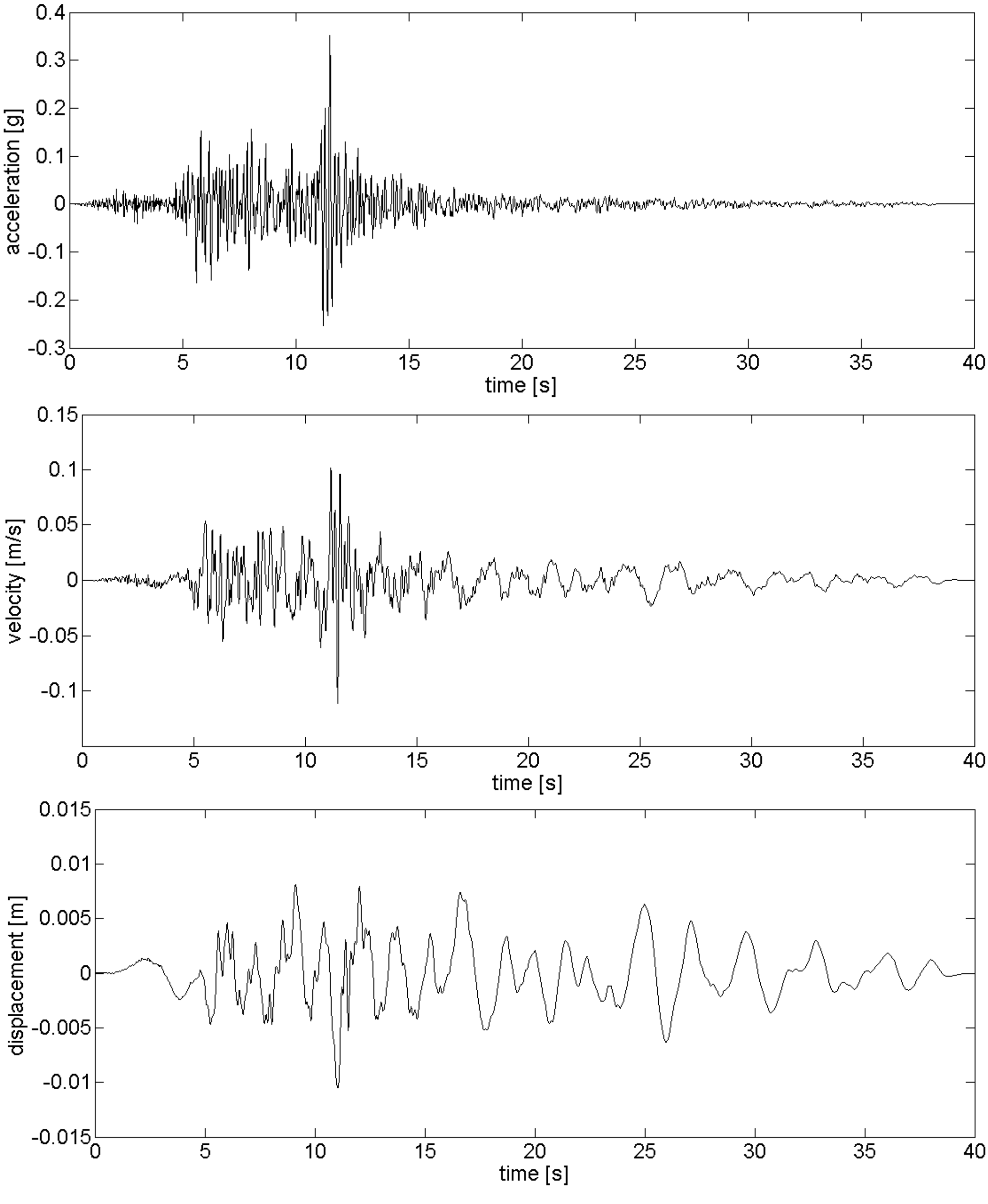

Figure 11.7. Acceleration, velocity and displacement time history scaled by 1.5.

The target and scaled trial acceleration response spectra are shown in Figure 11.8.

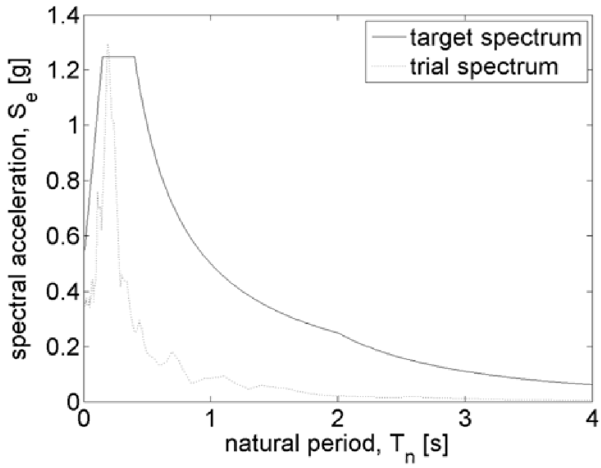

Figure 11.8. Target and scaled trial response spectra. Scaling is 1.5.

The soil profile is the full profile of 80 m soil as shown in Figure 2.7.

The analysis using the new bedrock time history is performed for both the equivalent linear and the nonlinear analyses. The result is shown as the surface acceleration response spectrum together with the prescribed surface acceleration defined by the Eurocode EC8 procedure. The response spectra are shown in Figure 11.9.

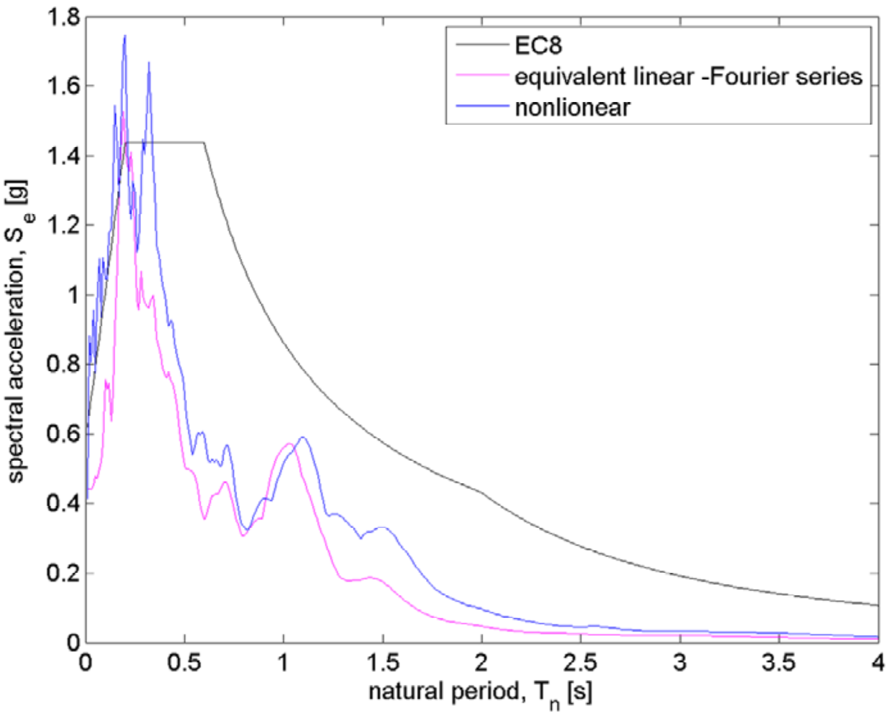

Figure 11.9. Surface acceleration response spectra using Northridge record.

The result using the new bedrock time history shows that the equivalent linear and nonlinear analyses gives similar results. For this record the response is generally below the design spectrum defined by Eurocode EC8. The peak for the response at the first mode of the soil around $T_n \approx 1.1\ \mathrm{s}$ is for this input motion also captured by the design spectrum.

Compared with the nonlinear response it is seen that the equivalent linear method tends to overdamp the response. The reason for this might be explained by the way the equivalent linear method incorporates the strain dependant damping as an effective strain proportional with the maximum strain. If the maximum strain is much larger than the majority of remaining strain cycles the effective strain should be lower than the prescribed 65 % of the maximum strain.

12. Conclusion

On the basis of the comparison of the analysis results the following conclusions can be made.

The Eurocode EC8 procedure is the fastest method to get an estimate of the seismic response at a given site. The procedure can be implemented with only basic knowledge of the site characteristics and seismic hazard for the area, and the procedure can therefore be used to get a qualified picture of the seismic load at a site. The Eurocode procedure only takes the soil effect into account in a simplified manner by including the top 30 m of soil. Therefore the procedure comes short in predicting the large amplification of the ground motion at the first period of the soil when soil deposits at a larger depth is present at the site. When the energy for the input motion is concentrated at small periods the Eurocode EC8 gives satisfactory results in that the design spectrum captures the amplification at larger periods.

An equivalent linear model can be implemented for a better estimate of the ground motion amplification at sites with deep soil deposits. The equivalent linear model takes all the soil layers and the strain dependency of the soil parameters into account. The model has shown to give satisfactory results, but some overestimated resonance effects can be calculated which will not happen in the field due to the varying stiffness of the soil throughout the duration of the earthquake. The equivalent linear method is not recommended for strain levels above 1 % since dynamic soil properties above this level are poorly described due to increasing nonlinearity in the soil response at these strain levels.

The nonlinear model gives satisfactory results both for low and high levels of strain. The model requires more extensive description of the constitutive model and therefore more laboratory testing is needed. The nonlinear analysis must be performed in the time domain which results in larger computational time but with today's computer power this should be no limitation.

It is important that good input motions are available for both the equivalent linear and nonlinear analyses. Both an amplitude and a phase spectrum must be given since estimations of the phase spectrum is attached with large uncertainty due to the complex structure of earthquake motions. Modified earthquake record are recommended as input motions for the analyses.

13. References

[*Abrahamson & Silva 1997*]: Empirical Response Spectral Attenuation Relationships for Crustal Earthquakes

N. A. Abrahamson & W. J. Silva, 1997
Seismological Research Letters
Volume 68, Number 1

[*Abrahamson 2000*]: State of the Practice of Seismic Hazard Evaluation, 2000

Norman A. Abrahamson
Pacific Gas and Electric Company

[*Andersen 2006*]: Linear Elastodynamic Analysis

Lars Andersen, 2006
Aalborg University
ISSN: 1901-7286

[*Bray 2007*]: Dynamical Shear Modulus & Material Damping

Jonathan D. Bray, 2007
University of California at Berkeley

[*Bray 2007b*]: Notes from the course Geotechnical Earthquake Engineering by professor

Jonathan. D. Bray, 2007
University of California at Berkeley

[*Chopra 2007*]: Dynamics of Structures - Theory and Applications to Earthquake Engineering

Anil K. Chopra, 2007
Pearson Prentice Hall
ISBN: 0-13-156174-X
3rd edition

[*dkimages.com 2008*]: dkimages.com

http://www.dkimages.com/discover/home/science/Earth-Sciences/Geology/The-Earth/Plate-Tectonics/Plates-Colliding/Plates-Colliding-5.html
Downloaded the 9th of April 2008

[*dkimages.com 2008b*]: dkimages.com
http://www.dkimages.com/discover/Home/Science/Earth-Sciences/Hydrologic-Sciences/Oceans-and-Seas/Ocean-Floor/Sea-floor-Spreading/Sea-floor-Spreading-07.html
Downloaded the 9th of April 2008

[*EN1998:2003*]: Eurocode 8: Design of structures for earthquake resistance - Part 1: General rules, seismic actions and rules for buildings
European committee for standardization, 2003
Final draft, Ref. No. prEN 1998-1:2003 E

[*Giardini et al. 2003*]: European-Mediterranean Seismic Hazard Map
D. Giardini, M.-J. Jiménez and G. Grünthal, 2003
European Seismological Commission
http://wija.ija.csic.es/gt/earthquakes
Downloaded the 12th of March 2008

[*Kramer 1996*]: Geotechnical Earthquake Engineering
Steven L. Kramer, 1996
Prentice Hall
ISBN: 0-13-374943-6

[*Lutes & Sarkani 2004*]: Random Vibrations - Analysis of Structural and Mechanical Systems
Loren D. Lutes & Shahram Sarkani, 2004
Elsevier Butterworth - Heinemann
ISBN: 0-7506-7765-1

[*Rathje et al. 2004*]: Empirical Relationships for Frequency Content Parameters of Earthquake ground Motions
Rathje, Faraj, Russel and Bray, 2004
EERI Earthquake Spectra

[*usgs.com 2008*]: U.S. Geological Survey
http://geomaps.wr.usgs.gov/parks/deform/gfaults.html
Downloaded the 9th of April 2008

[*usgs.com 2008b*]: U.S. Geological Survey
http://eqint.cr.usgs.gov/deaggint/2002
Downloaded the 6th of May 2008